Journal of Physics G: Nuclear and Particle Physics

NUCLEAR PHYSICS • OPEN ACCESS

Optical potentials for the rare-isotope beam era

To cite this article: C Hebborn *et al* 2023 *J. Phys. G: Nucl. Part. Phys.* **50** 060501

View the article online for updates and enhancements.

You may also like

- Isotope harvesting at FRIB: additional opportunities for scientific discovery
E Paige Abel, Mikael Avilov, Virginia Ayres et al.
- Low- to medium- cavities for heavy ion acceleration
Alberto Facco
- *r*-process nucleosynthesis: connecting rare-isotope beam facilities with the cosmos
C J Horowitz, A Arcones, B Côté et al.

This content was downloaded from IP address 42.116.20.44 on 04/05/2023 at 04:17

OPEN ACCESS
IOP Publishing
Journal of Physics G: Nuclear and Particle Physics
J. Phys. G: Nucl. Part. Phys. **50** (2023) 060501 (58pp)
https://doi.org/10.1088/1361-6471/acc348

Optical potentials for the rare-isotope beam era

C Hebborn[1,2], F M Nunes[1,3], G Potel[2], W H Dickhoff[4], J W Holt[5], M C Atkinson[2,6], R B Baker[7], C Barbieri[8,9], G Blanchon[10,11], M Burrows[12], R Capote[13], P Danielewicz[1,3], M Dupuis[10,11], Ch Elster[7], J E Escher[2], L Hlophe[2], A Idini[14], H Jayatissa[15], B P Kay[15], K Kravvaris[2], J J Manfredi[16], A Mercenne[17], B Morillon[10,11], G Perdikakis[18], C D Pruitt[2], G H Sargsyan[2], I J Thompson[2], M Vorabbi[19,20] and T R Whitehead[1]

[1] Facility for Rare Isotope Beams, East Lansing, MI 48824, United States of America
[2] Lawrence Livermore National Laboratory, PO Box 808, L-414, Livermore, CA 94551, United States of America
[3] Department of Physics and Astronomy, Michigan State University, East Lansing, MI 48824-1321, United States of America
[4] Department of Physics, Washington University, St. Louis, MO 63130, United States of America
[5] Department of Physics and Astronomy and Cyclotron Institute, Texas A&M University, College Station, TX 77843, United States of America
[6] Theory Group, TRIUMF, Vancouver, BC V6T 2A3, Canada
[7] Institute of Nuclear and Particle Physics, and Department of Physics and Astronomy, Ohio University, Athens, OH 45701, United States of America
[8] Dipartimento di Fisica, Università degli Studi di Milano, Via Celoria 16, I-20133 Milano, Italy
[9] INFN, Sezione di Milano, Via Celoria 16, I-20133 Milano, Italy
[10] CEA, DAM, DIF, F-91297 Arpajon, France
[11] Université Paris-Saclay, CEA, Laboratoire Matiére sous Conditions Extrêmes, F-91680 Bruyéres-Le-Châtel, France
[12] Department of Physics and Astronomy, Louisiana State University, Baton Rouge, LA 70803, United States of America
[13] NAPC–Nuclear Data section, International Atomic Energy Agency, A-1400, Vienna, Austria
[14] Division of Mathematical Physics, Department of Physics, LTH, Lund University, PO Box 118, S-22100 Lund, Sweden
[15] Physics Division, Argonne National Laboratory, Lemont, IL, 60439, United States of America
[16] Department of Engineering Physics, Air Force Institute of Technology, Wright-Patterson AFB, OH 45433, United States of America
[17] Center for Theoretical Physics, Sloane Physics Laboratory, Yale University, New Haven, Connecticut CT-06520, United States of America

 © 2023 The Author(s). Published by IOP Publishing Ltd Printed in the UK

[18] Department of Physics, Central Michigan University, Mount Pleasant, MI 48859, United States of America
[19] National Nuclear Data Center, Brookhaven National Laboratory, Upton, NY 11973-5000, United States of America
[20] Department of Physics, University of Surrey, Guildford, GU2 7XH, United Kingdom

E-mail: hebborn@frib.msu.edu

Received 18 October 2022, revised 9 February 2023
Accepted for publication 10 March 2023
Published 27 April 2023

Abstract

We review recent progress and motivate the need for further developments in nuclear optical potentials that are widely used in the theoretical analysis of nucleon elastic scattering and reaction cross sections. In regions of the nuclear chart away from stability, which represent a frontier in nuclear science over the coming decade and which will be probed at new rare-isotope beam facilities worldwide, there is a targeted need to quantify and reduce theoretical reaction model uncertainties, especially with respect to nuclear optical potentials. We first describe the primary physics motivations for an improved description of nuclear reactions involving short-lived isotopes, focusing on its benefits for fundamental science discoveries and applications to medicine, energy, and security. We then outline the various methods in use today to build optical potentials starting from phenomenological, microscopic, and *ab initio* methods, highlighting in particular, the strengths and weaknesses of each approach. We then discuss publicly-available tools and resources facilitating the propagation of recent progresses in the field to practitioners. Finally, we provide a set of open challenges and recommendations for the field to advance the fundamental science goals of nuclear reaction studies in the rare-isotope beam era. This paper is the outcome of the Facility for Rare Isotope Beams Theory Alliance (FRIB-TA) topical program 'Optical Potentials in Nuclear Physics' held in March 2022 at FRIB. Its content is non-exhaustive, was chosen by the participants and reflects their efforts related to optical potentials.

Keywords: optical potentials, nuclear reactions, phenomenological optical model, many-body theory

(Some figures may appear in colour only in the online journal)

1. Introduction

Nuclear reactions drive the chemical evolution of the Universe, enable a wide range of societally beneficial technologies on Earth, and provide a tool to study the structure of atomic

Original content from this work may be used under the terms of the Creative Commons Attribution 4.0 licence. Any further distribution of this work must maintain attribution to the author(s) and the title of the work, journal citation and DOI.

nuclei and properties of the nuclear force in the laboratory. In particular, nuclear reactions involving exotic short-lived isotopes are fundamental to address numerous open questions in contemporary nuclear science research to be investigated at frontier radioactive ion beam facilities, such as the Facility for Rare Isotope Beams (FRIB). Nuclear reaction theories with quantified uncertainties will be crucial to maximize the scientific impact of rare isotope facilities worldwide. However, even the simplest reactions that involve light nuclei at low center-of-mass energies are challenging to understand from fundamental *ab initio* nuclear theory [1]. The continued development of microscopic models that capture salient features of the quantum many-body problem, such as antisymmetry and multiple scattering, is therefore needed to advance nuclear reaction science in the rare-isotope beam era.

The nuclear optical model is the primary tool to reduce the complexity of quantum many-body scattering into a form that is tractable across a large range of energies, target isotopes, and reaction channels. The idea is to replace fundamental two-body and many-body forces between projectile and target with a complex and energy-dependent two-body local potential $U(r, E) = V(r, E) + \mathrm{i}W(r, E)$, in analogy with the scattering and absorption of light in a dielectric medium with complex index of refraction [2–4]. The imaginary part, $W(r, E)$, of the nuclear optical model potential (OMP) accounts for the loss of flux in the elastic scattering channel due to open reaction channels (e.g. inelastic, pick-up, break-up, and similar reactions) dictated by the projectile energy E. The energy dependence of the optical potential accounts for temporal non-localities due to virtual excitations of the nucleus and implicitly accounts for spatial nonlocalities that arise from exchange scattering on indistinguishable nucleons in the target. Formally, spatial nonlocality gives rise to a momentum-dependent potential, but for elastic scattering this can be approximated [5] in terms of an equivalent energy-dependent local mean field. During the last 60 years, the nuclear optical model has been broadly applied to analyze the elastic scattering of pions, nucleons and heavier ions by nuclei, over a wide range of energies [2–4]. Inelastic scattering was included by the coupled-channels formalism [6, 7] and consideration of dispersion effects from the requirement of causality [8] allows for the description of both bound and scattering states by the same complex nuclear mean field [9–11].

Following decades of refinements [12–16], the phenomenological optical model has achieved an impressive description of nucleon–nucleus scattering on stable target isotopes up to projectile energies $E \leqslant 200$ MeV. The functional form of modern phenomenological optical potentials includes complex-valued volume, surface, and spin–orbit terms, together with a central Coulomb interaction

$$\begin{aligned} U(r, E) = {} & V_V(r, E) + V_D(r, E) + \mathrm{i}W_V(r, E) + \mathrm{i}W_D(r, E) + V_{so}(r, E)\vec{l} \cdot \vec{s} \\ & + \mathrm{i}W_{so}(r, E)\vec{l} \cdot \vec{s} + V_C(r). \end{aligned} \tag{1}$$

The energy dependence in equation (1) is typically decoupled from the radial dependence, e.g.

$$V_V(r, E) = v_V(E) f(r, R_V, a_V), \tag{2}$$

where the form factor $f(r)$ is usually defined as a Woods–Saxon shape characterized by a radius R and diffuseness a, i.e.

$$f(r, R, a) = \frac{1}{1 + \mathrm{e}^{(r-R)/a}}. \tag{3}$$

Note that other radial dependencies can be used, such as Gaussian and squares of Woods–Saxon form factors. Whereas the real and imaginary volume terms (V_V, W_V) are proportional to form factors, the real and imaginary surface contribution (V_D, W_D) and the spin–orbit contributions (V_{so}, W_{so}) are proportional to the radial derivatives of these form factors. In

general, the fitted parameters that describe the energy and geometry dependence also vary with the mass number A and isospin asymmetry $\delta = (N - Z)/A$. In total, approximately 40 fitted parameters are used in the construction of the widely used non-dispersive phenomenological global optical potential of Koning and Delaroche [14]. Enforcing the appropriate dispersion relations

$$\mathrm{Re}\{U(E)\} = -\frac{1}{\pi}\mathcal{P}\int \mathrm{d}E' \frac{\mathrm{Im}\{U(E')\}}{E - E'}, \tag{4}$$

allows the number of parameters to be significantly reduced. Moreover, the description of both elastic scattering at incident energies below 5 MeV and the bound states is improved as compared to non-dispersive approaches. For nuclear reactions involving unstable isotopes, for which scattering data are scarce, the quality of phenomenological optical potential extrapolations is uncertain. For this purpose, microscopic or semi-microscopic optical potentials derived from fundamental nucleon–nucleon and many-nucleon forces may provide useful starting points.

Since the 1950s, several approaches have been developed to derive nucleon–nucleus optical potentials starting from microscopic many-body theory. These include the Watson multiple scattering theory, Feshbach projection operator formalism, and Green's function theory. Before briefly presenting each approach, let us define the many-body Hamiltonian for the $(A + 1)$-body system

$$\mathcal{H} = H_A(\vec{r}_1,\ldots,\vec{r}_A) + h_0 + V(\vec{r}, \vec{r}_1,\ldots,\vec{r}_A), \tag{5}$$

where H_A is the Hamiltonian for the A-particles of the target nucleus with eigenstates satisfying $H_A\Phi_k = \epsilon_k\Phi_k$, h_0 is the kinetic energy of the projectile, and V is the many-body interaction potential between projectile and nucleons in the target. The exact eigenvalues and eigenstates of the $(A + 1)$-particle system satisfy $\mathcal{H}\Psi = \mathcal{E}\Psi$.

The aim of the multiple scattering theory of Watson [17] and its later extension by Kerman, McManus, and Thaler [18] is to derive an equation for the optical potential in terms of free-space nucleon–nucleon scattering amplitudes. This can be formally justified only under certain assumptions, including the so-called 'impulse approximation', whereby it is assumed that the projectile nucleon is traveling at sufficiently high energy that it interacts strongly with only one or few nucleons of the target at some instant in time. The theory is therefore expected to be valid at energies sufficiently above the excitation energies of the nucleus, i.e. larger than roughly 60 to 100 MeV, where impacts of Pauli-blocking and three-body forces are diminished. In the impulse approximation and at leading order, the nucleon–nucleus optical potential with kinetic energy E can be represented as [18]

$$\hat{U}(\vec{k}', \vec{k}; E) = \sum_{\alpha=p,n}\int \mathrm{d}^3\vec{p}\,' d^3\vec{p} \,<\vec{k}'\vec{p}\,'|\hat{\tau}_\alpha(E)|\vec{k}\vec{p}>\rho_\alpha\left(\vec{p}\,' + \frac{\vec{k}'}{A}, \vec{p} + \frac{\vec{k}}{A}\right)\delta^3(\vec{k}' + \vec{p}\,' - \vec{k} - \vec{p}), \tag{6}$$

where the momenta $\vec{k}'$ and $\vec{k}$ are the final and initial momenta of the projectile in the frame of zero total nucleon–nucleus momentum, α sums over target neutrons and protons. The quantity $\hat{\tau}_\alpha(E)$ represents a nucleon–nucleon amplitude, and ρ_α the ground-state density of the target for protons (p) and neutrons (n). Note that extensions of this approach going beyond the impulse approximation and including three-body forces are possible and will be discussed further in the text.

At lower projectile energies, where Pauli blocking and three-body forces play an enhanced role, optical model potentials may be constructed using either the Feshbach projection formalism or Green's function theory. Neglecting first the antisymmetrization between the

projectile and the constituent nucleons in the target, Feshbach derived [19] an equation for the projection $P\Psi(\vec{r}, \vec{r}_1,\ldots,\vec{r}_A) = \phi_0(\vec{r})\Phi_0(\vec{r}_1,\ldots,\vec{r}_A)$ of the total wave function onto the elastic scattering channel of the form

$$\left(h_0 + \mathcal{V}_{00} + \sum_{j,k\neq 0} \mathcal{V}_{0j} G_{jk} \mathcal{V}_{k0}\right)\phi_0 = E\ \phi_0, \tag{7}$$

where Φ_0 is the ground state of the target and $E = \mathcal{E} - \epsilon_0$ is the nucleon–nucleus relative energy defined from the ground-state target energy ϵ_0. We define in equation (7); the Green's function matrix element G_{jk}

$$G_{jk} = \lim_{\eta \to 0^+} \frac{1}{E - H_{jk} + \mathrm{i}\eta}, \tag{8}$$

from the Hamiltonian matrix element H_{jk} and coupling potentials between the elastic scattering channel and the inelastic ones $\mathcal{V}_{jk}$,

$$H_{jk} = h_0\delta_{jk} + \mathcal{V}_{jk} + \epsilon_k\delta_{jk} \quad \text{and} \quad \mathcal{V}_{jk} = \langle\Phi_j|V|\Phi_k\rangle. \tag{9}$$

The optical potential is then identified as

$$V_{\mathrm{opt}} = \mathcal{V}_{00} + \sum_{j,k\neq 0} \mathcal{V}_{0j}\frac{1}{E - H_{jk} + \mathrm{i}\eta}\mathcal{V}_{k0} \tag{10}$$

with $\eta \to 0^+$. The potential is complex, energy dependent, and nonlocal. This formulation was later extended [20] to treat inelastic scattering processes and to properly account for antisymmetrization between projectile and target. An alternative derivation of the optical potential makes use of the language of second-quantized many-body theory and Green's functions. Here the propagation of particles and holes in a quantum many-body system is characterized by the one-body Green's function [21]

$$G(\vec{r}, t; \vec{r}', t') = -\mathrm{i}\langle\Phi_0|\hat{T}\,[\hat{a}_H(\vec{r}, t)\ \hat{a}_H^\dagger(\vec{r}', t')]|\Phi_0\rangle, \tag{11}$$

where $\hat{T}$ is the time ordering operator, $a_H^\dagger$ and a_H are creation/annihilation operators in the Heisenberg representation. The time Fourier transform $G(\vec{r}, \vec{r}'; E)$ of the one-body Green's function can be expressed in terms of the free Green's function $G_0(\vec{r}, \vec{r}'; E)$, defined from the free Hamiltonian $H_0 = h_0 + H_A$, and the nucleon irreducible self-energy $\Sigma^\star(\vec{r}, \vec{r}'; E)$ through the Dyson equation [21]

$$G(\vec{r}, \vec{r}'; E) = G_0(\vec{r}, \vec{r}'; E) + \int \mathrm{d}^3\vec{y} \int \mathrm{d}^3\vec{y}'\ G_0(\vec{r}, \vec{y}; E)\ \Sigma^\star(\vec{y}, \vec{y}'; E)\ G(\vec{y}', \vec{r}'; E). \tag{12}$$

The self energy can then be shown [22, 23] to play the role of a nonlocal potential that governs the spectrum of overlap functions $\phi_0(\vec{r}\ ) = \langle\Phi_0|a(\vec{r}\ )|\Psi\rangle$ associated with positive-energy elastic scattering states of the $(A+1)$-body system according to the Schrödinger equation

$$-\frac{\nabla_r^2}{2\mu}\phi_0(\vec{r}\ ) + \int \Sigma^\star(\vec{r}, \vec{r}'; E)\ \phi_0(\vec{r}')\ \mathrm{d}^3r' = E\phi_0(\vec{r}\ ), \tag{13}$$

where $\mu = [A/(A+1)]m_N$ is the reduced mass and m_N is the nucleon mass. Hence, $\Sigma^\star(\vec{r}, \vec{r}'; E)$ can be identified with the nucleon–nucleus optical potential as well as providing a similar interpretation for the properties of a removed nucleon [23].

Having briefly reviewed the different formalisms used to derive optical potentials, the rest of the paper is organized as follows. In section 2, we motivate the need for modern optical

potentials to address a wide range of applications from fundamental science discoveries to astrophysics to nuclear energy and security. In section 3, we review recent advances in constructing optical potentials from phenomenological, semi-microscopic and microscopic approaches with emphasis on the nucleon–nucleus potential. We also comment on the use of microscopic optical potentials to inform phenomenology and discuss limitations and model uncertainties of the two-body approximation used in nearly all optical model applications. In section 4, we present new tools and resources to facilitate the propagation of recent (and future) progress in the field of nuclear optical models to experimentalists and practitioners. In section 5, we compare the different approaches presented in this work and discuss their accuracy for different systems. We end with a summary and outlook.

2. Applications of optical potentials

2.1. Direct reactions to probe exotic nuclei

Direct reactions have played a foundational role in the development of our understanding of nuclear structure and will be an essential tool in the FRIB era [24]. In 1950, Butler had already observed that proton angular distributions following the (d, p) reaction yield information about the transferred neutron [25]. The rapid development of reaction theory thereafter, reliant on optical potential models, fostered their use to explore many facets of nuclear structure. More specifically, direct reactions have been instrumental in enriching our knowledge concerning shell evolution, weak binding, pairing, symmetries, deformation and applications to nuclear astrophysics and fundamental symmetries.

In the mid-eighties, the development of radioactive-ion beams (RIBs) and new experimental techniques enabled the study of nuclei away from stability, revealing exotic structures and challenging the usual description of nuclei. In particular, in regions with extreme neutron-to-proton ratios, nuclei exhibit single-particle levels with a non-standard spin-parity ordering, forming the so-called *islands of inversion* [26–28]. Exploring nuclei far from stability helped elucidate mechanisms for shell evolution, such as the ubiquitous action of the tensor force [28, 29]. Even more surprising, halo nuclei can be found close to the drip lines. These nuclei present a strongly clusterized structure, in which one or two loosely-bound nucleons have a high probability of presence far from the rest of the nucleons. With several major facilities around the world now capable of delivering beams of short-lived nuclei at Coulomb barrier energies and beyond, in conjunction with specifically tailored instrumentation, a wealth of direct-reaction data is expected.

In the absence of a universal, fully *ab initio* description of nuclear reactions and their connection to nuclear structure, the theoretical description of the reaction process is often simplified into a few-body one, where both projectile and target can be seen as composed of one or more clusters of nucleons. In this few-body picture, the structure of the nuclei involved in the reaction is described through an effective interaction reproducing properties of the low-energy spectrum of the nuclei while the interactions between the clusters making up the projectile and the target are simulated through optical potentials accounting in an effective fashion for the neglected many-body structure. These cluster-cluster (or nucleus-nucleus) optical potentials generalize the concept of nucleon–nucleus optical potentials. The accuracy of the nuclear-structure information inferred from experimental data is therefore strongly influenced by the reliability of both the optical potential and the few-body reaction model.

Among all nuclear reactions, elastic scattering, in which both the projectile and the target nuclei remain in their ground states and the beam is deflected from its incident direction, constitutes one of the simplest probes. The diffraction pattern of the angular distribution can

be used to infer the size of the nucleus [30]. Resonant elastic scattering is also a powerful tool for exploring isobaric analog resonances with RIBs [31]. The difference between the incoming flux and the elastic one defines the reaction cross section, which corresponds to processes in which the colliding species exchange energy and/or mass. As their magnitude grows with the spatial extension of the projectile, reaction cross sections have played a key role in the discovery of halo nuclei [32, 33].

Inelastic scattering is defined as an excitation of the target and/or the projectile during the collision process. The magnitude of inelastic scattering cross sections provide information about the system's response to nuclear and electromagnetic probes [34], associated with the degree of collectivity of the populated states. A high degree of collectivity is then often associated with the excitation of a rotational band in deformed nuclei, or with vibrations of the nuclear surface—it is anticipated that inelastic scattering will be a powerful complement to Coulomb excitation studies in the FRIB era, especially in probing octupole deformation [35].

Another key nuclear-structure quantity is the Gamow–Teller (GT) strength, which provides an essential connection to nuclear β decays. GT strength distributions are typically probed with charge-exchange reactions in which a proton in a target nucleus is exchanged for a neutron in the projectile nucleus, or vice-versa. Charge-exchange cross sections also provide insights on the isovector densities, i.e. the difference between proton and neutron densities inside the nucleus [36], and play a role in understanding double-β decay nuclear matrix elements [37, 38].

One-nucleon transfer reactions, such as (d, p) and (p, d), at energies a few MeV per nucleon above the Coulomb barrier in both the entrance and exit channels (typically between $\sim$5 and 50 MeV/nucleon, depending on the Q value), are highly selective probes to obtain information about the nuclear response to nucleon addition and removal (single-particle strength) [39–42]. The absolute value of the cross section is proportional to the single-particle content of the populated state, namely the spectroscopic factor, while the shape of the angular partial differential cross section is a strong signature of its orbital angular momentum. The evolution of the single-particle strength along an isotopic/isotonic chain [43, 44] is an ideal tool to explore correlations as a function of neutron–proton asymmetry, in particular as one approaches the nucleon drip lines.

Multiple-nucleon transfer reactions, in which several nucleons are transferred from the projectile to the target and vice-versa, are also commonly used to probe clustering and pairing effects. In particular, α-transfer cross sections for processes such as (^{6}Li, d) carry information about the α clustering inside the nucleus (see, for example, [45]), and can be used to infer reaction rates that are of astrophysical interest (see, for example, [46–49] and section 2.3). Two-nucleon transfer reactions give insights on pairing modes and pairing correlations [50–53]. Quasi-free scattering reactions, mentioned below, which knock out multiple nucleons [54–57] and or clusters of nucleons, e.g. alpha particles [58], can probe similar properties.

The structure of loosely-bound exotic nuclei can also be studied through breakup reactions [59–66] since the counting statistics are high owing to the fragile nature of these nuclei. When performed on heavy targets, the Coulomb repulsion between the projectile's clusters and the target dominates, while on light targets, their nuclear interaction is responsible for most of the breakup cross section. Consequently, the mechanisms driving the dissociation, and hence the properties of the exotic nuclei probed by the reaction, depend strongly on the nature of the target. For example, electromagnetic strength functions and capture rates of astrophysical interest can be extracted from Coulomb-dominated breakup observables [34, 46, 48, 67–72].

Inclusive measurements of one-nucleon breakup at intermediate energies (>50 MeV/nucleon), often referred to as one-nucleon removal, or heavy-ion knockout, reactions [73–76],

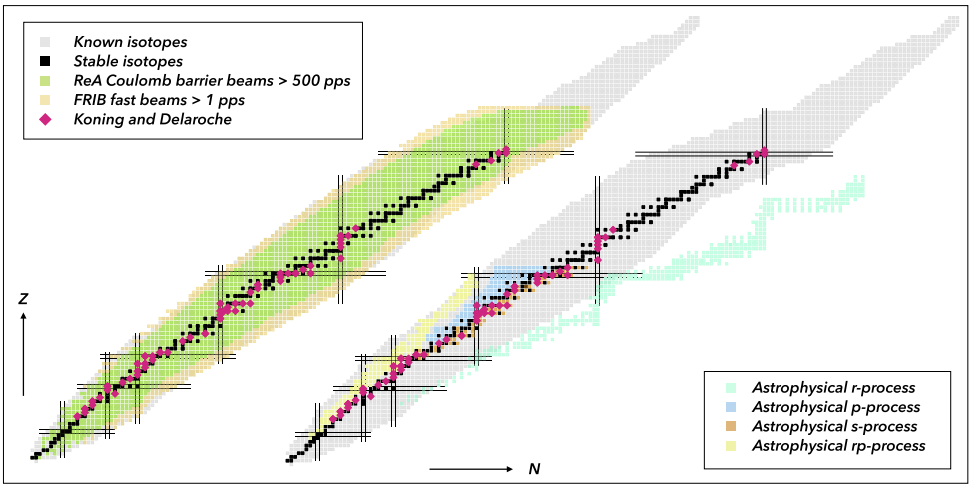

Figure 1. The chart of nuclides showing estimates of the reach of reaccelerated beams at FRIB and 'fast' fragmentation beams at FRIB and the well-known astrophysical processes. Also indicated (pink diamonds) are the nuclei whose properties were used to constrain the Koning and Delaroche optical potential [14], highlighting the dramatic extrapolations made.

have even higher counting statistics because only one fragment is measured after the collision. This type of inclusive reaction typically uses a beryllium or carbon target and is the favored probe for nuclei at the limits of stability for which only low-intensity beams are available. The standard associated observable is the parallel-momentum distribution of the remaining core. It acts as a key probe of the single-particle structure of the projectile, as it carries information on the spin, parity and energy of single-particle states [73, 74, 77, 78]. These reactions have therefore been widely used to study the shell structure evolution across regions of the nuclear chart, i.e. from stable to exotic nuclei at the drip lines. An open question in the field has been raised by such studies, relating to the nucleon asymmetry dependence of the quenching of cross sections on the difference between proton and neutron separation energies [79–81]. This issue ties together many of the direct-reaction probes mentioned in this section (see recent review in [82] and references therein).

Quasifree $(p, 2p)$ and (p, pn) scattering reactions are also a key probe of the single-particle degrees of freedom of exotic nuclei [83–85]. Contrary to one-nucleon removal reactions and transfer, quasifree scattering probes the inner part of the single-particle wave function. This is a consequence of the high energies at which these measurements are performed (typically above 200 MeV/nucleon).

To interpret reaction measurements, to arrive at a more fundamental understanding of the nuclear structure and reactions, and plan new experiments, it is crucial to develop accurate reaction models coupled with realistic interactions between the relevant nuclei. In the context of the direct reactions discussed here, optical potentials are responsible for most of the uncertainties beyond the description of the bound states [86]. Historically, optical potentials have been fitted to elastic-scattering data on stable targets. Thus, these interactions are not well constrained for exotic nuclei. Figure 1 illustrates the nuclei used to derive the Koning and Delaroche [14] optical model parametrization (pink diamonds), overlaid on the beams expected to be available at FRIB, both for reaccelerated (Coulomb barrier) beams of >100 particles per second (pps) and for 'fast' beams of >1 pps. Juxtaposed, figure 1 also

contains the regions of the nuclear chart relevant for the various astrophysical processes. Direct reactions involving these nuclei can be used to extract astrophysical rates [46, 48, 49]. It is clear that, in the FRIB era, using current phenomenological optical potentials carries tremendous uncertainties when extrapolating to the driplines.

In order to enhance the accuracy of our predictions concerning the reactions to be measured at FRIB, and to provide the associated quantified uncertainties, there is an urgent need for developing optical potentials across the whole nuclear chart at energies ranging from a few MeV up to 400 MeV. These next-generation interactions should include more physics constraints in order to reliably cover the variety of reactions to be studied at FRIB and ultimately provide a comprehensive and accurate account of exotic nuclei.

2.2. Compound-nuclear reactions

Compound-nuclear reactions play an important role in nuclear physics and in applications. Their cross sections are the required input for astrophysical simulations that describe stellar evolution and nucleosynthesis and for modeling processes that are relevant to medical isotope production, national security applications, and generating energy.

In a compound-nuclear reaction, a projectile fuses with a target to produce a highly-excited intermediate nuclear system which equilibrates and subsequently decays by particle evaporation, fission, or gamma emission. Compound reactions are very slow; at very low energies they produce narrow, isolated resonances and can be described in the framework of the *R*-matrix formalism [87]. With increasing projectile energy, the resonances begin to overlap, forming the unresolved-resonance region (URR) and, at even higher energies, one enters a region in which the statistical Hauser–Feshbach (HF) formalism is applicable [88]. The demarcation between the various regimes depends on the projectile type and on the structure of the compound nucleus (CN) formed. For reactions involving well-deformed nuclei with large level densities (e.g. n+^{155}Gd), the region of strongly overlapping resonances lies at much lower energies than for reactions involving nuclei near closed shell (e.g. n+^{208}Pb), see figure 2.

The HF formalism describes the average cross section for forming a CN at energy E_{ex} by fusing projectile a and target A (channel α) and subsequent decay into reaction products c and C (channel χ)

$$\sigma_{\alpha\chi}(E) = \sum_{J\pi} \sigma_{\alpha}^{CN}(E_{ex}, J, \pi) G_{\chi}^{CN}(E_{ex}, J, \pi) W_{\alpha\chi}(E_{ex}, J, \pi). \tag{14}$$

Here $\sigma_{\alpha}^{CN}(E_{ex}, J, \pi)$ is the CN formation cross section for the α channel. The quantities $G_{\chi}^{CN}(E_{ex}, J, \pi)$ describe the competition between the decay channel of interest (χ) and all other competing channels. Calculating G_{χ}^{CN} requires nuclear structure information, such as gamma-ray strength functions, fission barriers, and level densities [15]. These are traditionally written in terms of products of transmission coefficients (TCs) and level densities (in the residual nuclei). The TC for gamma emission is related to the gamma-ray strength function, the TC for fission describes tunneling through fission barriers. All other TCs describe the probability for particles to be emitted from the CN and are obtained from a potential-model or coupled-channels calculation that uses a nucleon–nucleus optical potential: $T_{\beta} = 1 - |S_{\beta\beta}^{\rm opt}|^2$, where $S_{\beta\beta}^{\rm opt}$ denotes the optical-model S-matrix, that can be obtained from projecting out all non-elastic channels coupled in the calculation.

Equation (14) above also contains a width fluctuation correction factor, $W_{\alpha\chi}(E_{ex}, J, \pi)$, which accounts for remnant correlations between the incoming and outgoing channels [90]. It is a reminder that the reaction cannot be completely separated into two independent processes.

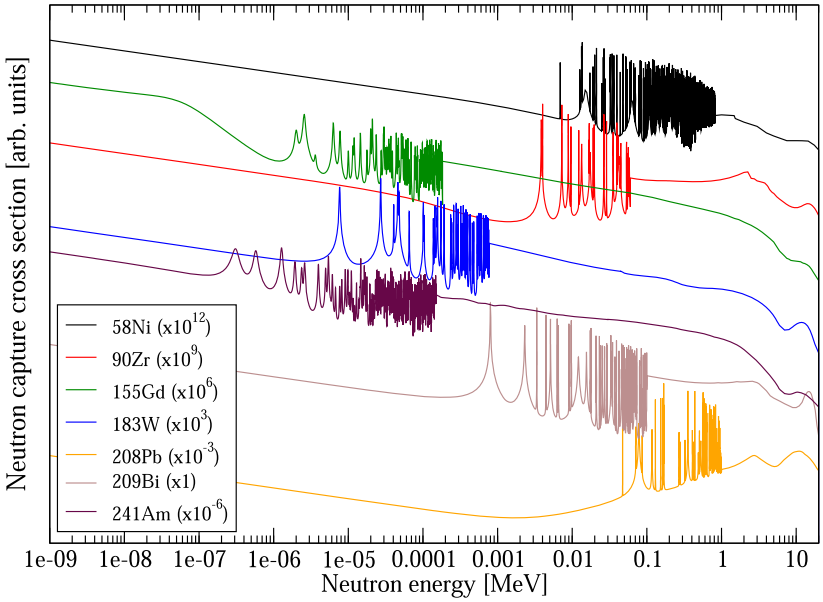

Figure 2. Evaluated neutron capture cross sections for various stable targets [89]. The depicted evaluations are based on a combination of calculations and measured data (not shown) and illustrate the different energy regimes: resolved resonance region (RRR) at lower energy where individual resonances can be distinguished, unresolved resonance region (URR) at intermediate energy where resonance peaks are still visible but overlapping, Hauser–Feshbach (HF) regime at higher energy where the cross section has a smooth dependence on energy, representing an average over strongly overlapping resonances. The high-energy behavior of the cross sections can be described in an average way using the HF formalism.

Similarly, in most realistic cases (and in all nuclear reaction evaluations) there are additional, non-compound, reaction processes that have to be accounted for when describing reaction observables. For that reason, statistical reaction codes have capabilities well beyond the evaluation of the HF expression. They include descriptions for direct reactions, pre-equilibrium reactions, as well as CN reactions. As detailed in section 2.1, the description of direct-reaction observables, in turn, requires OMPs. Statistical reaction codes also typically contain subroutines or auxiliary codes to generate transmission coefficients using OMPs. In addition, they need nuclear structure information—most modern ones can read this from databases, such as the Reference Input Parameter Library (RIPL-3) [15]. Much work has been devoted to improving statistical reaction calculations. Nuclear structure inputs have received much attention over the past two decades, with multiple theoretical and experimental efforts aimed at providing more reliable inputs for gamma-ray strength functions and nuclear level densities in particular (see [91–95] and references therein).

Similarly, a large number of optical potentials have been made available for use with statistical reaction codes [15]. This includes phenomenological nucleon–nucleus potentials, such as the spherical potential by Koning and Delaroche [14], the semi-microscopic nucleon–nucleus potential by Bauge *et al* [96–98], and the dispersive nucleon–nucleus potential by Morillon and Romain [99]. For deformed nuclei, the relevant nucleon–nucleus transmission coefficients are generated using coupled-channels calculations. Multiple efforts have focused on developing appropriate coupling schemes and requisite potentials [100–102]. To describe

fusion or emission of composite particles, optical potentials for light ions (t, ^{3}He, α, etc) are required. These tend to have larger uncertainties, as there is less available data to place constraints on the shapes and parameters of those potentials.

As they take various inputs, statistical reaction calculations are affected by multiple sources of uncertainty: nuclear-structure information for the various possible decay channels may be lacking, some reaction mechanisms, e.g. pre-equilibrium contributions, are not sufficiently well-known and optical model uncertainties also affect the predicted cross sections. Calculations for neutron-induced reactions on actinides are known to be sensitive to the coupled-channels optical potential utilized [101, 102].

Level densities can be estimated by extrapolating from known discrete levels, and (ideally) by measuring resonances in the interaction of two subsystems of the nucleus. Much better physical accuracy is possible if an optical potential is known for the scattering of those two subsystems. That is because we can simplify R-matrix theory when we can ignore interferences between resonances, and convert an average-ratio of widths to a ratio of average widths $\langle\Gamma\rangle$. Then the ratio of average width reads

$$\frac{\langle\Gamma\rangle}{D} = \frac{T_\beta}{2\pi}, \tag{15}$$

where D is the average level spacing. The transmission coefficient T_β comes from the S-matrix element for optical-model scattering, as explained above. Thus, given level densities and optical potentials we can estimate average widths. These estimates are the basis of the HF model of statistical reactions and decays that uses Porter–Thomas [103] distributions with these statistical averages and also neglects interference between resonances.

These approximations should be tested to gauge the accuracy of the HF model. Much work has gone into improving the average-ratio approximation, and now width fluctuation corrections (WFC) are standard in HF models [104]. The neglect of interference still needs to be tested but should be reasonable for angle-integrated data if not for angular distributions. Improvements have also been given by Simonius [105] to equation (15) when the widths are large, since the transmission coefficient has a maximum value of one.

One overall test of all these approximations is to derive the resonance parameters for a typical HF model using the common approximations, and then see whether a full R-matrix calculation with those parameters gives the HF predictions. The results of such a comparison for $n + {}^{14}$N elastic, inelastic and transfer reactions have been recently calculated. Figure 3 shows the ^{14}N(n, α) cross sections as a function of neutron energy. We see that, as might be expected, the best HF calculation (HF with WFC: the solid black line) is closest to the best R-matrix statistical model (Ap: the solid blue line). The agreement is not perfect and this is only a comparison between models, but it gives hope that, around the unresolved resonance region, there is a domain where the R-matrix resonance treatment can match up with the HF statistical treatment. This should help to constrain both the resonance parameters and optical potentials in the two regimes.

It is instructive to briefly focus on specific ways that observables may inform optical potential development and vice-versa. The connection between experiment and theory is, of course, facilitated via interpretative or predictive calculations. In the rest of this section, we will spotlight some examples of information exchange between experiment and theory. Nuclear reaction yields are related to optical potentials through the transmission coefficients discussed above. The shapes of the angular distributions of emitted particles are observables that theoretical calculations can reproduce. Typically, the transmission coefficients for the emitted particles will need to be modified to precisely fit the experimental data. The new experimentally constrained transmission coefficients will correspond to a new set of optical

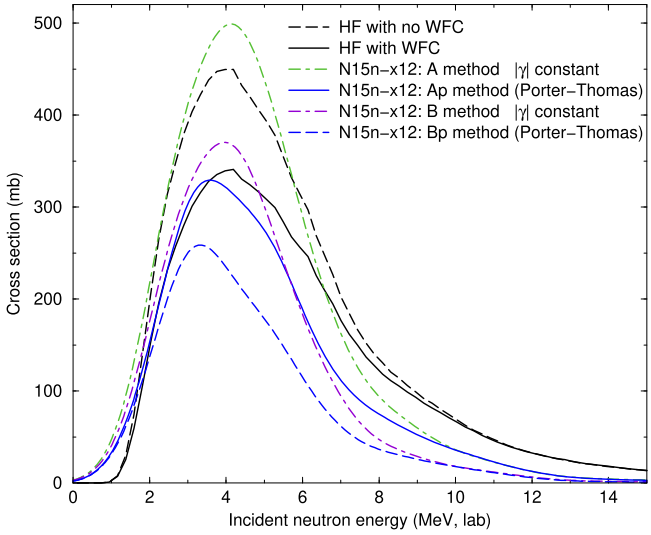

Figure 3. ^{14}N(n, α) cross sections as a function of neutron energy. The HF curves are standard Hauser–Feshbach calculations, without and with the width fluctuation corrections (WFC). The A curves follow Simonius [105] and the B curves are the linear approximation given in the text. The Ap and Bp curves use the standard Porter–Thomas statistical distributions [103] for the *R*-matrix parameters, while A and B curves have fixed amplitude sizes but random signs.

potential parameters that are now phenomenologically constrained and available for future calculations. These new parameters, locally fitted as they are, do not necessarily carry any predictive value away from the vicinity of the target nucleus considered. This shortcoming is becoming quite an issue for nuclear astrophysics applications in which a theoretical prediction is, for most participating nuclei, the only possible way to determine the thermonuclear reaction rates of interest (see e.g. figure 1). A second way to inform nuclear theory from experimental data is by reproducing evaporation spectra from highly excited compound nuclei. While the so-called evaporation technique [106] is typically suitable for determining the level densities of the excited compound systems, recently, it has been demonstrated in the literature [107] that the evaporated particle spectra can also provide some insight into optical potential properties.

Beam time at premier experimental facilities such as FRIB is very expensive and the number of available hours at large-scale radioactive ion beam facilities is often limited. This raises the degree of importance placed on high-quality, reliable, and accurate simulations to support the value of the proposed experiment. Optical potentials are necessary ingredients of any such simulation or theoretical prediction. The value of such predicted cross sections is profound for astrophysics applications involving thousands of species away from stability (for example for r-process or i-process nucleosynthesis). Typically predictions are collected into reaction rate libraries like the widely used JINA REACLIB [108]. An improved optical potential thus can influence fields beyond nuclear physics that make use of such libraries. Lastly, theoretical cross section calculations are typically collected into databases (e.g. TENDL [109]) that are available for use with various simulation tools such as GEANT4 [110] and MCNP [111] that are broadly utilized by experimentalists to optimize their instrumentation and interpret raw data.

2.3. Astrophysically relevant reactions

Another area in which optical potentials are ubiquitous is nucleosynthesis. Astrophysical modelling for a wide range of astrophysical sites requires large network of reactions. These cannot all be measured, and instead, models use global optical potentials for the task. In some scenarios, the reaction rates are needed away from stability, and typically the existing parametrizations are extrapolated without an estimate of uncertainties (as alluded above). In this section, we discuss a few examples to illustrate the ways in which a global optical potential, with quantified uncertainties and valid away from stability, can benefit the field.

First, we consider neutron capture reaction rates with medium mass and heavy nuclei away from stability. These are thought to be responsible for synthesizing the majority of elements heavier than iron in the Universe through the so-called rapid neutron capture process (r-process). The nucleosynthetic path of the r-process involves isotopes that are very neutron-rich and are located closer to the neutron dripline than the valley of stability, where the optical potential has been more thoroughly tested and constrained (see figure 1). The standard optical potential parametrization suggested by Bohr and Mottelson takes into account the large neutron–proton asymmetry away from stability through an isospin-dependent isovector term

$$U_{\rm iso} = \frac{1}{2}\, t_z\, \delta\, U_{\rm sym}, \tag{16}$$

where t_z is the nucleon isospin component, $\delta = (N - Z)/A$ and $U_{\rm sym}$ is the so-called symmetry potential.

The symmetry potential is currently under active research investigation. Phenomenological and semi-microscopic optical model parametrizations adjust the imaginary potential to agree with experimental data [107]. It has been already suggested in 2007 [112] and recently corroborated by experimental evidence [107] that the isovector component, constrained by data near stability, does not adequately reproduce the effect of the neutron–proton asymmetry that exists in nature. More experimental data and theoretical investigations are needed to quantify this deficiency of modern theories. Still, the above works suggest a significant effect on neutron captures relevant to the r-process but also on the less neutron-rich nuclei near stability that may be of interest to nucleosynthesis occurring under conditions with lower temperatures and neutron densities compared to the r-process, such as the i-process.

Significant as the effect of neutron excess may be, current theory does not appear to be sensitive to it. Reaction rate calculations with the typically-used optical potentials developed by Koning and Delaroche (KD) [14] and by Jeukenne, Lejeune and Mahaux (JLM) [113, 114] produce very similar results even though the latter one is based on a microscopic calculation. In figure 4, a number of neutron capture rate calculations using the two potentials are shown for Fe, Mn, Co, and Ni isotopes spanning from stability up to several neutrons towards the dripline. Despite the increasing neutron excess, the calculations reproduce a smooth change with neutron number. The difference between the reaction rates computed with KD and JLM decreases for increasing A, suggesting that no difference in the treatment of neutron excess exists between the semi-microscopic and the phenomenological potential away from stability. While we tested only two examples, there is no reason to assume that other potentials based on similar phenomenological approaches would behave differently with increasing neutron excess unless the theoretical description of the effect of neutron–proton asymmetry is fundamentally improved.

Nucleosynthesis in massive stars and in the proton-rich regions predicted to occur in neutrino-driven winds during core-collapse supernovae involves rates of (n, p) and (n, α) reactions at temperatures from approximately 1 GK down to hundreds of MK. In addition, photodisintegration

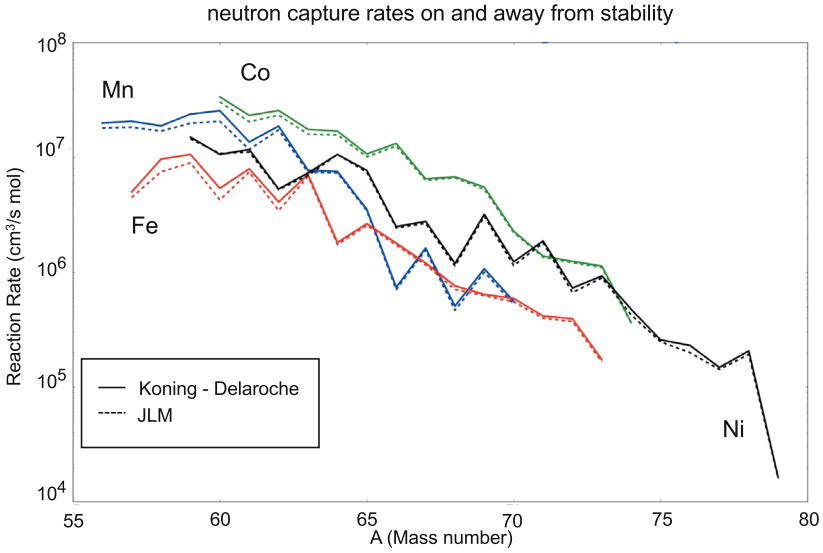

Figure 4. Neutron capture rate calculations using the Koning–Delaroche and JLM optical potentials for Fe, Mn, Co, and Ni isotopes far away from stability. Despite the increasing neutron excess, the calculations produce a smooth change with neutron number. Moreover, the resulting reaction rates are in increasingly better agreement with each other as the neutron number increases, suggesting that, if anything, the semi-microscopic JLM potential converges to the phenomenological Koning–Delaroche potential for neutron-rich nuclei. This suggests that there is no meaningful benefit in using the JLM potential compared to the KD one away from stability.

reactions (γ, p) and (γ, α) contribute to the production of the so-called p-nuclei, a class of isotopes shielded from the neutron-induced nucleosynthesis processes [115, 116]. Unfortunately, data in the astrophysically-interesting region below 1 MeV are sparse and of lower precision. At the same time, the focus of most evaluated neutron reaction data libraries is in the broader region of 0–20 MeV, and this energy range translates to very few data at energies below 1 MeV. The fine details of the cross section at these low energies, which can influence strongly nucleosynthesis calculations, are therefore often not included. The accurate determination of these reactions rates requires quantitative and predictive nucleon–nucleus optical potentials at energies reaching way below 1 MeV.

We should also note the central role optical potentials play in sensitivity studies, particularly those involving nuclei away from stability. These are essential tools for nuclear astrophysics that guide the experimental and modeling efforts [117]. Typically, a sensitivity study involves calculating the same astrophysics ensemble multiple times, each time changing the value of a 'parameter' that enters the calculation and recording how the results of the calculation change. In nuclear astrophysics, the most common 'parameters' modified are the values of *individual reaction rates* (see for example [118]). Ideally, reaction rates should change systematically, connecting with the uncertainties of the underlying theory. An example of such a calculation using the currently available optical potentials is shown in figure 5 for proton-rich unstable nuclei relevant Reprinted (figure) with permission from [170], Copyright (2018) by the American Physical Society.for the ν-p process in supernovae. One can note in figure 5 that these uncertainties are not smooth in mass numbers and in isospin asymmetry.

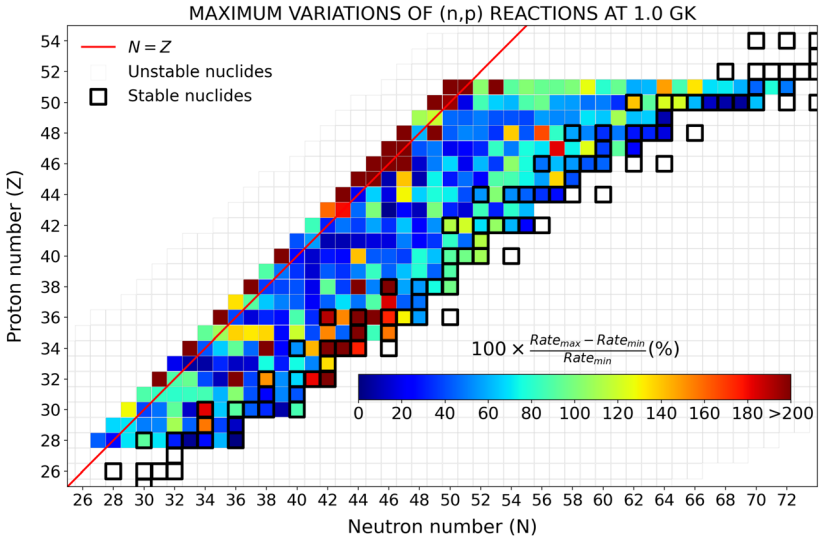

Figure 5. Maximum variation of the reaction rates at 1 GK for (n, p) reactions with isotopes relevant to the neutrino-p process when the JLM scaling parameters λ_x are varied within the estimated valid range.

Such sensitivity studies are based on the assumption that the uncertainty of the varied parameters is known to some reasonable degree in order for the result to be valuable. To perform useful sensitivity studies, we need optical potentials that reproduce the changing nuclear structure away from stability and have well-quantified uncertainties.

Although so far we have focused on nucleon–nucleus optical potentials, astrophysics also has a dire need for global optical potentials on light ions, particularly α-nucleus optical potentials. There are many α-induced reactions relevant for nuclear astrophysics due to the heavy abundance of helium in the Universe after the Big Bang. Chemical elements above ^{56}Fe are formed either via the slow neutron capture process (s-process) or through the rapid neutron capture process (r-process). The main neutron sources for the s-process occurring in asymptotic giant branch stars are (α, n) reactions on heavy nuclei such as ^{13}C and ^{22}Ne. In proton-rich explosive stellar environments such as novae and x-ray bursts, the dominant nucleosynthesis (p, γ) reaction sequence is halted at several waiting point nuclei due to low (p, γ) reaction Q-values resulting in a (p, γ)-(γ, p) equilibrium. α-capture on these waiting point nuclei allows the nucleosynthesis of heavier nuclei via the 'αp-process', a sequence of (α, p) reactions followed by (p, γ) proton captures, which eventually leads to the successive proton captures in the rapid proton capture process (*rp*-process) to synthesize heavier proton-rich nuclei.

To effectively explain the observed abundances of chemical elements from such stellar environments and nucleosynthesis processes, accurate stellar models are required. These models require nuclear input parameters such as nuclear masses and reaction rates [118–121]. At present, many of the astrophysically-relevant (α, γ), (α, n), and (α, p) reaction rates have not been experimentally constrained within relevant Gamow energies, where measurements are hindered by low counting rates. The reaction cross sections of relevant α-induced reactions are instead deduced using HF statistical model calculations.

Statistical HF calculations for α-induced reactions require a robust set of α-OMPs. Throughout the years, there have been various efforts to determine such OMPs [122–125].

These OMPs are determined by fitting available elastic-scattering angular distribution data. Compared to the amount of scattering data currently available for neutrons, protons and deuterons, the amount of available α scattering data are rather sparse, specially for nuclei further away from stability. This is generally the case for $A = 3$ and $A = 4$ projectiles compared to neutrons/protons. Additionally, elastic scattering data are generally obtained for higher energies due to the influence of the Coulomb barrier. The α-OMPs by Avrigeanu *et al* [124, 125] has been derived using α scattering data for target atomic masses ranging from 45 to 209. The McFadden and Satchler α-OMPs [122] have recently been shown to agree with available experimental data within a factor of $\sim$2 for target atomic masses $A = 20 - 50$ [126]. While these α-OMPs can reasonably reproduce experimental reaction cross sections for certain target masses and energies, for experimentally-inaccessible regions of the nuclei chart, they can introduce significant uncertainties for the deduced reaction rates affecting various nucleosynthesis calculations. In order to overcome these difficulties, a cohesive effort by the nuclear physics community is desired to obtain more scattering data which would aid in significantly improving the nucleon-, deuteron- and α-OMPs for more accurate theoretical reaction rate calculations.

2.4. Nuclear data for energy, security, medical, and other applications

A predictive theoretical capability of total, elastic and reaction cross sections is vital for a wide range of applications [127]. Improved optical potential calculations enable sophisticated modeling and guide the experimental efforts necessary to advance the technology readiness level within a given application. Below, we list several specific areas in which more comprehensive and reliable optical potentials would have significant impact.

2.4.1. Energy and security applications. Most energy and security applications require high-quality evaluated cross sections for neutron-induced reactions up to 20–30 MeV, such as those present in evaluated nuclear data libraries like ENDF/B-VIII.0 [128]. The highest-priority targets are actinides and structural/engineering materials. High-quality optical models provide the starting point for reliable descriptions of reactions needed for modern comprehensive evaluations of neutron induced reactions (e.g. see a recent evaluation of U-238 and U-235 neutron induced reactions [129] adopted into the ENDF/B-VIII.0 library [128]). Because of the high societal impact of these applications, many (but not all) relevant cross sections have been thoroughly examined, and sophisticated uncertainty quantification techniques developed and applied [130–132]. The extensive high-quality experimental data collected to inform the relevant cross sections mean that phenomenological models are in their range of validity, provided sufficient physics—such as selection of the appropriate reaction model and detailed structural information—are considered.

There are still needs for OMP development for materials used in next-generation reactor architectures. In some designs such as those involving molten salts, potentials are needed for isotopes beyond typical structural materials and actinides. Experimental data suitable for improving a phenomenological potential on these isotopes are not always available, especially because the bulk of single-nucleon scattering measurements were conducted more than thirty years ago. Also relevant are reactions on light elements which are important both in their own right and because they can provide important constraints on reverse reactions that are difficult to access experimentally but important for neutron economy (e.g. ^{16}O(n, α)^{13}C to improve knowledge of ^{13}C(α, n)^{16}O or vice-versa).

2.4.2. Medical applications. An important application is the production of isotopes used in medical diagnosis and treatment [133]. The two major methods for isotope production are (1) reactor-based fission, capture, and (n, p) reactions and (2) charged-particle-induced reactions using fast charged-particle and/or neutron beams [134–136]. For reactor-based isotope production, neutron-induced reaction cross sections similar to those in the energy and security applications are important, so there can be significant overlap in the theoretical and experimental tools needed to constrain these cross sections [135]. For charged-particle-induced reactions, much higher energies are required: up to tens of MeV in commercial cyclotrons such as those found in hospital settings, and up to hundreds of MeV for dedicated accelerator facilities such as Los Alamos Neutron Science Center (LANSCE).

Isotope production requires not only nuclear physics information which can be partially obtained via an optical model, but also efficient chemical separation techniques that allow the produced isotope to be extracted. As such, the most important reactions are those that change the number of protons and thus the chemistry of the target, facilitating chemical separation and increasing the specific activity of the product. For charged-particle beams, the charge-exchange reactions (p, xn), (d, xn), (α, xn) are the most important [137–141]. In a similar vein, the most important neutron-induced reactions in the reactor-based setting are (n, p), fission, or multi-step reactions with subsequent β- or α-decay, yielding a change in element of the reaction products [135]. In some cases a direct production of the parent radionuclide is feasible (e.g. ^{100}Mo (n, $2n$) reaction is used to produce ^{99}Mo parent for production of the very important ^{99}Tc generators) [139]. In each of these cases, secondary particle reactions often contribute significantly to reaction yields, compounding the importance of proper reaction modelling to consider all relevant channels. Because of the inherently complicated nature of these reactions, it should be noted that the OMP provides only the first ingredient required for reliable predictions of the needed cross sections, and that additional information—such as from a statistical reaction and pre-equilibrium model—is essential. As currently-available OMPs have been developed to describe p, n, d, or α scattering, several OMPs across a wide range of energies may be needed simultaneously to describe secondary particle production and follow-on reactions [15].

A further medical application is radiotherapy, where cross section information at energies up to 250 MeV/nucleons are important. For example, in a proton radiotherapy procedure, the dose delivered in the beam entrance region (before the Bragg peak) depends heavily on the elastic scattering of protons on tissue, which is one of the easiest quantities to cleanly predict using a suitable OMP and reaction code. However, this information must be combined with atomic and radiological data that are often absent or highly uncertain. As is the case in compound nuclear reactions that combine nuclear structure and OMP information, knowing the relative uncertainty of the OMP versus other reservoirs of uncertainty (e.g. atomic data) can help focus efforts on reducing the most impactful uncertainties first. There are also important quantities that the OMP cannot fully inform, for example, activation data or the production cross section for positron-emitting radionuclides (e.g. ^{11}C). As uncertainty quantification is still developing for many other types of physics data entering medical and energy/security applications, better OMP uncertainty assessments can potentially provide a methodological guidepost for other fields.

2.4.3. Space applications. The interaction of radiation with space-based systems is important to understand for both national security and industry. Radiation shielding in space is a balance between maximizing protection and minimizing the amount of shielding material, as there is a strong cost motivation to minimize the overall weight of the system [142]. In addition, radiation effects on electronic systems are often difficult to directly study in

space-like environments [143]. Relevant models for both these cases often lack experimental data [142]. Much like in other applications outlined above, secondary particle production contributes significantly to the relevant doses. Knowledge of neutron production from proton-induced reactions is very important and double-differential cross sections of produced neutrons may be needed. In addition, gamma rays produced by inelastic scattering can potentially have a large impact on overall dose delivered to a space-based system (for example, an electronics circuit) by incoming neutrons [143]. Given that these reaction cross sections are often poorly known, predictive and uncertainty-quantified OMPs, in concert with other theoretical inputs, can have a significant impact. In particular, a recent survey of nuclear data needs for space radiation protection has identified significant shortcomings in experimental data [144]. Previous work has been done using optical models to predict nuclear fragmentation processes relevant for space applications [145, 146].

3. Review of strategies to build nucleon–nucleus optical potentials

3.1. Standard and dispersive phenomenological approaches

3.1.1. Standard optical potentials. Early developments of optical potentials sought to describe single-nucleon cross sections phenomenologically, using a local, complex, one-body potential (1)–(2) with parameters varying smoothly in E and A, analogous to the refractive index for an absorptive medium. By the 1960s, enough cross section data had been collected to contemplate training a 'global' optical potential suitable for predicting elastic scattering cross sections across a broad range of nuclei and energies, with Becchetti and Greenlees the first to do so [12]. Increases in computational power and the size of experimental databases led to potentials with a growing number of free parameters and better empirical performance, including the spherical CH89 [13] ($40 \leqslant A$, $10 \leqslant E \leqslant 65$ MeV) and the Koning and Delaroche [14] ($24 \leqslant A \leqslant 209$, 1 keV $\leqslant E \leqslant 200$ MeV) potentials, which remain widely used. Most recent phenomenological efforts include additional physics, such as enforcing dispersivity, including non-locality, and/or describing deformation via a coupled-channels approach, each of which can improve the accuracy needed for applications [15]. To simplify interpretation in terms of nuclear asymmetry, many single-nucleon potentials adopt a Lane-consistent form where the OMP is partitioned into isoscalar and isovector components so that the neutron and proton OMPs differ only by a change in sign of the asymmetry-dependent components [98, 147]. Besides the high-visilibity global efforts, over the decades many hundreds of experimental papers have included isotope- or region-specific optical-potential analyses to assess the impact of their newly collected data (for example, [148]). However, the basic formula for developing a phenomenological OMP remains essentially unchanged since the 1950s: select a suitable collection of functional forms dependent on A, E, and/or δ, compile experimental scattering data, predict reaction observables given an OMP, and optimize OMP parameters according to χ^2 minimization.

As an example, consider the Koning–Delaroche OMP [14], one of the most widely used OMPs since its introduction in 2003. The nominal range of validity in energy is 1 keV to 200 MeV. Both global and several local versions are available, spanning near-spherical systems with $24 \leqslant A \leqslant 209$. To train the OMP, the authors used hundreds of proton and neutron differential elastic scattering and analyzing power data sets from $27 \leqslant A \leqslant 209$ collected from the 1950s to the 1990s, as well as proton reaction cross section data and neutron total cross section data on natural and isotopic targets. The potential itself includes six subterms with Woods–Saxon-like radial dependence separated from their energy dependence, with a total of forty-six free parameters. Optimization was done using a combination of 'computational steering' and χ^2 minimization, whereby a user manually guided potential

parameters until predicted cross sections were visually close to experimental values, then invoked a simulated annealing algorithm to find a parameter-vector optimum. The success of the KD global OMP in reproducing its training data, particularly the elastic-scattering angular distributions and neutron total cross sections above the resolved-resonance region, as well as its ease of use, have led to its widespread adoption as a default OMP in reaction codes such as TALYS [149, 150] and Finite Range with Exact Strong COuplings (FRESCO) [151].

There are limitations of this approach that are discussed in more detail in section 3.3.

3.1.2. Dispersive optical potentials. The Dispersive Optical Model (DOM), first introduced by Mahaux and Sartor [8–10], is an optical model which makes use of a dispersion relation (4) that relates the imaginary part of the potential to its real part over all energies. Equation (4) is a very powerful constraint that provides a variety of advantages over non-dispersive optical models, helping to reduce the number of model parameters (e.g. see [152]) and to achieve a better description of neutron-induced cross sections for energies below $\sim$5 MeV [153] compared to traditional OMPs like Koning–Delaroche [14]. Dispersion integrals given by equation (4) can be solved numerically [154] or analytically for selected imaginary potentials [10, 155, 156]. Several different dispersive OMPs have been derived (starting from equation (4)) for a variety of use-cases. One class of dispersive OMPs was derived to describe deformed nuclei assuming a rigid-rotor structure like Rh, Au, W, Ta, Hf and actinides [157–159]. Another was derived for spherical nuclei that are soft relative to vibrations assuming a soft-rotator structure like Fe, Ni, Cr [160] and Zr [15]. Yet another class of dispersive coupled-channel potentials has been used to describe both elastic and inelastic scattering data in a broad energy range up to 200 MeV. These derived dispersive OMPs [101, 161–163] have been shown to be approximately Lane consistent, i.e., the same OMP holds for incident neutrons and protons [164, 165] and the parametrization becomes isospin dependent. The dispersion relation has also been used to provide a consistent description of both bound and scattering data in spherical nuclei [11, 166] in some cases allowing 'data-driven' extrapolations to the drip lines [167, 168].

We now briefly discuss efforts that augment the data set constraining the OMP to negative energies by taking in structure information (charge density, energy levels, particle number, etc), in addition to the elastic-scattering data corresponding to positive energies. As mentioned in the Introduction, the optical potential can be interpreted as the irreducible self-energy $\Sigma^{\star}(r, r'; E)$, in the Green's function formalism. Moreover, $\Sigma^{\star}(r, r'; E)$ generalizes the exact nucleon–nucleus optical potential of Feshbach to include both bound and scattering states (a more detailed discussion can be found in section 3.2.2). Connecting the optical potential to the Green's function, along with utilizing the dispersion relation in equation (4), allows for a complete description of the nucleus over both the positive- and negative-energy domains [11, 166]. Adjusting OMP parameters to describe data using equation (4) guarantees that the irreducible self-energy stays well-defined [169, 170]. Currently, there are DOM fits using this Green's function formalism for spherical targets ^{16,18}O, ^{40,48}Ca, ^{58,65}Ni, ^{112,124}Sn, and ^{208}Pb for $-200\,\text{MeV} < E < 200\,\text{MeV}$ [169–172]. In principle, a dispersive optical potential can be applied in the same mass-number and energy range as a typical non-dispersive potential (such as KD) can. Work is currently underway to implement a global parametrization of a fully-dispersive optical potential for spherical targets [173].

Noting that Hartree–Fock potentials are already inherently nonlocal, it was demonstrated that spatial nonlocality of the self-energy including its imaginary part must be treated explicitly in order to describe properties below the Fermi energy [166]. To satisfy the dispersion relation in equation (4), it is at present assumed that the energy dependence of the imaginary part is the same for all spatial coordinates, which simplifies the numerical effort. Typically, optical potentials approximate the spatial nonlocality with an energy

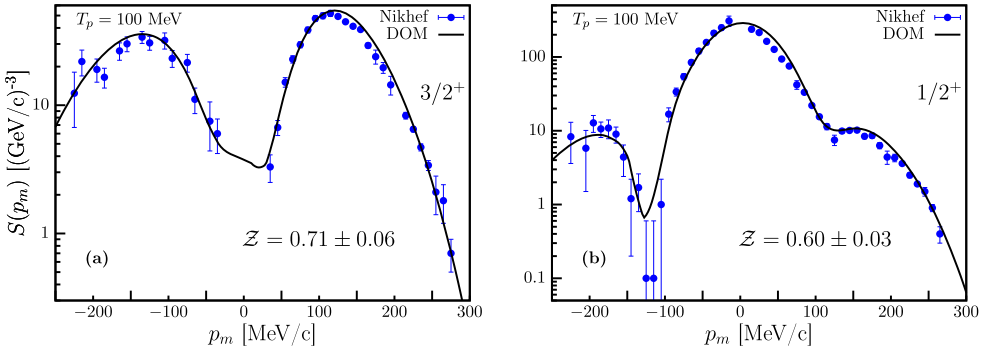

Figure 6. ^{40}Ca(e, $e'p$)^{39}K spectral functions in parallel kinematics, at an outgoing proton kinetic energy of 100 MeV. The solid line is the calculation using the DOM ingredients, while the points are from the experiment detailed in [179]. (a) Distribution for the removal of the $0d\frac{3}{2}$. The curve contains the DWIA for the $3/2^+$ ground state including a spectroscopic factor of 0.71. (b) Distribution for the removal of the $1s\frac{1}{2}$ proton with a spectroscopic factor of 0.60 for the $1/2^+$ excited state at 2.522 MeV. The figure is adapted from figure 5 of [170]. Reprinted with permission from [170], Copyright (2018) by the American Physical Society.

dependence [5]. However, this added energy dependence does not satisfy the dispersion relation, which would lead to an incorrect description of the negative-energy observables. Thus, the spatial nonlocality is treated explicitly with the so-called Perey–Buck form [5]

$$\mathcal{U}(\vec{r}, \vec{r}'; E) = U\left(\frac{r + r'}{2}; E\right) \mathrm{e}^{-\frac{(\vec{r}-\vec{r}')^2}{\beta^2}} \pi^{-3/2} \beta^{-3}, \tag{17}$$

where β is a nonlocality parameter which controls how much strength is distributed off the diagonal. It is worth noting that the functional form in equation (17) is chosen out of convenience, but is capable to represent essential features of microscopic potentials [174, 175]. With this treatment of the nonlocality, along with the dispersion relation in its subtracted form, quantities such as particle numbers, charge densities, and ground-state binding energies are included in the DOM fit. This allows for data-informed predictions of quantities such as the neutron skin of ^{48}Ca and ^{208}Pb (see [169, 171, 172, 176] for more details).

The ability to describe both bound and scattering states of a nucleus is particularly useful in the description of stripping, transfer and knockout reactions needed to fully utilize FRIB [177, 178]. As a specific example, we briefly present the DOM calculation of ^{40}Ca (e, $e'p$)^{39}K cross sections [170]. This reaction, measured at NIKHEF [179], can be described using a distorted-wave impulse approximation (DWIA), which assumes that the virtual photon exchanged by the electron couples to the same proton that is detected and that the final-state interaction can be described using an optical potential [180, 181]. The ingredients of the DWIA therefore require a distorted wave describing the outgoing proton at the appropriate energy and an overlap function for the removed proton and its associated spectroscopic factor. The DOM allows for a consistent DWIA analysis in that the bound state wave function, spectroscopic factor, and outgoing proton distorted wave can all be provided from the same self-energy. The resulting momentum distributions, shown in figure 6, came straight from the DOM self-energy—the ^{40}Ca(e, $e'p$)^{39}K data was not used in the DOM fit. The spectroscopic factors coming directly from the DOM self-energy show a good description of the data—thus updating the previously

obtained spectroscopic factors (found by scaling the previous DWIA analysis to match the data points). Furthermore, this analysis was also done for ^{48}Ca$(e, e'p)^{47}$K providing a new perspective on the quenching of spectroscopic factors [82, 182]. These results demonstrate how, provided that sufficient elastic-scattering and structure data is available to constrain the fit, the DOM potential applied in the appropriate reaction theory is a powerful way to consistently describe knockout reactions and aspects of transfer reactions relevant to FRIB science.

3.1.3. Uncertainty quantification. Uncertainty quantification (UQ) for OMPs is an emerging topic, with the majority of publications on the topic dating from the last five years. The earliest systematic attempt at OMP UQ was by the authors of the Chapel Hill global OMP [13], who used a bootstrap method to assess that the variances of parameters in their OMP were very small (on the order of a percent). An attempt to estimate uncertainties of potential parameters was discussed at the IAEA RIPL project, where rough estimates of geometry and potential depth uncertainties were given [15]. Recent analyses using Bayesian techniques [86, 131, 176, 183, 184] reveal much larger uncertainties (tens of percent for elastic-scattering observables and up to a hundred percent for single-nucleon transfer cross sections) indicating that the statistical assumptions used for training phenomenological potentials can impact predictions as strongly as the data used for training. Due to the absence of global OMPs with well-calibrated parametric uncertainties, OMP users often resort either to tuning OMP parameters by hand or to performing ad hoc UQ by comparing predictions from multiple OMPs—neither of which is easily extrapolated to the high-asymmetry regime that will be probed at FRIB. Recently, Pruitt, Escher and Rahman have developed an extension of the global spherical proton and neutron OMPs of KD [14] and CH89 [13] with uncertainty quantification of the potential parameters, called KDUQ and CHUQ [185]. The mass and energy range of validity are the same as the original KD and CH89, i.e $24 < A < 209$ and $0.001\,\text{MeV} < E < 200\,\text{MeV}$ for KDUQ and $40 < A < 209$ and $10\,\text{MeV} < E < 65\,\text{MeV}$ for CHUQ. This new development will support the quantification of uncertainties in reaction observables. A natural next step to improve the constraint of these parametrizations is to enforce dispersion relations, include data on highly asymmetric systems and bound observables.

3.2. Microscopic approaches

As previously discussed, the phenomenological models have been built using experimental data primarily from stable nuclei. Hence, it is uncertain whether the extrapolations of phenomenological optical potentials to unstable isotopes would be reliable. For this purpose, optical potentials based on microscopic or semi-microscopic nuclear structure calculations prove to be vital. This section contains a description of various recent attempts to link the OMP to the underlying interaction between nucleons in free space. All approaches have strengths and weaknesses as well as limitations to their applicability which are discussed below.

3.2.1. Constructing Green's function from beyond mean-field approaches: Feshbach formulation, nuclear structure model and optical potentials from effective Hamiltonians.
Feshbach formulation. One of the approaches used to integrate microscopic nuclear structure information into the construction of optical potentials is by using the Feshbach formulation [19], where the optical model potential for a nucleon scattering energy E is given by equation (10). Equation (10) can be obtained from the set of coupled differential equations written in terms of the reaction channels [19]. By solving this set of equations, the Green's

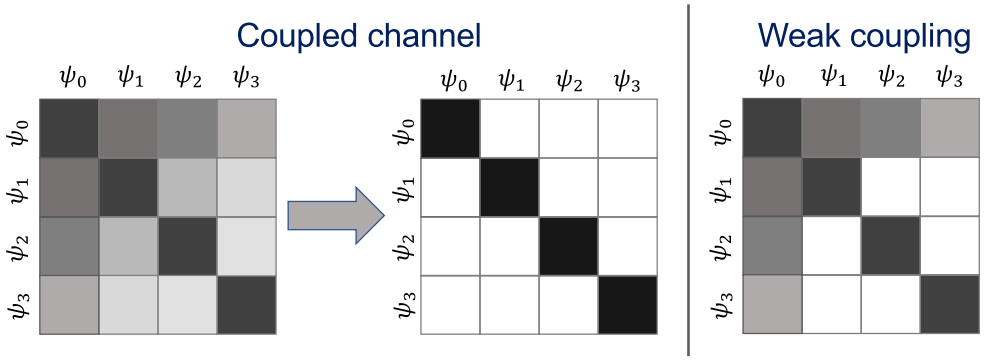

Figure 7. Schematic illustration of the obtention of the 'arrow' matrix from the weak coupling approximation. ψ_i correspond to the many-body states of the target, coupled together by the incoming nucleon.

function matrix G_{jk} can be diagonalized in the space of the excited states j, $k \neq 0$, but one can also use the weak coupling approximation [19, 186–189], which neglects the couplings between excited states, i.e. $\mathcal{V}_{jk} = \mathcal{V}_{0k}\delta_{j0}$. In this case the coupling potential is expressed in terms of an 'arrow' matrix (figure 7), and equation (10) becomes

$$V_{\rm opt} = \mathcal{V}_{00} + \sum_{j\neq 0} V_{0j} G_{jj} \mathcal{V}_{j0}, \tag{18}$$

where only the diagonal elements of the Green's function (8) enter. The coupling potentials and the Green's functions in the second term of equation (18) can be provided by nuclear structure calculations.

The method works best for the low-energy region where nuclear structure models can provide reliable and converged calculations (approximately $<$50 MeV). The versatility of this approach lies in the variety of structure calculations it can accommodate. However, the description of compound nucleus reactions, in which the relevant target-nucleon states are statistical in nature, is an open challenge.

Nuclear structure method. Another method is to construct the potential from a phenomenological effective NN interaction using the Green's function formalism. It is called the Nuclear Structure Method (NSM). The Green's function formalism allows the hierarchization of correlations and avoids double countings. Antisymmetrization due to the fermionic nature of nucleons is taken into account. The NSM was first proposed for realistic NN interactions by N Vinh Mau in the early 1970s [190]. Then it has been recast in order to be used with density functionals such as Skyrme or Gogny [191].

When dealing with a spherical target nucleus (without pairing), the NSM potential is made of two contributions: the Hartree–Fock potential and the Random Phase Approximation potential. The mean-field term is energy-independent. Its exchange term (Fock term) turns out to be nonlocal when using a finite-range interaction. The RPA contribution is a polarization contribution. The absorption results from taking into account the coupling to inelastic channels when the target nucleus is excited. Such excitations are described in the RPA formalism. This term is non-local, energy dependent and complex. The NSM can be interpreted as a Feshbach potential with consistent ingredients as the same functional is used all along the calculation. Hence in equation (18), V_{00} would be the equivalent of the Hartree–Fock potential in the NSM whereas V_{0i}'s would be provided by RPA.

A pioneering application of the method at lowest order with the Skyrme functional has demonstrated the ability of the Hartree–Fock potential to grasp the main features of the real part of the optical potential below 50 MeV incident energy [192]. Follow-up studies have included second-order terms with particle–particle (pp) and particle–hole (ph) correlations. The pp correlations are implicitly contained in the phenomenological NN interaction. particle–hole correlations are then taken into account explicitly through the Random Phase Approximation (RPA). In the beginning of the 1980s, several groups have worked on the NSM and related methods mostly using Skyrme interactions [191, 193, 194]. More refined versions of the NSM have been proposed including both inelastic excitations and (n, p) charge exchange [195–197]. The NSM has been used as well to determine α-nucleus potentials [198–200]. In the last decade, there has been a renewed interest in the NSM with Skyrme [201–203] and Gogny interactions [204–206]. The NSM describes with relative success, for both neutron and proton projectiles, the scattering off target nuclei such as: ^{16}O [203, 207, 208], ^{40}Ca [193, 195, 203, 204, 206], ^{48}Ca [203, 206] and ^{208}Pb [203, 208], for incident energy below 50 MeV. A calculation fully handling continuum and self-consistency has been proposed with Skyrme interactions [207]. The method has been applied to neutron scattering off ^{16}O below 30 MeV. This approach is particularly interesting because it allows one to circumvent the pitfall of RPA calculations in a harmonic oscillator (HO) basis that requires the introduction of ad hoc escape and damping widths [204]. Methods close to the NSM have also been used to describe proton inelastic scattering [209].

The NSM works well for incident energies below 50 MeV. Thus the method is complementary to g-matrix approaches in terms of energy range. In its current versions, it is limited to target nuclei well-described within RPA, typically double-closed shell nuclei. However, the extended reach of energy density functional based on structure calculations (pairing, deformation and odd number of nucleons) [210] suggests that further versions of the NSM will be suitable for a wide range of target nuclei. Some recent attempts have extended the approach to scattering off target nuclei with pairing using Hartree–Fock–Bogolyubov (HFB) formalism [211, 212]. The NSM will then be extended to include pairing correlations within the HFB formalism with Quasiparticle-Random-Phase Approximation (QRPA) on top of it. These new developments will eventually allow for the description of nucleon scattering off deformed target nuclei with pairing.

We mention here also approaches that employ Skyrme [213–217] or Gogny [218] functionals for infinite nuclear matter (see more extensive discussion of such methods in section 3.2.4). The optical potential is then obtained using the local density approximation (LDA) with a consistent density. This approach allows a satisfactory description of the elastic scattering observables for energies up to 100 MeV. In this context, there have been several attempts to fit new Skyrme functionals adding scattering constraints to the more usual structure ones [215–217, 219].

Optical potentials from effective Hamiltonians. While it is alluring to use a single interaction (e.g. Chiral) or pseudo–interaction (e.g. Gogny or Skyrme functionals) to construct the nuclear structure properties for the ground state, excitations, and subsequently the optical potential, it is also possible to combine effective Hamiltonians and interactions without lack of generality. This strategy has the advantage of potentially reducing computational costs or increasing the many-body expansion with respect to a calculation that treats every component on equal footing.

Over the years, several approaches have used different effective interactions and microscopic methods to construct the optical potential. The approach based on Hartree–Fock [191, 220] consists in defining the real part of a local potential based on an appropriate Skyrme functional. It is extended with additional couplings and

absorption [208, 221]. Eventually, one can consider the optical potential as arising from particle–vibration coupling, even extended in the continuum [209]. Another prominent example is the nuclear field theory, where single-particle and collective degrees of freedom are combined, eventually employing phenomenological coupling instead of a single consistent Hamiltonian or functional [222]. The nuclear field theory have been lately expanded, both in functional form [223], and using an effective coupling between multipolar vibrations and mean field [224]. The coupling between degrees of freedom has been recast as the solution to the Dyson equation [225], closely relating several structure and reaction observables [226–229]. However, it is difficult for an explicit Dyson procedure to treat cases where symmetry breaking is prominent, e.g. deformed nuclei, both in terms of guaranteeing symmetry restored final states and adequate computational costs.

The generator coordinate method (GCM) can tackle symmetry restoration in both even and odd nuclei. It is also appealing for its analogy with the resonating group method [230]. Developing effective Hamiltonians has the advantage of both formal consistency within the projection procedure that is difficult to maintain using functionals and simplifying the numerical calculations, all with excellent agreement with experimental structure observables [231]. The GCM has been used to calculate scattering properties of stable and exotic nuclei in several cases [230, 232, 233]. There is further work ongoing in connecting the microscopic structure description in the GCM and the reaction observables in the form of the construction of microscopic optical potential for deformed nuclei.

3.2.2. Computing the self-energy from ab initio predictions of nuclei: self-consistent Green's function and inversion of propagator using ab initio wavefunctions. As discussed in previous sections, the irreducible self-energy $\Sigma^{\star}(E)$ generalizes the exact nucleon–nucleus optical potential of Feshbach to include both *bound* and *scattering* states [8, 23, 234]. Diagonalizing the self-energy leads to the one-body Green's function, also known as the propagator (see equation (12)). Hence, many-body Green's function theory provides a well-grounded connection between structure and reactions [21] and it enables the direct computations of the self-energy based on the best accurate *ab initio* methods. We present the state-of-the-art frontiers and challenges of the Green's function approach in the following.

Ab initio computations of the self-energy for finite nuclei can be approached in two ways: (a) either by direct application of propagator theory to calculate its Feynman diagram expansion, as done in the Self- consistent Green's Function (SCGF) [235–237]; or (b) inverting the propagators computed using an *ab initio* wave function approach, as done in the coupled-cluster method (CCM) [238], the No-Core Shell Model (NCSM), and the Symmetry-Adapted No-Core Shell Model (SA-NCSM) [239]. *Ab initio* methods can construct the optical potential from chiral interactions, or other effective field theory (EFT) forces so that they provide a direct link to the underlying symmetry and symmetry-breaking patterns of quantum chromodynamics. They also provide a systematic approach to quantify theoretical uncertainties arising from the nuclear force and the controlled many-body approximations. Typical calculations for finite nuclei involve large but truncated model spaces that lead to a discretization of the scattering continuum. In most cases, the greatest challenges relate to dealing with such discretization and to handling a large number of degrees of freedom needed to resolve the dynamics at several scattering energies [240, 241]; a very demanding task if compared to typical successful *ab initio* computations of low-energy nuclear structure.

Direct computations of the self-energy. The SCGF approach involves computing a converged series of Feynman diagrams based on prescriptions that are aimed at preserving conservation laws. Modern nuclear physics applications exploit the Nambu–Gorkov formulation to include pairing in spherical open-shell nuclei [242] and follow the algebraic

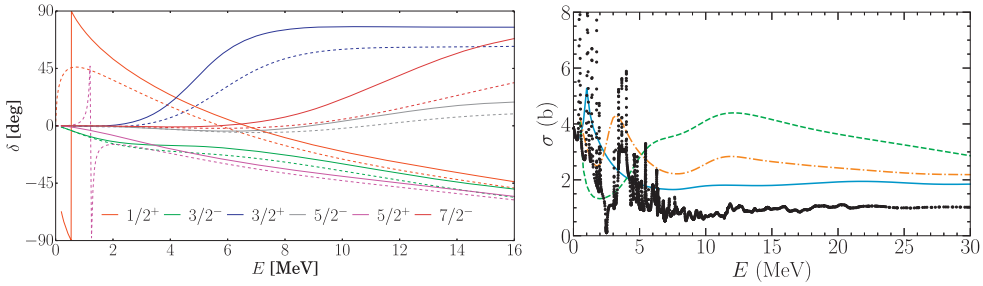

Figure 8. *Left*: A comparison of n-^{16}O phase shifts obtained with SCGF calculations using only the correlated mean field Σ^{∞} at $N_{\max} = 11$ (solid lines) and with the NCSM/RGM (dashed lines), which includes only the ground state of ^{16}O, at $N_{\max} = 11$. Both calculations have been made using $\mathrm{NNLO_{opt}}$ nucleon–nucleon interaction and $\hbar\Omega = 18$ MeV. *Right:* comparison of the predicted SCGF total cross section for elastic n-^{16}O as a function of the energy when including different portions of doorway states: only the correlated mean field Σ^{∞} (dashed green line), with half of the 2p1h and 2h1p configurations (dotted dashed orange line), and with complete ADC(3) (solid blue line). Computations are based on the $\mathrm{N2LO_{sat}}$ interaction. The experimental data is also shown (black dots). Reprinted with permission from [249], Copyright (2019) by the American Physical Society.

diagrammatic construction (ADC) technique to devise a systematically improvable hierarchy of many-body truncations [237]. Up to third order, or ADC(3), accurate ground state observables and low-energy spectroscopy are achieved for several chains of isotopes near the oxygen, calcium, nickel, and tin regions [243–246]. The Nambu–Gorkov approach has been applied only at second order for open shells nuclei and it is now being implemented to the previously unavailable ADC(3) level [247, 248].

In SCGF theory the self-energy is naturally split into a mean-field part, denoted as $\Sigma^{(\infty)}$, and a dynamic contribution, $\widetilde{\Sigma}(E)$, which is energy dependent and accounts for coupling to the virtual inelastic channels that give rise to the dispersion relation (4). Exploratory SCGF computations of optical potentials are reported in [174, 236]. The $\Sigma^{(\infty)}$ from SCGF agrees qualitatively well with direct scattering computations with the no core-shell model with resonating group method (NCSM/RGM, see [1] for a recent review and references therein) when virtual excitations of the target are suppressed, as seen in [249] and illustrated in figure 8 which compares the n-^{16}O phase shifts obtained with both methods. To reach a more predictive description of single-particle bound states and resonances, we include virtual states of the target nucleus. By including low-lying excitations of ^{17}O, the no-core-shell model with continuum (NCSMC) accounts effectively for virtual target excitations and leads to two bound states, namely $1/2^+$ and $5/2^+$. For SCGF, virtual excitations, contained in $\widetilde{\Sigma}(\omega)$, correct single-particle states and generate a large number of narrow resonances across all scattering energies. Results for low energy states are shown in [249] and there is qualitative accord with the observation.

In the SCGF approach, the biggest challenge for an *ab initio* theory is calculating $\widetilde{\Sigma}(\omega)$. The SCGF-ADC(3) construction contains correlations from all two-particles one-hole (2p1h) and one-particle two-holes (1p2h) configurations and has a direct impact on the absorption of the optical model. This is demonstrated for elastic neutron scattering off ^{16}O by the right-hand side of figure 8, where all 2p1h doorway states contribute to the solid blue line and are then gradually frozen until only the mean-field $\Sigma^{(\infty)}$ remains (dashed green line) [249]. The 2p1h states become insufficient already at intermediate energies, where more complex

configurations must enter into play. Truncations well beyond third order, ADC(n) with $n \gg 3$, will most likely resolve this problem but will require groundbreaking advances in nuclear many-body theory to automatically generate and efficiently sample the exponentially growing number of diagrams.

Inversion of propagators using ab initio wave functions. The indirect approach first evaluates the one-body Green's function in configuration space,

$$G_{\alpha\beta}(E) = \left\langle \Phi_0 \left| a_\alpha \frac{1}{E - (\mathcal{H} - \epsilon_0) + \mathrm{i}\eta} a_\beta^\dagger \right| \Phi_0 \right\rangle + \left\langle \Phi_0 \left| a_\beta^\dagger \frac{1}{E + (\mathcal{H} - \epsilon_0) - \mathrm{i}\eta} a_\alpha \right| \Phi_0 \right\rangle . \tag{19}$$

where α and β label the single-particle states and with $\eta \to 0^+$. One then inverts equation (12) for each scattering energy E to calculate the optical potential. To compute $G_{\alpha\beta}(E)$, the completeness of eigenstates $|\Psi^{A\pm1}\rangle$ can be used, which requires computationally intensive calculations of many eigenstates, but in practice, the inverse Hamiltonian operator in equation (19) is evaluated using one of a few available Lanczos algorithm methods [240, 250] (see also [237, 251, 252] and references therein). Note that if one evaluates equation (19) in the Lehmann representation using the completeness over $|\Psi^{A\pm1}\rangle$, one is evaluating the overlap functions $\langle\Psi_n^{A+1}|a_\alpha^\dagger|\Phi_0\rangle$ that are in fact solutions. In this case, the approach is equivalent to computing a discretized set of scattering waves and then solving an inverse scattering problem.

The viability of the propagator inversion scheme was demonstrated for oxygen and calcium isotopes using the particle attached and removed CCM, as discussed in [238] and is being applied within NCSM frameworks [239, 253]. The SA-NCSM provides useful features for nucleon–nucleus scattering such as its suitability describing deformation. *Ab initio* descriptions of spherical and deformed nuclei up through the calcium region are now possible in the SA-NCSM [254–256] without the use of interaction renormalization procedures and effective charges. It has also been shown that the SA-NCSM can use significantly reduced model spaces as compared to the corresponding ultra-large conventional NCSM model spaces without compromising the accuracy of results for various observables. This allows the SA-NCSM to accommodate larger model spaces needed for clustering, collective, and continuum degrees of freedom, and to reach heavier nuclei such as ^{20}Ne [255, 257], ^{21}Mg [258], ^{22}Mg [259], ^{28}Mg [260], as well as ^{32}Ne and ^{48}Ti [261]. Moreover, the construction of self-energies for light nuclei starting from the NCSM/RGM and its extension to the NCSMC are also currently being developed and are of interest as scattering states are included explicitly in the many-body basis. As the NCSMC reproduces low-energy scattering and bound-state observables [262–269] for light nuclei, the optical potentials derived within this theory, along with the reach of the symmetry-adapted RGM (SA-RGM) to intermediate-mass nuclei [256, 270], are expected to be accurate in a similar range of energies and masses.

Challenges and opportunities. Computationally, the most demanding task is the accurate evaluation of the self-energy for all relevant scattering energies. Methods that scale polynomially with the mass number, such as SCGF and CCM, are presently limited to simple excitations (e.g. 2p1h and 2h1p) throughout the energy range and converge with respect to the model space up to $\approx$160 MeV [174, 271]. However, more complex configurations that are important at intermediate energies are missing (see figure 8). The NCSM family of methods is complementary and it performs a truncation based on the number of HO excitations, which has two advantages. First, correlated multiple particle–hole configurations are well included at low energies (e.g. SA-NCSM can capture giant resonances, which is important to describe

scattering from 1 to 15 MeV per nucleon) but high scattering energies may pose a challenge. Second, it ensures the exact separation of the motion of the center of mass.

Indeed, calculations of the one-body Green's function that use laboratory coordinates may pose issues due to spurious center-of-mass motions in both the target and the $A \pm 1$ systems. Model spaces in typical *ab initio* computations are sufficiently large to decouple the intrinsic and the center of mass wave functions [272]. Moreover, this separation is even exact for NCSM calculations with HO-excitation truncations [273]. Nevertheless, the zero point motion of the center of mass is *still present* and it can be a source of spuriosity. Johnson discussed the technical difficulties with expressing a self-energy in a pure laboratory system [274, 275] and suggested that a proper optical potential theory should be expressed in Jacobi coordinates. Center of mass corrections are seen to be sizeable for light nuclei, such as ^{16}O but become quickly negligible at larger masses where the self-energy approaches the one in the laboratory frame. We note that the NCSM/RGM and NCSMC methods routinely compute scattering among observables by handling these center-of-mass corrections [1]. A similar development could also be valuable for reformulating the SCGF self-energy in proper relative projectile-target coordinates.

A related technical question is the discretization of the scattering spectra due to the finite model spaces. Both the Green's function and the optical potential (i.e. the self-energy) develop a real and an imaginary part in the continuum. For practical applications, the finite size of the model space implies a set of discrete poles both in equation (19) and in the spectral representation for $\Sigma^{\star}(E)$. The correct continuum spectrum is recovered only taking the limit $\eta \to 0$ while *at the same time* letting the density of intermediate states diverge (as per the complete set of configurations in an infinite model space). Ideally, one would like to use a finite η to impose a width as big as the distance between two neighboring levels, and check that predictions for observables are unaffected by variations of η around such central value. Note that the technical issue of handling the $\eta \to 0$ limit is more compelling for the inversion propagator approaches, since the diverging poles in equation (19) can lead to instabilities in the inversion process. This has been studied with the CCM method using Berggren bases with the continuum [276, 277]. For all cases, however, it should be clear that the choice for η sets the energy resolution of the optical potential being computed. A higher resolution requires a higher density of intermediate states, posing stronger demand on the *ab initio* method being employed.

To conclude, constructing the self-energy starting from microscopic computations with a single realistic Hamiltonian allows for a consistent description of the target structure and reaction dynamics, to derive a nucleon–nucleus optical potential and calculate elastic scattering observables. Contrary to phenomenological approaches whose applicability is limited by the reliability of extrapolations, microscopic optical potentials rely only on the knowledge of nuclear interactions and can be built in principle for any nucleus accessible by the theory. Such nucleon–nucleus optical potentials could be also used for microscopic descriptions of (d, p) and (d, n) [42].

Although elegant and with controlled approximations, *ab initio* methods are computationally intensive, they require suitable approximations and still have to face important challenges. In all cases, the quality of constructed microscopic potentials will reflect the current status of high performance computing resources and the accuracy of the many-body approach used. In particular, the coupling to possible intermediate states strongly influences the absorption from the elastic channel, i.e. the magnitude of the elastic scattering cross section. Moreover, the diffraction pattern, i.e. the position of the minima in the elastic-scattering angular distribution, is determined by the root mean square radius of the target posing important requirements on the quality of the realistic nuclear force used. The most

compelling issue is to advance *ab initio* methods to reach complete and stable description of intermediate configurations. Novel approaches as those discussed in [278, 279] will be key to reach full predictive power at medium energies.

3.2.3. Multiple scattering approach. The theoretical approach to the elastic scattering of a nucleon from a nuclear target pioneered by Watson [17, 280], made familiar by Kerman, McManus, and Thaler (KMT) [18], and further developed as spectator expansion of multiple scattering theory [281–284] is receiving renewed interest as an approach to the optical potential that can combine advances in nuclear structure with, e.g. chiral nucleon–nucleon (NN) interactions. A theoretical motivation for the spectator expansion derives from our present inability to calculate the full many-body problem when the projectile energy exceeds about 40–50 MeV (see sections 3.2.1 and 3.2.2). In this case, an expansion is constructed within a multiple scattering theory assuming that two-body interactions between the projectile and one of the nucleons in the target nucleus play the dominant role. In the spectator expansion the leading (first) order term involves two-body interactions between the projectile and one of the target nucleons, the next-to-leading (second) order term involves the projectile interacting with two of the target nucleons, and so forth. Hence, this expansion derives its ordering from the number of target nucleons interacting directly with the projectile, while the residual target nucleus remains 'passive'. Due to the many-body nature of the free propagator for the nucleon-target system, there is an additional aspect to consider in the ordering of the spectator series. The expansion of chiral NN forces not only leads to two-body forces but naturally introduces three-body forces at next-to-next-to-leading order. The latter will not contribute to the leading order in the spectator expansion. The calculation of an optical potential relies on basic input quantities. For the leading order those are fully-off-shell NN amplitudes (or *t*-matrices), representing the current understanding of the NN force, and fully-off-shell one-body density matrices representing the current understanding of the ground state of the target nucleus. For any higher order, additional input like 3N amplitudes and two-body density matrices for the target will be needed.

The standard approach to elastic scattering of a strongly interacting projectile from a target of A-particles is the separation of the Lippmann–Schwinger equation for the transition amplitude T

$$T = V + VG_0(E)T \tag{20}$$

into two parts, namely an integral equation for T

$$T = U + UG_0(E)PT, \tag{21}$$

where U is the optical potential operator defined by a second integral equation

$$U = V + VG_0(E)QU. \tag{22}$$

In the above equations the operator $V = \sum_{i=1}^{A} v_{0i}$ consists of the two-body NN potential v_{0i} acting between the projectile and the ith target nucleon. The free propagator $G_0(E)$ for the projectile-target system is given by

$$G_0(E) = \frac{1}{E - H_0 + \mathrm{i}\eta} \tag{23}$$

with $\eta \to 0^+$. Though most applications use targets with 0^+ ground states, there is no need for this to be the case [285]. In fact, to develop optical potentials valid for exotic nuclei, a variety of targets with different ground state spin configurations will need to be considered.

The operators P and Q in equations (20) and (21) are projection operators with $P + Q = 1$, and P being defined such that equation (21) becomes a one-body equation. In this

case, P is conventionally taken to project on the elastic channel, such that $[G_0, P] = 0$, and is defined as $P = |\Phi_0\rangle\langle\Phi_0|/\langle\Phi_0|\Phi_0\rangle$. With these definitions, the transition operator for elastic scattering can be defined as $T_{el} = PTP$, in which case equation (21) can be written as

$$T_{el} = PUP + PUPG_0(E)T_{el}. \tag{24}$$

The choice of the projector P fixes the scattering problem to be considered. A projection onto the target ground state is the appropriate choice to derive an optical potential describing the elastic scattering of a nucleon from a target nucleus, but when considering e.g. inelastic scattering in a coupled-channel approach, this P-space should contain the excited states under consideration. To our knowledge, this has not been attempted in a multiple scattering approach.

The expression for the optical potential in equation (22) contains the projection operator Q and thus, even in the leading order term where U is defined as $U = \sum_{i=1}^{A} \tau_{0i}$, the quantity τ_{0i} cannot readily be identified with a NN amplitude derived in free space. Working in momentum space, it is straightforward to formulate an integral equation for the Watson optical potential [286]

$$\tau_{0i} = v_{0i} + v_{0i}G_0(E)Q\tau_{0i} = \hat{\tau}_{0i} - \hat{\tau}_{0i}G_0(E)P\tau_{0i}, \tag{25}$$

where $\hat{\tau}_{0i}$ is the NN t-matrix given as a solution of a regular two-body Lippmann–Schwinger equation, in which only the many-body Green's function $G_0(E)$ needs to be considered. The standard impulse approximation turns this Green's function into a two-body propagator. It should be noted that the above equations follow in a straightforward derivation and correspond to the first-order Watson scattering expansion [17, 280]. The integration of equation (25) taking into account contributions from the Q space corresponds to an averaging over inelastic channels and thus should only be applied for energies higher than ∼30–40 MeV. Unfortunately, a similar formulation as in equation (25) cannot be made in coordinate space. Here the closest to treating the operator Q is the averaging suggestion made by Kerman, McManus, and Thaler [18] leading to the KMT factor (A-1)/A in the optical potential. [286] showed that the explicit treatment of the operator Q is especially important for scattering from very light nuclei, where the KMT factor is not close to one. The importance of an explicit treatment of Q for nuclei far off the valley of stability needs to be explored. Studies of reaction cross sections of the helium isotopes at energies below 100 MeV revealed that treating Q exactly or via KMT did not lead to major differences: however, not treating Q at all caused discrepancies of more than 10% in the reaction cross section.

A further equally important consideration for obtaining the optical potential is to find a solution to equation (22), which still has a many-body character due to the propagator $G_0(E)$. The standard impulse approximation assumes closure, i.e. ignores target excitations. For projectile energies above ∼80 MeV this is generally assumed to be a good approximation and errors have not been studied yet. In the impulse approximation and at leading order, the nucleon–nucleus optical potential for a certain kinetic energy E is given by equation (6). Let us now discuss a possible extension of this formalism to include effects of the antisymmetrization and to go beyond the impulse approximation.

The treatment of Pauli antisymmetry effects follows the philosophy growing out of the early work of Watson [287, 288] and developed via the spectator expansion in [289]. In the lowest order the two-body antisymmetry is achieved through the use of two-body t-matrices which are themselves antisymmetric in the two 'active' variables (corresponding to the weak binding limit in [288]).

Going beyond the impulse approximation in the spirit of the spectator expansion means consider that more nucleons of the target are active. At the next order in the expansion, one

needs to consider that two nucleons of the target i and j are active. The optical potential would depend on propagators $\mathcal{G}_{0j}$ that have the structure of three-body channel Green's functions. One can describe these propagators within a single particle description as

$$\mathcal{G}_{0j}(E) = \frac{1}{E - h_0 - h_j - \sum_{i \neq j} v_{ij} - H^j + i\eta}, \tag{26}$$

where $\eta \to 0^+$, H^j is the residual target Hamiltonian involving $(A-1)$ particles (excluding particles 0 and j), h_j is the kinetic energy operator for nucleon j, and v_{ij} is the interaction between target nucleons i and j. One can then project this Green's function onto a fixed number of eigenstates of the residual target Hamiltonian H^j. Due to the presence of v_{ij} an exact solution will require fully-off-shell two-body density matrices for the target nucleus as well as three-body dynamics. Two-body density matrices from *ab initio* structure models are calculable in principle, so there is an opportunity to consistently estimate the contribution of the next order in the spectator expansion, and thus have a better understanding of its convergence as function of projectile energy as well as mass number. This will be a very challenging enterprise. A first attempt with nuclear densities derived from HFB mean field calculations for heavier nuclei was made in [290, 291] where the interaction v_{ij} was taken as the corresponding nuclear mean field. The result of this study showed that at projectile energies above 100 MeV the second-order correction is almost negligible, while starting to be evident in the spin observables at energies below 100 MeV. At about 50 MeV, the second-order correction is quite visible in the differential cross section.

Another approach to take into account the beyond-leading-order effects of three-body forces was implemented in [292] by constructing a density-dependent NN interaction that treats the 3N force in an approximate way [293, 294]. For energies above 100 MeV, few effects were noticeable in the differential cross sections, though some effects were observed in the analyzing power and spin rotation function.

Explicit calculation of the leading order term in the Watson approach. For explicit calculations of reaction observables from the leading order term in the spectator expansion, equation (6), one needs both, structure information (fully-off-shell one-body density matrices) and reaction information (NN amplitudes). Current *ab initio* calculations of multiple scattering theory are limited in their applicable mass range due to the available *ab initio* structure inputs. To reach target nuclei beyond the $A \sim 40$ range, one-body density matrices will need to be calculated from other structure models, e.g. SCGF, CCM and In-Medium Similarity Renormalization Group (IM-SRG).

Recent work [295] showed that including the spin of the struck target nucleon has an effect on the elastic scattering spin observables for neutron-rich systems, which implies consistent calculations incorporating this term may be necessary to study nuclei off the valley of stability. This additional term requires both, a scalar and spin-dependent one-body density matrix, and guarantees that the scalar (Wolfenstein A), vector (Wolfenstein C), and tensor (Wolfenstein M, G, H, and D) parts of the NN interaction are included[21]. For $J = 0$ to $J = 0$ transitions, it has been shown that only A, C, and M contribute due to parity invariance, though this likely holds for other transitions between the same spin states. Future work to develop *ab initio* treatments of inelastic scattering in this framework are becoming possible and will allow for further study of the tensor (Wolfenstein M, G, H, and D) parts of the NN interaction.

In addition to the theoretical uncertainties arising from the spectator expansion of the multiple scattering theory (e.g. next-to-leading-order effects for three-body forces, as well as

[21] For the definition and derivation of Wolfenstein amplitudes see [296, 297].

energy-dependencies of the NN t-matrix [298])—which are expected to be small in the energy regime above 60 MeV—there are additional theoretical uncertainties propagating from the nuclear-structure calculations. This includes both model-related uncertainties (e.g. any residual dependence on the size of the model space), as well as uncertainties from the underlying NN interaction (e.g. uncertainties associated with truncating a chiral effective field theory at a certain order, dependence on the fits of the low-energy constants (LECs), and others). Different approaches can be taken to address each of these uncertainties, but an accounting of them is necessary to extract reliable information about reaction observables.

Explicit calculation of the leading order term in the g-matrix approach. This approach starts directly from the general expression for the leading-order term of equation (6) and realizes that from quite general considerations [299] the two-body (NN) amplitude $\hat{\tau}_\alpha$ can be recast as

$$\langle \vec{k}'\vec{p}\,'|\hat{\tau}_\alpha(E)|\vec{k}\ \vec{p}\,\rangle = \int \frac{\mathrm{d}\vec{z}}{(2\pi)^3}\, \mathrm{e}^{\mathrm{i}\vec{z}\cdot(\vec{W}'-\vec{W})}\, g_{\vec{z}}\left[\frac{1}{2}(\vec{W}'+\vec{W});\, \vec{b}',\, \vec{b}\right], \tag{27}$$

where $g_{\vec{z}}$ represents a reduced interaction at the local coordinate $\vec{z}$. In this expression $\vec{W}=\vec{k}+\vec{p}$, and $\vec{b}=(\vec{k}-\vec{p})/2$, the prior total and relative two-body momenta, respectively. The same applies to the post momenta, denoted by primed marks. Additionally, the $\vec{z}$ coordinate is given by the average $\vec{z}=(\vec{r}\,'+\vec{s}\,'+\vec{r}+\vec{s})/4$, the center of gravity of the four coordinates of the two-particles, $\vec{r}$, $\vec{r}\,'$, $\vec{s}$, $\vec{s}\,'$.

Assuming a density-dependent *NN* effective interaction, in [299] it is demonstrated quite generally that the folding potential in momentum space can be expressed as the sum of two terms,

$$U(\vec{k}',\vec{k};E) = \sum_\alpha \int \mathrm{d}\vec{P}\ \hat{\rho}_\alpha(\vec{q};\vec{P})\ \hat{\tau}_0(E+\epsilon_\alpha) + U_1(\vec{k}',\vec{k};E), \tag{28}$$

where

$$U_1(\vec{k}',\vec{k};E) = -\sum_\alpha \int_0^\infty \mathrm{d}z\ \tfrac{4\pi z^3}{3} \int \tfrac{\mathrm{d}\vec{P}}{(2\pi)^3} \int \mathrm{d}\vec{q}\,'\, \hat{\jmath}_1(z|\vec{q}\,'-\vec{q}|)\ \rho_\alpha(\vec{q}\,';\vec{P})\, \partial_z g(\rho_z, E+\epsilon_\alpha). \tag{29}$$

Here $\hat{\jmath}_1(x)=3j_1(x)/x$, with $j_1(x)$ being the spherical Bessel function of order 1 and $\rho_\alpha(\vec{q};\vec{P})=\varphi^\dagger_\alpha(\vec{P}+\frac{1}{2}\vec{q})\,\varphi_\alpha(\vec{P}-\frac{1}{2}\vec{q})$, with φ_α the target single-particle wave function with energy ϵ_α. Note that in the sum only occupied states should be considered. While $\hat{\tau}_0$ represents the momentum-space free t-matrix (as present in the KMT term of the optical potential [300–302]), the fully off-shell g-matrix can be modeled with the infinite nuclear matter Brueckner–Hartree–Fock g-matrix. Assuming weak isospin asymmetry, the gradient term $\partial_z g=[\partial g/\partial\rho][\partial\rho/\partial z]$, is evaluated at a local isoscalar density ρ_z. The resulting nonlocal potential $U(\vec{k}',\vec{k};E)$ has been applied to nucleon elastic scattering, as reported in [303, 304] An interesting interpretation of equation (29) for U_1 is that intrinsic medium effects take place mostly at the surface of the target, as modulated by $\partial_z\rho$, the gradient of the density [303].

Finally, let us emphasize that there are other similar approaches which construct in coordinate space nucleon- and nucleus-optical potentials, folding microscopic neutron and proton densities with nucleon–nucleon effective interactions [305–312].

3.2.4. Nuclear matter approaches: Whitehead–Lim–Holt potential, G-matrix solutions of the Brueckner–Bethe–Goldstone and the JLM folding model. Compared to finite nuclei, infinite homogeneous nuclear matter represents a conceptually simpler physical system to study. In particular, calculations of the nucleon optical potential in nuclear matter avoid many of the technical difficulties and practical limitations faced when computing the nucleon optical potential directly in a finite system. When combined with a local density approximation, the nuclear matter approach can also be used to construct nucleon–nucleus optical potentials, provided that the isoscalar and isovector densities of the target nuclei are known. A significant advantage is that the nucleon optical potential in nuclear matter only needs to be computed once over a wide range of densities and proton fractions and then may be applied across large regions of the nuclear chart. Hence, the nuclear matter approach is naturally suited for the construction of global optical potentials, which will be vital for the future of reaction theory for rare isotopes. However, the assumptions of the nuclear matter approach that allow for the ease of constructing global nucleon–nucleus optical potentials also omit phenomena such as surface effects, resonances, and spin–orbit interactions. The nuclear matter approach also tends to produce an overly absorptive imaginary term at high energies. Some of these shortcomings may be straightforwardly remedied while for others the solution remains unclear, for more details see [313]. Ultimately, the quality of theoretical predictions for reaction cross sections from optical potentials derived within the nuclear matter approach must be assessed by comparisons to experimental data.

The framework for utilizing nuclear matter calculations of the optical potential for finite nuclei was built by Jeukenne, Lejeune and Mahaux in the late 1970s [113, 114]. They implemented the Local Density Approximation (LDA)

$$\begin{aligned} U(E;\, r)_{\rm LDA} &= V(E;\, r)_{\rm LDA} + iW(E;\, r)_{\rm LDA} \\ &= V(E;\, k_f^p(r),\, k_f^n(r))_{\rm NM} + iW(E;\, k_f^p(r),\, k_f^n(r))_{\rm NM}{}' \end{aligned} \tag{30}$$

which relates the optical potential at a given position in the nucleus with the optical potential of nuclear matter (denoted by NM) with the same local density and isospin asymmetry through the neutron $k_f^n(r)$ and proton $k_f^p(r)$ Fermi momenta. A key finding of [113] is that the LDA is insufficient for reproducing elastic-scattering data, which requires a modification called the Improved Local Density Approximation (ILDA) that takes into account the nonzero-range of the nuclear force

$$U(E;\, r)_{\rm ILDA} = \frac{1}{(t\sqrt{\pi})^3} \int U(E;\, r')_{\rm LDA} e^{\frac{-|\vec{r}-\vec{r}'|^2}{t^2}} {\rm d}^3 r'. \tag{31}$$

The ILDA introduces a Gaussian smearing of the optical potential over the range of densities probed across the length scale t, typically chosen to be around $t \sim 1.2$ fm, the effective range of the nuclear force. The most important consequence is that the optical potential in the interior of the nucleus changes little, while the surface diffuseness of the optical potential increases due to finite-range effects.

Whitehead–Lim–Holt global optical potential. Recent advances [314, 315] in the nuclear matter approach to constructing microscopic nucleon–nucleus optical potentials incorporate consistent two-body and three-body forces [316] at various orders in the chiral expansion. The nucleon self-energy in nuclear matter is calculated in the framework of many-body perturbation theory (MBPT) [317, 318], which has already been used to produce accurate models of the nuclear equation of state [319–323]. In addition to MBPT, there are other many-body frameworks for microscopically calculating the self-energy. One notable example is the work of Rios in SCGF theory [324].

In MBPT, the first-order (or Hartree–Fock) contribution to the nucleon self energy in isospin-symmetric nuclear matter is given by

$$\Sigma^{(1)}_{2N}(k) = \sum_{1} \langle \vec{k}\ \ \vec{h}_1 s s_1 t t_1 | \bar{V}_{2N} | \vec{k}\ \ \vec{h}_1 s s_1 t t_1 \rangle n_1, \tag{32}$$

where $\vec{k}$, s, t are the momentum, spin, and isospin of the projectile, n_1 is the occupation probability $\theta(k_f - h_1)$ for a filled state with momentum $\vec{h}_1$ below the Fermi surface, and the summation is over intermediate-state momenta $\vec{h}_1$, spins s_1, and isospins t_1.

The second-order perturbative contributions to the nucleon self energy in symmetric nuclear matter are expressed as

$$\Sigma^{(2a)}_{2N}(k; E) = \frac{1}{2} \sum_{123} \frac{|\langle \vec{p}_1 \vec{p}_3 s_1 s_3 t_1 t_3 | \bar{V}_{2N} | \vec{k} \vec{h}_2 s s_2 t t_2 \rangle|^2}{E + \epsilon_2 - \epsilon_1 - \epsilon_3 + i\eta} \bar{n}_1 n_2 \bar{n}_3, \tag{33}$$

$$\Sigma^{(2b)}_{2N}(k; E) = \frac{1}{2} \sum_{123} \frac{|\langle \vec{h}_1 \vec{h}_3 s_1 s_3 t_1 t_3 | \bar{V}_{2N} | \vec{k} \vec{p}_2 s s_2 t t_2 \rangle|^2}{E + \epsilon_2 - \epsilon_1 - \epsilon_3 - i\eta} n_1 \bar{n}_2 n_3, \tag{34}$$

where the occupation probability for particle states above the Fermi momentum is $\bar{n}_i = \theta(k_i - k_f)$. The second-order contributions $\Sigma^{(2a)}$ and $\Sigma^{(2b)}$ are energy-dependent and complex. In equations (33) and (34), the single-particle energies E and ϵ should be computed self-consistently according to

$$E(k) = \frac{k^2}{2M} + \mathrm{Re}\ \Sigma(k; E(k)). \tag{35}$$

The use of chiral nuclear forces provides several advantages to the phenomenological nuclear forces of the past. By virtue of being an effective field theory, chiral makes a concrete connection to the underlying theory of quantum chromodynamics through its symmetries. Furthermore, chiral nuclear forces are calculated in a perturbative expansion that allows for a direct method of uncertainty quantification by assessing order-by-order convergence [325].

The wide applicability of the nuclear matter approach and uncertainty quantification capabilities of chiral EFT were employed in [326] to construct both the first microscopic global optical potential and the first global optical potential with uncertainty quantification. Both of these advances are central to the development of reaction theory for the rare-isotope beam era, where theoretical predictions for thousands of exotic isotopes will be needed to drive scientific discovery and answer fundamental science questions in nuclear astrophysics. Present microscopic optical potentials have sizable uncertainties, which may be reduced within a Bayesian framework that incorporates experimental nucleon–nucleus scattering and reaction data in Bayesian likelihood functions. In [326], five separate global optical potentials were generated from a set of chiral potentials of different order in the chiral expansion and with varied momentum-space cutoffs. These global optical potentials are expressed in terms of Woods–Saxon functions that are parametrized in terms of energy, target mass, and target isospin asymmetry (E, A, δ). Assuming the five optical potentials are drawn from a multivariate Gaussian distribution in the space of optical potential parameters, one can then propagate statistical uncertainties to scattering observables. This multivariate Gaussian distribution of nucleon–nucleus optical potentials is referred to as the Whitehead–Lim–Holt (WLH) global optical potential.

In figure 9, the real (left panel) and imaginary (right panel) terms of the WLH optical potential for $n+^{40}$Ca at $E = 5$ MeV and $E = 100$ MeV are shown in coordinate space. As the energy increases, the real term decreases in depth while the imaginary term increases in depth.

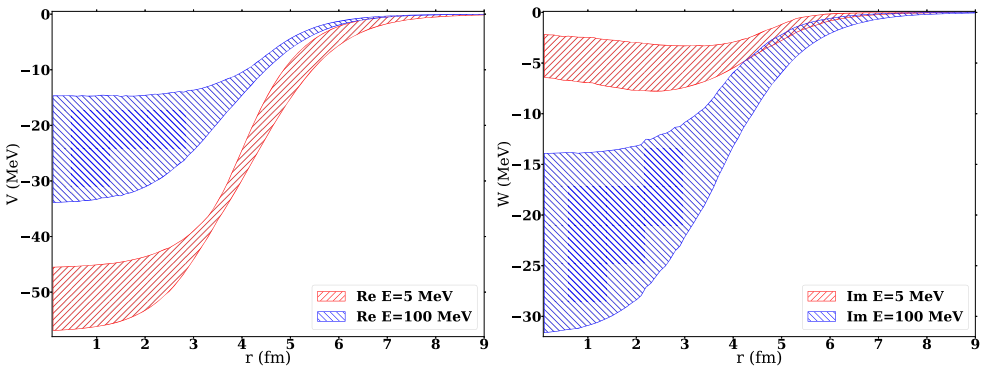

Figure 9. The real (left) and imaginary (right) terms of the WLH global optical potential for $n+^{40}$Ca at $E = 5$ MeV (red) and $E = 100$ MeV (blue).

Both terms have larger uncertainties as the energy increases reflecting the enlarging uncertainties of chiral EFT at high energies. These potentials can be easily applied in open source reaction codes to propagate uncertainties to reaction observables. The WLH global optical potential yields good reproductions of experimental elastic scattering cross sections for projectile energies of $E \lesssim 150$ MeV. Total reaction cross sections calculated from WLH are in good agreement with data up to moderate energies, and then overestimate data at larger energies due to an overly absorptive imaginary term. Beyond energies of $E \lesssim 150$ MeV, predictions of the WLH optical potential are expected to have greater discrepancies with data along with larger uncertainties. Predictions of WLH for a wide range of reactions are shown in section 5.

G-matrix solutions of the Brueckner–Bethe–Goldstone. The nuclear matter approach also gives access to direct inelastic scattering observables. In this case, the effective interaction used to build the microscopic optical potential also serves to build the transition potentials that enter the definition of the relevant Distorted Wave Born Approximation (DWBA) or coupled-channels equations. For instance, nucleon elastic and inelastic scattering were modeled from g-matrix solutions of the Brueckner–Bethe–Goldstone equations in nuclear matter—two well-known examples are the Melbourne [327] and the Santiago g-matrices [328]—and one-body density matrices through the calculation of non-local optical and transition potentials (an example of the application to inelastic scattering with the Melbourne g-matrix and RPA beyond mean-field approach is given in [329, 330]).

JLM folding potential. As these approaches have proven less suited at incident energy below 30–50 MeV, one pragmatic solution to cover the missing low-energy range, quite important for energy applications and experimental programs at RIBs, is to still rely on effective interactions derived from nuclear matter calculations but which are slightly renormalized to account for selected scattering observables. One such approach is the JLM folding model mentioned above, which has been extensively used to describe elastic and inelastic scattering of protons, neutrons, and composite particles within the double folding method, for both spherical and deformed targets. A global Lane-consistent parametrization of the JLM interaction was given by Bauge *et al* in 2001 [98] by adjusting the interaction to reproduce many elastic scattering and charge-exchange observables between 1 keV and 200 MeV. Many reactions were studied with this parametrization starting with HFB ground state densities and transition densities from the QRPA nuclear structure calculations. Recent examples are the determination of inelastic scattering to discrete states and to the continuum

for neutron scattering below 30 MeV off spherical [331], and axially-deformed targets such as actinides within the coupled-channel framework [332], as well as the modeling of proton inelastic scattering off unstable targets [333]. The method's ability to provide accurate reaction observables is mostly related to the quality of the nuclear structure input, so it was intensively used to challenge structure theory with hadron scattering observables. Despite its phenomenological content, the method has displayed good predictive capabilities especially for direct inelastic scattering, as no inelastic observables are used to constrain the interaction. However, its phenomenological aspect makes the method's precision hard to improve beyond the use of better nuclear structure input, and it relies on simplified nuclear matter calculations with old-fashioned bare interactions. Moreover, resulting potentials from the JLM folding model are local and non-dispersive, while the optical potential is known to be non-local and to obey dispersion relations. The spin–orbit component is ad hoc—it does not stem from an underlying nuclear matter calculation—and uses a simple form factor given as a derivative of the microscopic density. This approach could thus be revisited starting from modern nuclear matter calculations such as those described above.

One aspect of inelastic scattering that deserves attention is the rearrangement correction in [334], which has a large renormalization effect on inelastic cross sections [335]. This correction, which stems from the density dependence of the effective interaction used for inelastic scattering, is still now applied in an ad hoc manner when folding models are used. We stress that this correction, which has been known for a long time to induce modifications as large as the difference between the *t*- and the *g*-matrix [334], should be described from more fundamental principles in order to reach a better description of inelastic scattering within the microscopic framework of folding and full-folding approaches.

3.3. Synergies between microscopic approaches and phenomenology

There are three main limitations of the standard phenomenological approach that was presented in section 3.1. First, in selecting a potential form and parametrization (such as a Gaussian nonlocality), the practitioner makes simplifying assumptions about the physics at hand, pushing any unknown physics into changes of the potential parameters. As such, any extrapolation away from the region of training data is perilous, especially to weakly bound systems near the drip lines that will be probed with FRIB. Second, training phenomenological potentials requires copious training data, the vast majority of which was collected between 1960 and 2000 in direct kinematics at smaller facilities such as university cyclotrons and tandem accelerators. Without additional high-precision p, n, d, t, ^{3}He, α scattering data, it is unlikely that traditional phenomenological OMPs can be meaningfully improved (except by including additional physical input such as, e.g. deformation information), nor can microscopic approaches be rigorously tested. If new phenomenological OMPs are to be developed using data from radioactive beams in inverse kinematics, low statistics and large uncertainties in the reaction theory used to constrain these OMPs with non-elastic cross sections present serious problems. Finally, past optimization approaches for phenomenological OMPs have focused almost exclusively on finding 'best-fit' parameters but lack meaningful parametric uncertainties. Even the best phenomenological potentials fail to achieve χ^2/N values of $\approx$1 that would indicate reasonable reproduction of the training data, an indication that either important physics are missing from the phenomenological forms, training data uncertainties are underestimated, or both.

While the phenomenological approaches described in section 3.1 offer better accuracy in describing scattering on stable targets, their predictability in unknown regions is weak. Similarly, phenomenological optical potentials that provide an excellent description of one

reaction channel, can fail to describe other channels. In contrast, microscopic approaches, having the correct symmetries, are more promising for extrapolations. However, as detailed in section 3.2, the wide range of microscopic approaches have their own shortcomings. It is therefore appropriate to develop strategies that marry the best of the two worlds. We next discuss some explicit ways in which microscopic approaches can benefit from an appropriate phenomenological calibration.

It is well-known that for a model to be able to reproduce the scattering diffraction pattern, it is essential that the same model describe the size of the system correctly. This is particularly relevant to *ab initio* methods, since various parametrizations of the chiral potentials used in these models may not reproduce accurately the root mean square radius (see e.g. [336] for selected medium-mass nuclei). Hence, for the description of reactions at low energies, it is important that modern nuclear forces employed in the calculations capture nuclear radii [337] while ensuring the proper treatment of dominant correlations, as discussed next.

Particle threshold energies (or resonance energies) are another important quantity for most reactions and become even more relevant for reactions involving nuclei at the limits of stability. In this regard, microscopic models cannot provide the level of precision needed for an adequate description of the reaction (of the order of 0.1 MeV). As such, often microscopic approaches find ways to adjust their calculations such that the model reproduces the thresholds exactly [265, 269]. Given that it is unlikely that many-body methods will reach the level of precision needed in the near future, one should better understand how these different adjustments affect the optical potential and propagate to complex reaction observables.

As remarked in section 3.2, with the exception of the NCSM and derivatives (NCSMC, SA-NCSM, etc), optical potentials derived from *ab initio* methods contain only simple excitations, up to 2p1h or 2h1p. In addition, collective correlations may be suppressed for some methods and chiral potential parametrizations employed [338]. This leads to an underestimation of the flux removed from the elastic channel, and thus an overestimation of the elastic-scattering cross section[22]. While *ab initio* NCSM-type approaches are applicable to medium mass, currently it is not feasible to extend NCSM methods to heavy systems to include the level of complexity required for a good description of the total absorption occurring in the scattering (for example configurations beyond 2p2h [238, 339]). Consequently, some groups have devised strategies to incorporate the missing physics by hand as for example the method discussed in section 3.2 involving doorway states.

A microscopically derived optical potential with known uncertainties, that has been well-calibrated on the important inputs discussed above, has the potential to perform much better than any phenomenological approach when exploring unknown regions of the nuclear chart. There are a few well identified aspects in which the microscopic optical potential can provide critical information to phenomenology.

First and foremost, since the nucleon–nucleon force contains the correct isospin symmetry, microscopic approaches should in principle provide important guidance with respect to the isospin dependence of the optical potential. This is particularly relevant to scientific programs in facilities with rare isotope beams. Not only is the optical potential isospin dependence important, but also it is critical to know how it varies with beam energy. Future studies focused on extracting the isospin dependence of the microscopic optical potential from first-principles are encouraged.

Another equally important aspect of the optical potential is the radial dependence of the spin–orbit force. While there is a reason to model the radial dependence of the central force

[22] By construction, NCSM-type approaches include higher orders of complexity in the model and therefore do not, in principle, have the same issue, however, they are limited to applications on light to medium-mass nuclei.

after the density distribution in the target nucleus, the basis for the radial dependence of the spin–orbit force is not well established and for simplicity is taken to be the derivative of the central term. Microscopic studies focused on determining the radial dependence of the spin–orbit force will be very helpful to reduce ambiguous model dependencies in the global optical potential.

Finally, as stated a number of times throughout this white paper, a microscopic optical potential is intrinsically non-local. However, most phenomenological potentials have preferred to make the global potential local to avoid the additional computational cost, with the exception of some DOM potentials (see section 3.1.2). This simplification introduces a very strong energy dependence in the parameters. Despite it not being directly probed through elastic scattering, the off-shell effects associated with non-locality do show up in other reaction channels [340, 341] and therefore should be considered. In view of the incredible advances in computing capacity, a non-local global optical potential is now feasible and microscopic approaches should provide guidance to the radial form and its range. Current microscopic studies have already shown that the simple Gaussian form for the non-locality factor used by Perey and Buck (introduced in section 3.1.2) is not sufficient [276, 342, 343]. But one should also assess whether it is appropriate to separate this non-local factor in the first place. Further microscopic studies along these lines will help establish a form for the non-local potential that can then be used in phenomenology.

3.4. Model uncertainties beyond pairwise effective potentials

Complex reactions as discussed in section 2 are often described within a few-body model and the dynamics are obtained from a Hamiltonian including the relevant degrees of freedom and the corresponding pairwise interactions between the clusters. Thus, even when the full dynamics is calculated, there is still a model uncertainty emerging from the reductions of the many-body model into the few-body model. Quantifying the uncertainty introduced through this simplification is not trivial. In this section, we discuss the first steps taken toward this goal.

As an illustration, we consider reactions involving the deuteron, typically described within a three-body model consisting of a neutron, a proton, and a target that consists of A nucleons, interacting through pairwise phenomenological potentials. An exact solution to this three-body problem is provided by the Faddeev formalism [344]. While the Faddeev formalism enables a correct description of the three-body dynamics, its predictive power is limited, in part, by the uncertainties in the effective phenomenological nucleon–nucleus potentials that implicitly include the three-cluster interaction npA. Additionally, the formal projection of the many-body problem onto the three-particle space gives rise to an irreducible three-body force (3BF) which cannot be decomposed into a sum of pairwise interactions [345] and thus cannot be constrained using nucleon–nucleus scattering data. Efforts to quantify the effects of the irreducible nucleon–nucleon–nucleus forces have been carried out in [346, 347] by utilizing multiple scattering theory to estimate the lowest order contributions to the 3BF arising from the excitation of nucleons inside the nucleus A. While those works demonstrated that the 3BF corrections to the pairwise potentials had a significant impact on deuteron-induced reaction observables, there is some ambiguity coming from how the phenomenological potentials are defined that does not allow for the disentanglement of irreducible three-body contributions.

The effects of the 3BF can be quantified without ambiguities by adopting microscopically computed nucleon–nucleus potentials and grounding all calculations on a single microscopic Hamiltonian using the same NN interactions. Uncertainties arising from the omission of the irreducible 3BF in three-body model calculations were performed for deuterium-^{4}He

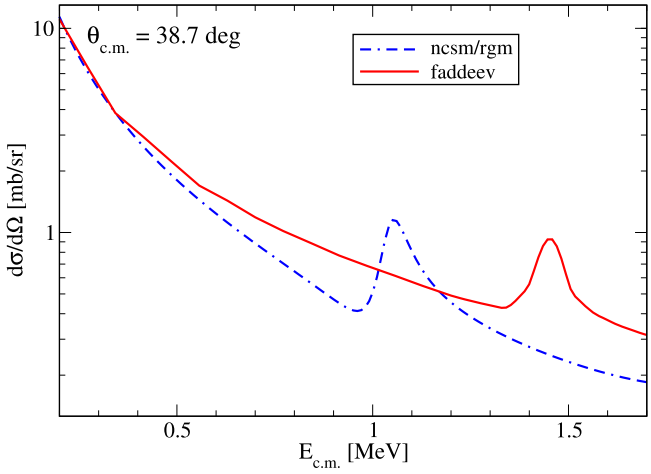

Figure 10. The differential cross section for elastic $d + \alpha$ scattering as a function of the center-of-mass energy $E_{c.m.}$ at the scattering angle $\theta_{c.m.} = 38.7$ deg. The solid lines shows phase shifts computed using the NCSM/RGM while the Faddeev results are depicted by dashed lines. The model space for the Faddeev calculation is restricted to a total two-body angular momentum of $J_{np} \leqslant 3$ and $J_{n/p-\alpha} \leqslant 9/2$ for the np and n/p-α subsystems [348].

scattering and the ^{6}Li ground state [348]. This system has the advantage that it can be well-described using microscopic reaction theory. First, the NCSM/RGM [349, 350] was used to compute effective $n/p - \alpha$ potentials. Then the three-body Faddeev equations [351] are used to compute the ^{6}Li ground state as well as $d + \alpha$ scattering observables. In parallel, the same scattering observables are obtained directly from NCSM/RGM. The comparison between the two approaches discloses the effects of the 3BF, arising from the antisymmetrization. The study finds that the irreducible three-body force has a sizable effect on observables. Specifically, the Faddeev approach yields a ^{6}Li ground state that is approximately 600 keV shallower than the one obtained with the NCSM/RGM. Additionally, the d-α three-body calculations yield a 3^+ resonance that is located approximately 400 keV higher in energy compared to the NCSM/RGM result (see figure 10). The shape of the d-α angular distributions computed using the two approaches also differ, owing to the different position of the 3^+ resonance.

While the utilization of the NCSM/RGM allows for the determination of the contributions to the 3BF stemming from Pauli exclusion effects, a similar study based on the no-core-shell model with continuum [352, 353] (NCSMC) is necessary for the quantification of additional components arising from excitations of the nucleons in ^{4}He. Lastly, a similar study that encompasses several nuclei and a broader energy range can shed light on the mass and energy dependence of the 3BF. Such work would inform the parametrization of the latter and thus lead to improved three-body calculations for reactions.

4. Tools and resources

As discussed in section 3, there are multiple efforts to build reliable optical potentials which are constructed from different approaches and have therefore various forms, e.g. local/non-local and parametrized/numerical. To facilitate the development of accurate optical potentials

and their use in applications, it is essential to efficiently share our codes and newly-developed optical potentials. Having access to well-documented publicly-available reaction codes is a real asset to developers of potential. In this way, the potentials for various observables, such as direct and compound nuclear reaction cross sections (see section 2), can be easily tested and their accuracy can be quantified. From the user side, because parametrizations of optical potentials often involve many functionals, integrating new optical potentials in a reaction code can be cumbersome.

To streamline the use of these potentials and to compare efficiently their accuracies for reaction observables, it is time to list available resources in one platform. To fulfill these needs, in the context of the workshop 'Optical potentials in nuclear physics' held in March 2022 at FRIB [354] gathering reaction codes and optical potential parametrizations was created. We briefly present here the different resources that this website contains (more details can be found in this website and in the references therein). Let us emphasize that the list presented is non-exhaustive, this is a selected overview of tools available to the community. In the future, the website will be updated with any resources that developers want to share.

Reaction codes. Because optical potentials approximate the absorption from the elastic channel, their accuracy is often evaluated by looking at elastic scattering and polarization data. Different codes, Scattering WAves off NonLocal Optical Potentials in the presence of Coulomb interaction (SWANLOP) [355, 356], Schrödinger Integro-Differential equation Solver (SIDES) [357], equations Couplées en Itérations Séquentielles (ECIS) [358], Optical Model with Nonaxiality (OPTMAN) [359–361] and FRESCO [151], provide these observables for any numerical potential given as input. These solvers have complementary advantages, we emphasize here some of their capabilities. SWANLOP and SIDES, developed by Arellano, Blanchon *et al*, can handle non-local optical potentials exhibiting a Gaussian non-locality, such as the one proposed in the early work of Perey and Buck [5]. Moreover, SWANLOP can read optical potentials expressed in both coordinate and momentum spaces. ECIS and OPTMAN, developed respectively by Raynal and Soukhovitski, are connected to a comprehensive database of parameters of local optical potentials as part of the IAEA RIPL project [15], allowing to calculate consistently scattering cross sections for many targets in a broad energy range. FRESCO [151], developed by Thompson, also contains a wrapper code SFRESCO, that can be used to fit the optical potentials parameters to experimental data.

For more complex direct reactions, such as transfer and breakup, the codes FRESCO and NonLocal Adiabatic Transfer (NLAT) [362] are the tools of choice. FRESCO calculates virtually any direct or multi-step nuclear reaction which can be expressed in terms of countable coupled-channels. In particular, FRESCO provides various cross sections for breakup and transfer, obtained within the Continuum Discretized Coupled-Channel method [363–368] (CDCC), Coupled Reaction Channels [369, 370] (CRC) or the DWBA. *R*-matrix and Lagrange methods allow non-local potentials to be included non-iteratively. NLAT, developed by Titus *et al*, calculates transfer cross sections for single-nucleon transfer reactions, (d, p), (d, n), (n, d) or (p, d), including nonlocal nucleon-target interactions, within the finite-range adiabatic distorted wave approximation [371] (ADWA) and DWBA. This code is suitable for deuteron induced reactions in the range of $E_d \sim 10$–70 MeV.

To compute compound reactions (see section 2.2), TALYS [149, 150], Yet Another Hauser Feshbach Code (YAHFC) [372] and EMPIRE [373], relying on the HF formalism [88], are available. These three codes, which have been widely used by the community, provide predictions of nuclear reactions, including direct, pre-equilibrium and compound nucleus reactions, through multiple different methods and inputs. In particular, they can treat various optical models, spherical or deformed, through coupled-channels methods. These codes are also connected to different optical potential libraries, EMPIRE is connected to RIPL

database [15], and both YAHFC and TALYS have some popular global parametrizations integrated in the code. There are some ongoing efforts to update YAHFC to integrate the extended global spherical proton and neutron optical potentials of CH89 [13] and KD [14] with uncertainty quantification of the potential parameters, respectively CHUQ and KDUQ [185] (see section 3.1).

To solve coupled-channels problems in nuclear physics, the subroutine RMATRIX [374], developed by Descouvemont, is also a practical tool as it can be easily integrated in any code. This routine takes in input local or non-local coupling potentials at different nucleus-nucleus distances. It also includes an efficient way to deal with long-range potentials with propagation techniques, which significantly speeds up the calculations.

Available optical potential parametrizations. A comprehensive database of parameters for local optical potentials for many targets in a broad energy range was developed during the IAEA RIPL project [15]. A retrieval code (OMGET) is available from the RIPL3 webpage [375] at tab 'OPTICAL'. This is a FORTRAN code that can prepare inputs for the optical solvers ECIS and OPTMAN using the RIPL OMP library.

As emphasized in section 3.1, there are a multitude of phenomenological optical potentials that have been developed for the last fifty years. Some of these parametrizations for neutron-, proton-, deuteron- and α-target systems have been collected by Kay in an excel spreadsheet. Having such a compilation of phenomenological potentials makes it easier for the user who wants to compare observables obtained with various optical potentials. This spreadsheet is a work in progress and any suggestion is welcome.

Another recent effort has been made by Pruitt, Escher and Rahman to quantify the uncertainties of the potential parameters in the global spherical proton and neutron optical potentials of KD [14] and CH89 [13] with uncertainty quantification, the so called KDUQ and CHUQ [185]. The mass and energy range of validity are the same as the original KD and CH89, i.e $24 < A < 209$ and $0.001\,\text{MeV} < E < 200\,\text{MeV}$ for KDUQ and $40 < A < 209$ and $10\,\text{MeV} < E < 65\,\text{MeV}$ for CHUQ. The optical potential parameters and tools for sampling are available in the supplemental material of [185].

The recently developed microscopic global WLH nucleon–nucleus potential with quantified uncertainties [314] (see section 3.2.4) has been parametrized to be easily integrated into modern reaction codes, using a local Woods–Saxon form with parameters that vary smoothly in energy, mass, and isospin asymmetry. This global potential is valid for targets with mass $12 \leqslant A \leqslant 242$ and energies $0 \leqslant E \leqslant 150\,\text{MeV}$. A python script sampling the WLH global parametrization can be downloaded on the website [376].

Recommendations. Historically, optical potentials have been parametrized using a local Woods–Saxon radial form with parameters depending smoothly on the beam energy and mass of the target. Because these global potentials have simple expressions, they are easily shared and often used for applications. In general, the newly developed microscopic optical potentials are non-local and do not have an analytical parametrization. To facilitate collaboration between theorists and experimentalists, we propose recommendations for the non-local optical potentials to be shared as easily as possible between makers and users.

Consider the case where the non-local potentials do not couple different partial waves lj. The radial forms $U_{lj}(r, r'; E)$, defined on a two-dimensional (r, r') radial grid, may then be represented as a matrix and their eigen-expansions determined. At the specific incident energies E where these potentials are targeted, some of its eigenvectors will have much higher overlaps with the scattering wave functions than the others. It would therefore be more efficient if just the eigensolutions with the largest product of overlaps and eigenvalues could be retained without significant loss of accuracy. These eigenvectors would be the one-dimensional form factors, such as $f_{i,lj,E}(r)$ corresponding to eigenvalues $\lambda_{i,ljE}$, in the expansion

$$U_{lj}(r, r'; E) = U_{ljE}(r)\ \delta(r - r') + \sum_{i=1}^{n} \lambda_{i,ljE}\ f_{i,lj,E}(r)\ f_{i,lj,E}(r'). \tag{36}$$

The evaluator would choose expansion size n just sufficient to describe the important physical effects that are not described by the local potential.

As well as saving space in publications, these separable expansions would allow the fast solution of the scattering equations without needing R-matrix or Lagrange mesh bases that require solving a set of linear equations defined by the radial grid. That is because the scattering equation with a potential like equation (36) can be solved by the method of equation (5) of [377], where a linear combination of inhomogeneous solutions (from each $f_{i,lj,E}(r)$ as a driving term) is added to the regular solution to reproduce the effects of the potential (36). Groups of only $n + 1$ linear equations now need to be solved.

Further efficiency would follow if the form factors $f_{i,lj,E}(r)$ could have analytic forms in their radial and energy dependence. In general, the principal eigenvectors will not have analytic shapes, but if the potential makers could fit some parametrized analytic forms, this would make the interchange of non-local potentials even easier.

Despite the recent efforts to treat non-local optical potentials, there are still many methods and codes that have not been generalized to non-local interactions. To move forward as a community, we suggest that reaction codes need to be extended to deal with both local and non-local potentials.

5. Comparing approaches

In this section, we provide a critical assessment and comparison of the different approaches presented in this work, both in order to illustrate the content of the previous sections, and to set the stage for the next one. We show in figures 11–14 a systematic comparison of predictions for a variety of observables. We consider two broad categories: phenomenological (solid lines) and microscopic or semi-microscopic (dashed lines) models. The models for which an uncertainty quantification (UQ) study has been performed are represented by their 95% uncertainty band. The acronyms used in this section, referring to the optical potentials discussed throughout this paper, are listed in table 1. Features of each optical potential, e.g. applicability in mass and in energy, are summarized in table 2.

In figure 11 we show angular differential cross sections for elastic scattering of neutrons and protons on ^{40,48}Ca, ^{16}O, and ^{12}C at several beam energies, indicated by each line on the figure around zero degree. The overall reproduction of the data is encouraging: the agreement of all phenomenological models (KD, DOM-STL, MR, MBR, KDUQ), semi-microscopic (JLMB) and most microscopic models (MST-B, MST-V, NSM, WLH) is excellent at small angles, while both the consistency between approaches and the agreement with the data deteriorates at larger angles. This is to be expected since large scattering angles receive contributions from other non-elastic channels, e.g. inelastic excitation, transfer and breakup, tracing back to the imaginary part of the optical potentials. Another positive feature, the diffraction pattern of maxima and minima in the angular distribution agrees well with the data, suggesting that the bulk properties of the matter density distribution (such as the mean squared radius) are reproduced.

In addition to these general remarks, there are a number of specific aspects that emerge from these comparisons:

- In contrast with the other *ab initio* models, the SCGF optical potential, featured in the n+^{40}Ca calculation, shows a consistent over-prediction of the elastic cross section,

Table 1. List of abbreviations used to denote the OMPs discussed in the text.

	List of abbreviations
KD	Koning–Delaroche
KDUQ	Koning–Delaroche with Uncertainty Quantification
DOM (STL)	Dispersive Optical Model (Saint Louis)
MR	Morillon–Romain
MBR	Morillon–Blanchon–Romain
NSM	Nuclear Structure Model
SCGF	Self-Consistent Green's Function
MST-B	Multiple Scattering Theory—Burrows
MST-V	Multiple Scattering Theory—Vorabbi
WLH	Whitehead–Lim–Holt
JLMB	Bruyères Jeukenne–Lejeune–Mahaux

Table 2. Summary of the Optical Potential models discussed in the text, identified with the acronyms detailed in table 1 and used in figures 11, 12, 13, and 14. In the second and third columns, we indicate the applicability ranges in terms of mass and bombarding energy, respectively. The fourth column (D.) identifies dispersive potentials, while the fifth one differentiates between microscopic (Mic.), i.e. based on structure calculations, and phenomenological potentials. The sixth column indicates whether an uncertainty quantification (UQ) analysis has been performed. The seventh column (Bib.) points to the relevant references and the eighth column (Sec.) to the section in which the model is discussed.

	Mass	Energy	D.	Mic.	UQ	Bib	section
KD	$24 \leqslant A \leqslant 209$	$1\ \text{keV} \leqslant E \leqslant 200\ \text{MeV}$	×	×	×	[14]	3.1.1
KDUQ	$24 \leqslant A \leqslant 209$	$1\ \text{keV} \leqslant E \leqslant 200\ \text{MeV}$	×	×	✓	[185]	3.1.1
DOM (STL)	C, O, Ca, Ni, Sn, Pb isotopes	$-\infty < E < 200\ \text{MeV}$	✓	×	✓	[172] [176]	3.1.2
MR	$12 < Z < 83$	$E < 200\ \text{MeV}$	✓	×	×	[99]	3.1.2
MBR	$12 < Z < 83$	$E < 200\ \text{MeV}$	✓	×	×		3.1.2
NSM	^{40}Ca, ^{48}Ca, ^{208}Pb	$E < 40\ \text{MeV}$	✓	✓	×	[204]	3.2.1
SCGF	O, Ca, Ni isotopes	$E < 100\ \text{MeV}$	✓	✓	×	[249]	3.2.2
MST-B	$A \leqslant 20$	$E \gtrsim 70\ \text{MeV}$	×	✓	×	[295]	3.2.3
MST-V	$4 \leqslant A \leqslant 16$	$E \gtrsim 60\ \text{MeV}$	×	✓	×	[292] [285]	3.2.3
WLH	$12 \leqslant A \leqslant 242$	$0 \leqslant E \leqslant 150\ \text{MeV}$	×	✓	✓	[326]	3.2.4
JLMB	$A > 30$	$1\ \text{keV} < E < 340\ \text{MeV}$	×	✓	×	[96] [98]	3.2.4

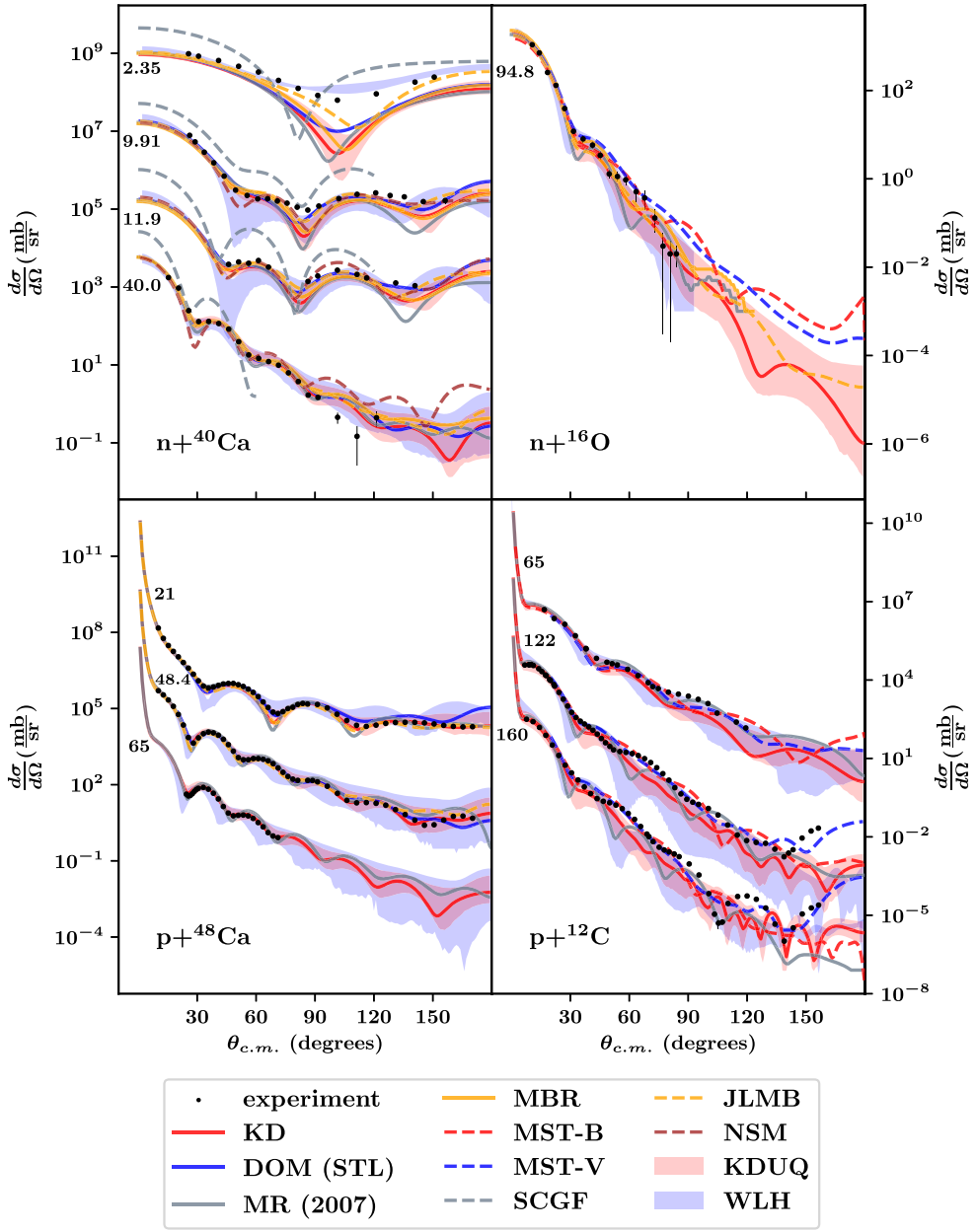

Figure 11. Elastic-scattering angular differential cross sections for neutrons on ^{40}Ca and ^{16}O and protons on ^{48}Ca and ^{12}C, computed making use of the optical models indicated in the legend. The numbers by the curves around zero degree correspond to the nucleon bombarding energies in MeV. The shaded areas correspond to 95% confidence intervals.

resulting from a lack of absorption. This is likely a consequence of the fact that the level density at energies relevant for scattering phenomena is typically underpredicted by current *ab initio* calculations, leading to a small imaginary component in the optical potential. Note that the predictions presented here have been obtained with the NNLO-sat chiral interactions, using other two- and three-nucleon forces will influence the diffraction pattern and the absorption. One should also emphasize that the *ab initio*-derived SCGF potential is the only one shown in figures 11–12 that does not rely on static densities or mean field approximations. This characteristic is shared by all methods discussed section 3.2.2.

- For the $n+^{40}$Ca at 2.35 MeV, only WLH is able to reproduce the shape of the angular distribution and absolute value of the cross section. That can be easily understood by noting that WLH is the only calculation including the contribution of compound elastic processes, which are important for this case. Note that if these contributions were included in the other calculations (KD, DOM-STL, MR, MBR, JLMB and KDUQ), they may also reproduce the data.
- The calculations based on multiple scattering theory (MST-B, MST-V) are only applied to the $n+^{16}$O and $p+^{12}$C elastic scattering at high energies, consistent with their range of validity. These two models exhibit a similar level of agreement when compared to the data. Although they are similar for smaller angles, there are significant differences at larger angles. This may result from the different treatment of spin used in both approaches as discussed in section 3.2.3.
- The approach based on an RPA description of the collective low-energy nuclear spectrum (NSM) are designed to be used at lower energies, where they indeed perform well.
- The semi-microscopic model JLMB is accurate over the whole energy range, as its parameters were adjusted to reproduce neutron and proton elastic scattering observables in the 1 keV–200 MeV energy range for $A \geqslant 40$. One can see here that although the JLMB was not fitted on lighter nuclei, it agrees fairly well with experimental data on ^{16}O target. This indicates that the JLMB remains a good starting point for $A < 40$ nuclei.
- WLH performs well for all energies considered, however, the uncertainty intervals from WLH are larger than those from KDUQ. This is particularly evident for $p+^{48}$Ca scattering at large angles. While KDUQ was fitted to data, WLH results from a microscopic calculation of the nucleon–nucleon interaction in nuclear matter and therefore there is no reason why these uncertainties should be of the same magnitude.

We now turn to energy distributions (total cross sections in figure 12 and reaction cross sections in figure 13). As for the angular distribution, here the phenomenological potentials agree well with the $n+^{40,48}$Ca data at all energies. This is expected for the DOM parametrization which was fitted to reproduce both ^{40,48}Ca data. However, since the MR, MBR, KD and KDUQ global optical potentials were only fitted to ^{40}Ca data, the good agreement with the ^{48}Ca data suggest that the mass and isospin dependencies of these parametrizations are accurate. The WLH also agrees well with the data within its uncertainty, although the uncertainty interval is very large. For this observable too, the current imperfections of SCGF *ab initio* calculations are apparent. Even if the available data are more scarce for the reaction cross sections than for the total cross sections, the picture drawn by the comparisons in figure 13 is similar to that from figure 12. The reaction cross section is largely associated with the imaginary part of the optical potential, reflecting the role of the open reaction channels in removing flux from the elastic one.

While the phenomenological approaches perform well, the NSM approach underestimates the reaction cross section, which might point to the fact that it fails to account for important

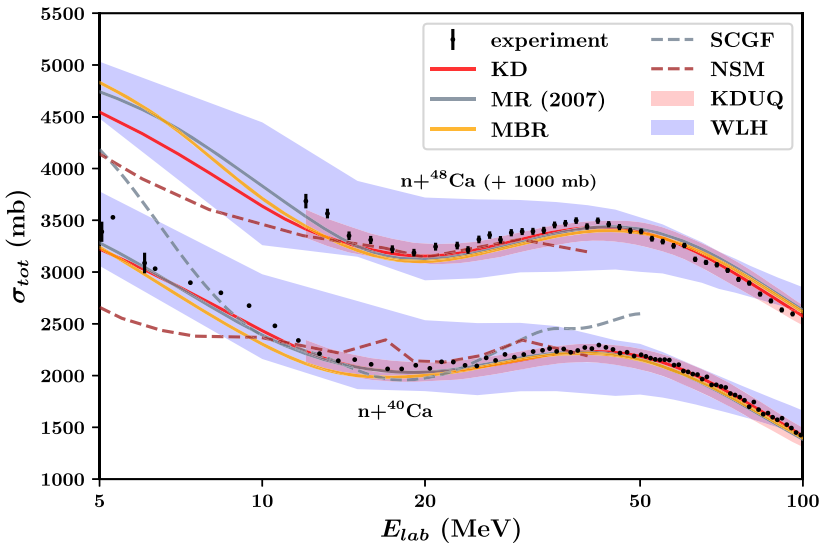

Figure 12. Total cross section as a function of neutron bombarding energy for ^{40,48}Ca. The shaded areas correspond to 95% confidence intervals.

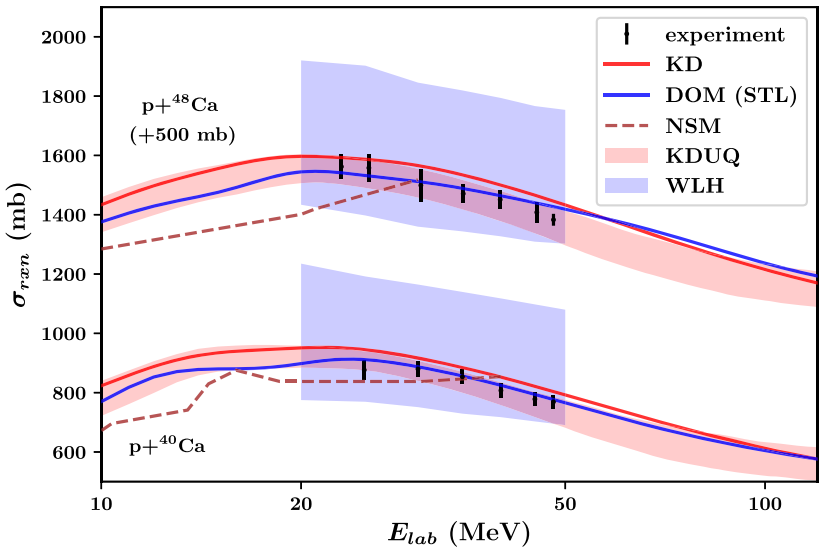

Figure 13. Reaction cross section as a function of proton bombarding energy for ^{40,48}Ca. The shaded areas correspond to 95% confidence intervals.

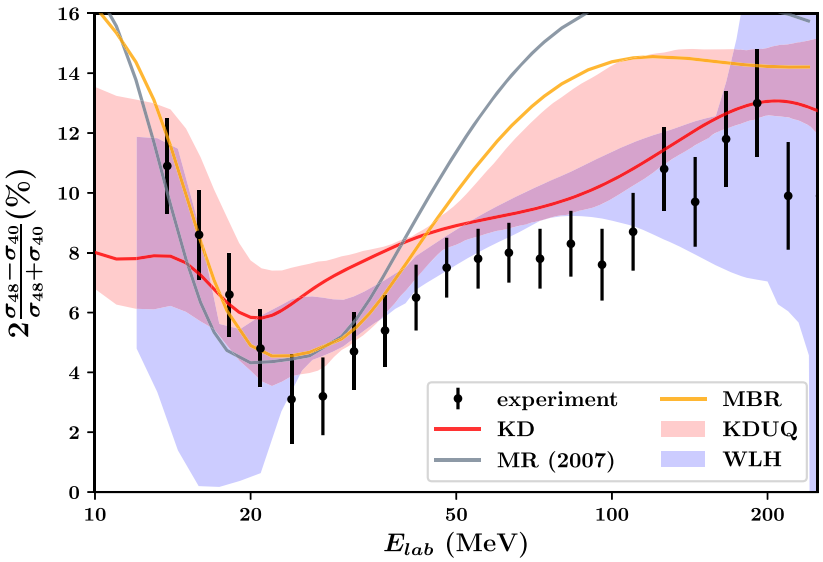

Figure 14. Asymmetry of the total cross section between ^{40}Ca and ^{48}Ca, defined as twice the ratio between the difference and the sum of the total cross sections, expressed in percentage. The shaded areas correspond to 95% confidence intervals.

reaction processes at lower energies. Since the NSM takes explicitly into account direct excitation of collective states in the low-lying spectrum, this result suggests that other reaction channels, such as compound nucleus formation, charge exchange, and transfer, need to be included in order to account for the total absorption. Note that the sharp variation in the NSM results compared to the other potentials can be explained by the discrete energy positions of the collective states predicted by RPA calculations, causing peaks in the reaction cross section and hence the total cross section. Overall, figures 12 and 13 reflect the difficulty encountered by microscopic theories in describing the variety of relevant reaction channels. However, the good behaviour of the WLH potential (despite its wide uncertainty interval), based on microscopic calculations of the nucleon–nucleon interaction in nuclear matter, is noteworthy.

Finally, we consider the asymmetry of the total cross section between ^{40}Ca and ^{48}Ca as shown in figure 14. This observable is very sensitive to the difference between neutron and proton densities, and the fact that all the models reproduce the trend reasonably well suggests that they can account for the isospin dependence of the cross section around stability. However, the WLH potential somewhat underpredicts the energy of the first dip at around 30 MeV. The uncertainty bands associated with KDUQ and WLH capture the data at the 95% confidence level, and contrary to the previous observables, they both have a similar width. A likely explanation is that uncertainties associated with ratios of observables obtained consistently within the same theory tend to cancel. In the WLH, all nuclei are derived consistently within the same framework, and uncertainties can be traced back to its specific approximations (included here are the truncation level of the chiral EFT). It is unclear how systematic uncertainties evolve for different nuclei in the case of phenomenological approaches. The phenomenological dispersive optical potentials MR and MBR perform remarkably well below 30 MeV, while KD is somehow worse. This situation is reversed above 40 MeV. While this ratio of observable offers, in principle, an excellent constraint for the isospin dependence of the optical potential, we must note the large experimental uncertainties associated with the

data in figure 14. Dedicated experimental efforts devoted to new measurements with extended range and improved error bars would be necessary for it to be useful in the extraction of the isospin dependence of the optical potential. Since exotic systems are characterized by an extreme neutron-to-proton ratio, we expect the cross section asymmetry to be a strong indicator of the reliability of potentials away from stability.

Overall, phenomenological optical potentials with quantified uncertainties perform well for stable nuclei even for observables and energies they have not been fitted to, as testified by their ability to reproduce the asymmetry data shown in figure 14. A rigorous estimation of the associated uncertainties, such as implemented in the KDUQ and WLH models, is a very desirable feature. We also want to stress the importance of the implementation of dispersivity in the DOM-STL, MR, and MBR phenomenological potentials. Some microscopic approaches provide a good reproduction of elastic scattering for their ranges of validity: low energy for NSM, and high energy for the multiple scattering potentials. However, advances in fully *ab initio* potentials, represented here by the SCGF and multiple scattering theory models, are still needed before they can be reliably used far from stability.

6. Outlook and recommendations

In conclusion, optical potentials are ubiquitous in nuclear physics. In this white paper, we discuss multiple ongoing efforts in the theory community aimed at improving their reliability and at quantifying associated uncertainties. Overall, results for nucleon elastic scattering on stable targets show that the various methods do capture most of the physics, although as expected discrepancies amongst the methods and with the data increase at backward angles. The situation for nuclei away from stability is much more dire and requires dedicated future programs. In this section, we summarize the key points that should be kept in mind moving forward.

First and foremost, improving the determination of the optical potential for rare isotopes requires a close collaboration between theory and experiment. Experiments specifically targeted on constraining the optical potential are an imperative. While recent *ab initio* advances on the optical potential are impressive, it is clear that to obtain predictability away from stability, a careful validation of the current methods for systems with large isospin asymmetry is essential. This implies working closely with the experimental community, such that theorists engage in both ends of the experimental endeavor, namely in providing input to experimental design and helping in the interpretation of the measurements. We emphasize the benefit of systematic studies, experimental setups that can measure multiple channels simultaneously or cover a range of beam energies. To obtain constraints on the isospin dependence of the optical potential, it is important to be able to extract observables that are particularly sensitive to isospin asymmetry. As such, experiments that span multiple isobars or measure a long isotopic chain are invaluable.

Secondly, future theoretical studies should strive to include uncertainty quantification in deriving the optical potential. The field is ripe for merging the knowledge obtained from microscopic approaches with experimental data within a Bayesian analysis. Such a statistical framework provides a natural avenue, not just for uncertainty quantification, but also for interpolating and extrapolating the optical potential, assessing the information content of various observables, and for quantitatively discriminating between models. Theorists must be better informed on the experimental data used, and a concerted effort needs to be made such that experimental error bars incorporated in the optical model constraints include not just statistical but also systematic errors.

Concerning the progress in theory, there are many thrusts that need to be pursued and the field can greatly benefit from stronger collaborations between theorists with differing expertise. In general, *ab initio* methods need to be expanded beyond current truncations, so they can include additional correlations and ameliorate the lack of absorption resulting from the unphysically low density of states. As more *ab initio* methods extend into the continuum, reaction data needs to be part of the standard protocols of validating *ab initio* theories (currently theorists use mostly bound state spectra and root mean square radii to determine the quality of their model). It is important to address nuclear collectivity in microscopic optical model approaches at a global level. Although going beyond two-particle two-hole contributions is very challenging for some many-body frameworks, the current status demonstrates that including higher-order correlations is unavoidable. There are a variety of structure quantities calculated within the microscopic approaches that serve as inputs to the construction of optical potentials (e.g. one-body densities and two-body densities). It is important that structure theorists calculate these quantities, test them for convergence and make them widely available.

Several recent studies have demonstrated the added benefit of including the dispersion relation, enforcing causality as a constraint on the optical potential. Especially when considering a global optical potential spanning several energy regimes, it is desirable to correct the optical potential such that the real and imaginary parts of the extracted interaction are related in the appropriate manner.

It is understood that non-locality does affect reactions beyond the elastic channel and therefore its impact should be carefully considered. While in principle the optical potential is non-local, following the earlier work by Perey and Buck, a global non-local nucleon optical potential remains to be implemented. Studies have shown that the Gaussian shape assumed in the Perey and Buck parametrization is likely too simplistic. Since the optical model non-locality cannot be measured directly, this information must come from theory. Non-locality should be inspected when extracting the optical potential from microscopic theories, particularly to understand its full off-shell behavior and the dependencies on model-space truncations. For most of the existing codes, local potentials are computationally much more efficient. However, methods to include non-local potentials can be very efficient when the optical potentials are expressed in separable form.

In addition to non-locality, we identified two other features of the optical potential that must rely mostly on theory. As one moves away from stability, details on the isospin dependence become ever more important. Even with the new facilities, experiment will not be able to cover the whole nuclear landscape and such extrapolations in isospin will be reliant on theory. Testing this aspect of the microscopically derived optical potential is of paramount importance. Another important term in the optical potential is the spin–orbit force. The interplay of the spin–orbit force and the central term has been shown to be very important for loosely-bound systems. Elastic scattering is not strongly sensitive to this term and therefore, again, theory must provide guidance.

Despite the discussion in this white paper being mostly focused on the nucleon optical potential, we must underline the necessity of optical potentials for complex probes (beyond the neutron and the proton). Many experimental programs at rare isotope facilities require the use of complex probes and progress on modern formulations for the nucleus-nucleus optical potential has been slow. Future theoretical studies should include global deuteron, triton, alpha and heavy-ion microscopic optical potentials, valid for nuclei away from stability.

Ultimately, progress in the theory for optical potentials does not immediately ensure integration into the many applications in our field. It is critical that tools be updated so that the whole community can benefit from their improvements. An integral part of this work was the

creation of a website for the purpose of concentrating in one place the existing relevant codes. These codes need to be regularly updated by their authors to incorporate the latest optical potential developments. Only then will the field fully benefit from the theoretical advances.

Finally, it must be noted that while there has been increasing interest by the many-body nuclear structure community in investigating the connection to the optical potential, the gap between the existing effort and the needs is still very large. Workforce development in this area is still critical and involves a particular skill set, including many-body nuclear formalisms, few-body reaction theory and modern statistical methods.

With the RIB factory in RIKEN in full force, FRIB having started operations earlier this year and numerous other facilities around the world, we expect a plethora of rare isotope data, directly relevant for the optical potential, in the coming years. Therefore, we anticipate this topic will need to be revisited in the next 5–6 years.

Acknowledgments

The authors thank H Arellano for giving information on the the SCL-Bruyères *g*-matrix approach for the optical potential and K Launey for critical feedback and insights in the SA-NCSM subsection. The authors also thank S Nikas and P Gastis for sharing the calculations plotted in figures 4 and 5. This work is supported by the U.S. Department of Energy, Office of Science, Office of Nuclear Physics, under the FRIB Theory Alliance award no. DE-SC0013617. The work at Lawrence Livermore National Laboratory (LLNL) is performed under the auspices of the U.S. Department of Energy under Contract DE-AC52-07NA27344 and was supported in part by the LLNL-LDRD Program under Project No. 21-ERD-006. The work at Brookhaven National Laboratory is sponsored by the Office of Nuclear Physics, Office of Science of the U.S. Department of Energy under Contract No. DE-AC02-98CH10886 with Brookhaven Science Associates, LLC. The work at Ohio University is supported by the U.S. Department of Energy Office of Science under Grants DE-FG02-93ER40756. This work was also supported by the U.S. Department of Energy Office of Science under grants DE-SC0021422, DE-SC0019209, DE-SC0019521, DE-AC02-06CH11357 and DE-NA0003841. This work is supported by the National Science Foundation under Grant no. PHY-1913728, PHY-2209060, PHY1652199, PHY1912643, and PHY2207756. Computing support for the NCSM/RGM and Faddeev results presented in figures 8 and 10 came from the LLNL Institutional Computing Grand Challenge program. Computing support for the SCGF results presented in figures 8 come from the DiRAC DiAL system at the University of Leicester, UK, (funded by the UK BEIS via STFC Capital Grants No. ST/K000373/1 and No. ST/R002363/1 and STFC DiRAC Operations Grant No. ST/R001014/1) and from the National Energy Research Scientific Computing Center (DOE Contract No. DE-AC02-05CH11231) using NERSC award NP-ERCAP0020946.

Data availability statement

The data that support the findings of this study are available upon reasonable request from the authors.

ORCID iDs

C Hebborn https://orcid.org/0000-0002-0084-2561

F M Nunes https://orcid.org/0000-0001-8765-3693
G Potel https://orcid.org/0000-0002-4887-7499
W H Dickhoff https://orcid.org/0000-0003-1738-3979
J W Holt https://orcid.org/0000-0003-4373-3856
M C Atkinson https://orcid.org/0000-0002-5423-1432
R B Baker https://orcid.org/0000-0002-3909-4425
C Barbieri https://orcid.org/0000-0001-8658-6927
M Burrows https://orcid.org/0000-0002-4574-4711
R Capote https://orcid.org/0000-0002-1799-3438
P Danielewicz https://orcid.org/0000-0002-1989-5241
Ch Elster https://orcid.org/0000-0002-2459-1226
J E Escher https://orcid.org/0000-0002-0829-9153
L Hlophe https://orcid.org/0000-0001-6675-6132
A Idini https://orcid.org/0000-0001-7624-8975
H Jayatissa https://orcid.org/0000-0001-8746-0234
B P Kay https://orcid.org/0000-0001-8675-0731
K Kravvaris https://orcid.org/0000-0002-1715-0967
J J Manfredi https://orcid.org/0000-0003-3703-7424
G Perdikakis https://orcid.org/0000-0002-8539-8737
C D Pruitt https://orcid.org/0000-0003-0607-9461
G H Sargsyan https://orcid.org/0000-0002-3589-2315
M Vorabbi https://orcid.org/0000-0002-1012-7238
T R Whitehead https://orcid.org/0000-0001-8909-2033

References

[1] Navrátil P, Quaglioni S, Hupin G, Romero-Redondo C and Calci A 2016 *Phys. Scr.* **91** 053002
[2] Hodgson P 1963 *The Optical Model of Elastic Scattering* (Oxford: Clarendon Press)
[3] Hodgson P 1971 *Nuclear Reactions and Nuclear Structure* (Oxford: Oxford University Press)
[4] Hodgson P 1997 The nuclear optical model: introductory overview *Proceedings of the Meeting on Nucleon–Nucleus Optical Model up to 200 MeV* (Paris: OECD)
[5] Perey F and Buck B 1962 *Nucl. Phys.* **32** 353
[6] Buck B 1963 *Phys. Rev.* **130** 712
[7] Tamura T 1965 *Rev. Mod. Phys.* **37** 679
[8] Mahaux C, Ngô H and Satchler G 1986 *Nucl. Phys.* A **449** 354
[9] Mahaux C and Sartor R 1991 *Nucl. Phys.* A **528** 253
[10] Mahaux C and Sartor R 1991 *Advances in Nuclear Physics* vol 20 ed J W Negele and E Vogt (New York: Plenum)
[11] Dickhoff W H, Charity R J and Mahzoon M H 2017 *J. Phys. G: Nucl. Part. Phys.* **44** 033001
[12] Becchetti F D and Greenlees G W 1969 *Phys. Rev.* **182** 1190
[13] Varner R, Thompson W, McAbee T, Ludwig E and Clegg T 1991 *Phys. Rep.* **201** 57
[14] Koning A J and Delaroche J P 2003 *Nucl. Phys.* **713** 231
[15] Capote R *et al* 2009 *Nucl. Data Sheets* **110** 3107
[16] Weppner S P, Penney R B, Diffendale G W and Vittorini G 2009 *Phys. Rev.* C **80** 034608
[17] Watson K M 1953 *Phys. Rev.* **89** 575
[18] Kerman A, McManus H and Thaler R 1959 *Ann. Phys.* **8** 551
[19] Feshbach H 1958 *Ann. Phys.* **5** 357
[20] Feshbach H 1962 *Ann. Phys.* **19** 287
[21] Dickhoff W H and Van Neck D 2008 *Many-Body Theory Exposed!* (Singapore: World Scientific) 2nd edn
[22] Bell J S and Squires E J 1959 *Phys. Rev. Lett.* **3** 96
[23] Dickhoff W and Charity R 2019 *Prog. Part. Nucl. Phys.* **105** 252
[24] Bonaccorso A 2018 *Prog. Part. Nucl. Phys.* **101** 1

[25] Butler S T 1950 *Phys. Rev.* **80** 1095
[26] Warburton E K, Becker J A and Brown B A 1990 *Phys. Rev.* C **41** 1147
[27] Thibault C, Klapisch R, Rigaud C, Poskanzer A M, Prieels R, Lessard L and Reisdorf W 1975 *Phys. Rev.* C **12** 644
[28] Otsuka T, Gade A, Sorlin O, Suzuki T and Utsuno Y 2020 *Rev. Mod. Phys.* **92** 015002
[29] Otsuka T, Suzuki T, Fujimoto R, Grawe H and Akaishi Y 2005 *Phys. Rev. Lett.* **95** 232502
[30] Di Pietro A *et al* 2010 *Phys. Rev. Lett.* **105** 022701
[31] Bradt J *et al* 2018 *Phys. Lett.* B **778** 155
[32] Tanihata I *et al* 1985 *Phys. Lett.* B **160** 380
[33] Tanihata I, Hamagaki H, Hashimoto O, Shida Y, Yoshikawa N, Sugimoto K, Yamakawa O, Kobayashi T and Takahashi N 1985 *Phys. Rev. Lett.* **55** 2676
[34] Aumann T and Nakamura T 2013 *Phys. Scr.* **2013** 014012
[35] Butler P A 2016 *J. Phys. G: Nucl. Part. Phys.* **43** 073002
[36] Frekers D and Alanssari M 2018 *Eur. Phys. J.* A **54** 177
[37] Cappuzzello *et al* 2018 *Eur. Phys. J.* A **54** 72
[38] Cappuzzello F *et al* 2023 *Prog. Part. Nucl. Phys.* **128** 103999
[39] Schiffer J P *et al* 2012 *Phys. Rev. Lett.* **108** 022501
[40] Lee J *et al* 2010 *Phys. Rev. Lett.* **104** 112701
[41] Wimmer K 2018 *J. Phys. G: Nucl. Part. Phys.* **45** 033002
[42] Timofeyuk N and Johnson R 2020 *Prog. Part. Nucl. Phys.* **111** 103738
[43] Schiffer J P *et al* 2004 *Phys. Rev. Lett.* **92** 162501
[44] Manfredi J *et al* 2021 *Phys. Rev.* C **104** 024608
[45] Aumann T and Bertulani C A 2020 *Prog. Part. Nucl. Phys.* **112** 103753
[46] Tribble R E, Bertulani C A, Cognata M L, Mukhamedzhanov A M and Spitaleri C 2014 *Rep. Prog. Phys.* **77** 106901
[47] Horowitz C J *et al* 2019 *J. Phys. G: Nucl. Part. Phys.* **46** 083001
[48] Nunes F, Potel G, Poxon-Pearson T and Cizewski J 2020 *Ann. Rev. Nucl. Part. Sci.* **70** 147
[49] Tumino A, Bertulani C A, La Cognata M, Lamia L, Pizzone R G, Romano S and Typel S 2021 *Annu. Rev. Nucl. Part.* **71** 345
[50] von Oertzen W and Vitturi A 2001 *Rep. Prog. Phys.* **64** 1247
[51] Potel G, Idini A, Barranco F, Vigezzi E and Broglia R A 2013 *Rep. Prog. Phys.* **76** 106301
[52] Frauendorf S and Macchiavelli A 2014 *Prog. Part. Nucl. Phys.* **78** 24
[53] Potel G and Broglia R A 2021 *The Nuclear Cooper Pair* (Cambridge: Cambridge University Press)
[54] Bertulani C 2006 *Nucl. Phys.* A **767** 155
[55] Simpson E C and Tostevin J A 2011 *Phys. Rev.* C **83** 014605
[56] Duer M *et al* 2022 *Nature* **606** 678
[57] Stevens S, Ryckebusch J, Cosyn W and Waets A 2018 *Phys. Lett.* B **777** 374
[58] Tanaka J *et al* 2021 *Science* **371** 260
[59] Bonaccorso A 2013 *Phys. Scr.* **T152** 014019
[60] Baye D and Capel P 2012 Breakup reaction models for two- and three-cluster projectiles *Clusters in Nuclei* (vol 2) vol 848 (Heidelberg: Springer)
[61] Bertulani C A 2005 *Phys. Rev. Lett.* **94** 072701
[62] Ogata K and Bertulani C A 2010 *Prog. Theor. Phys.* **123** 701
[63] Bonaccorso A and Brink D 2021 *Eur. Phys. J.* A **57** 171
[64] Summers N C, Nunes F M and Thompson I J 2014 *Phys. Rev.* C **89** 069901
[65] Moro A M and Lay J A 2012 *Phys. Rev. Lett.* **109** 232502
[66] Goldstein G, Baye D and Capel P 2006 *Phys. Rev.* C **73** 024602
[67] Baur G and Typel S 2007 *J. Phys. G: Nucl. Part. Phys.* **35** 014028
[68] Baur G, Bertulani C and Rebel H 1986 *Nucl. Phys.* A **458** 188
[69] Summers N C and Nunes F M 2008 *Phys. Rev.* C **78** 069908
[70] Ogata K, Hashimoto S, Iseri Y, Kamimura M and Yahiro M 2006 *Phys. Rev.* C **73** 024605
[71] Moschini L and Capel P 2019 *Phys. Lett.* B **790** 367
[72] Moro A M, Lay J A and Gómez Camacho J 2020 *Phys. Lett.* B **811** 135959
[73] Hansen P and Tostevin J 2003 *Annu. Rev. Nucl. Part. Sci.* **53** 219
[74] Tostevin J A 2006 *J. Phys.: Conf. Ser.* **49** 21
[75] Sauvan E *et al* 2004 *Phys. Rev.* C **69** 044603
[76] Sauvan E *et al* 2000 *Phys. Lett.* B **491** 1

[77] Tostevin J A, Bazin D, Brown B A, Glasmacher T, Hansen P G, Maddalena V, Navin A and Sherrill B M 2002 *Phys. Rev.* C **66** 024607
[78] Hebborn C and Capel P 2021 *Phys. Rev.* C **104** 024616
[79] Gade A *et al* 2008 *Phys. Rev.* C **77** 044306
[80] Tostevin J A and Gade A 2014 *Phys. Rev.* C **90** 057602
[81] Tostevin J A and Gade A 2021 *Phys. Rev.* C **103** 054610
[82] Aumann T *et al* 2021 *Prog. Part. Nucl. Phys.* **118** 103847
[83] Aumann T, Bertulani C A and Ryckebusch J 2013 *Phys. Rev.* C **88** 064610
[84] Moro A M 2015 *Phys. Rev.* C **92** 044605
[85] Gómez-Ramos M and Moro A M 2018 *Phys. Lett.* B **785** 511
[86] Lovell A E, Nunes F M, Catacora-Rios M and King G B 2020 *J. Phys. G: Nucl. Part. Phys.* **48** 014001
[87] Lane A M and Thomas R G 1958 *Rev. Mod. Phys.* **30** 257
[88] Hauser W and Feshbach H 1952 *Phys. Rev.* **87** 366
[89] Chadwick M *et al* 2006 *Nucl. Data Sheets* **107** 2931
[90] Hilaire S, Lagrange C and Koning A J 2003 *Ann. Phys.* **306** 209
[91] Goriely S *et al* 2019 *Eur. Phys. J.* A **55** 172
[92] Zelevinsky V and Horoi M 2019 *Prog. Part. Nucl. Phys.* **105** 180
[93] Larsen A C, Spyrou A, Liddick S N and Guttormsen M 2019 *Prog. Part. Nucl. Phys.* **107** 69
[94] Savran D, Aumann T and Zilges A 2013 *Prog. Part. Nucl. Phys.* **70** 210
[95] Bracco A, Lanza E G and Tamii A 2019 *Prog. Part. Nucl. Phys.* **106** 360
[96] Bauge E, Delaroche J P and Girod M 1998 *Phys. Rev.* C **58** 1118
[97] Bauge E, Delaroche J P, Girod M, Haouat G, Lachkar J, Patin Y, Sigaud J and Chardine J 2000 *Phys. Rev.* C **61** 034306
[98] Bauge E, Delaroche J and Girod M 2001 *Phys. Rev.* C **63** 024607
[99] Morillon B and Romain P 2007 *Phys. Rev.* C **76** 044601
[100] Nobre G P A, Palumbo A, Herman M, Brown D, Hoblit S and Dietrich F S 2015 *Phys. Rev.* C **91** 024618
[101] Soukhovitskiĭ E S, Capote R, Quesada J M, Chiba S and Martyanov D S 2016 *Phys. Rev.* C **94** 064605
[102] Soukhovitskiĭ E S, Capote R, Quesada J M, Chiba S and Martyanov D S 2020 *Phys. Rev.* C **102** 059901
[103] Porter C E and Thomas R G 1956 *Phys. Rev.* **104** 483
[104] Ernebjerg M and Herman M 2005 *AIP Conf. Proc.* **769** 1233
[105] Simonius M 1974 *Phys. Lett.* B **52** 279
[106] Voinov A V, Grimes S M, Brune C R, Hornish M J, Massey T N and Salas A 2007 *Phys. Rev.* C **76** 044602
[107] Voinov A V *et al* 2021 *Phys. Rev.* C **104** 015805
[108] Cyburt R H *et al* 2010 *Astrophys. J., Suppl. Ser.* **189** 240
[109] Koning A J, Rochman D, Sublet J C, Dzysiuk N, Fleming M and van der Marck S 2019 *Nucl. Data Sheets* **155** 1
[110] Agostinelli S *et al* 2003 *Nucl. Instrum. Methods. Phys. Res.* A **506** 250
[111] Schweda K and Schmidt D 2002 *Nucl. Instrum. Methods. Phys. Res.* A **476** 155
[112] Goriely S and Delaroche J P 2007 *Phys. Lett.* B **653** 178–83
[113] Jeukenne J P, Lejeune A and Mahaux C 1977 *Phys. Rev.* C **16** 80
[114] Jeukenne J P *et al* 1976 *Phys. Rep.* **25** 83
[115] Arnould M and Goriely S 2003 *Phys. Rep.* **384** 1
[116] Rauscher T, Dauphas N, Dillmann I, Fröhlich C, Fülöp Z and Gyürky G 2013 *Rep. Prog. Phys.* **76** 066201
[117] McKay J, Denissenkov P, Herwig F, Perdikakis G and Schatz H 2020 *Mon. Not. R. Astron. Soc.* **491** 5179
[118] Nikas S, Perdikakis G, Beard M, Surman R, Mumpower M R and Tsintari P 2020 arXiv:2010.01698
[119] Bliss J, Arcones A, Montes F and Pereira J 2020 *Phys. Rev.* C **101** 055807
[120] Denissenkov P A, Herwig F, Perdikakis G and Schatz H 2021 *Mon. Not. R. Astron. Soc.* **503** 3913
[121] McKay J E, Denissenkov P A, Herwig F, Perdikakis G and Schatz H 2019 *Mon. Not. R. Astron. Soc.* **491** 5179

[122] McFadden L and Satchler G 1966 *Nucl. Phys.* **84** 177
[123] Demetriou P, Grama C and Goriely S 2002 *Nucl. Phys.* A **707** 253
[124] Avrigeanu M and Avrigeanu V 2010 *Phys. Rev.* C **82** 014606
[125] Avrigeanu V, Avrigeanu M and Mănăilescu C 2014 *Phys. Rev.* C **90** 044612
[126] Mohr P 2015 *Eur. Phys. J.* A **51** 56
[127] Bernstein L A, Brown D A, Koning A J, Rearden B T, Romano C E, Sonzogni A A, Voyles A S and Younes W 2019 *Annu. Rev. Nucl. Part.* **69** 109–36
[128] Brown D *et al* 2018 *Nucl. Data Sheets* **148** 1
[129] Capote R *et al* 2018 *Nucl. Data Sheets* **148** 254
[130] Capote R, Smith D and Trkov A 2010 *EPJ Web Conf* **8** 04001
[131] Koning A 2015 *Eur. Phys. J.* A **51** 184
[132] Capote R *et al* 2020 *Nucl. Data Sheets* **163** 191
[133] Nichols A and Capote R 2014 *Nucl. Data Sheets* **120** 239
[134] Gul K *et al* 2001 Charged particle cross-section database for medical radioisotope production: diagnostic radioisotopes and monitor reactions *IAEA Technical Report* IAEA-TECDOC-1211 IAEA, Vienna, Austria
[135] Běták E, Caldeira A and Capote R e a 2011 Nuclear data for the production of therapeutic radionuclides *IAEA Technical Reports* Series No. 473 International Atomic Energy Agency, Vienna, Austria
[136] Paige Abel E *et al* 2019 *J. Phys. G: Nucl. Part. Phys.* **46** 100501
[137] Hermanne A *et al* 2018 *Nucl. Data Sheets* **148** 338
[138] Hermanne A, Tárkányi F, Ignatyuk A, Takács S and Capote R 2021 *Nucl. Data Sheets* **173** 285
[139] Tárkányi F *et al* 2019 *J. Radioanal. Nucl. Chem.* **319** 487
[140] Tárkányi F *et al* 2019 *J. Radioanal. Nucl. Chem.* **319** 533
[141] Engle J *et al* 2019 *Nucl. Data Sheets* **155** 56
[142] Slaba T C, Bahadori A A, Reddell B D, Singleterry R C, Clowdsley M S and Blattnig S R 2017 *Life Sci. Space Res.* **12** 1
[143] Quartemont N J, Peterson G, Moran C, Samin A, Wang B, Yeamans C, Woodworth B, Holland D, Petrosky J C and Bevins J E 2021 *Nucl. Instrum. Methods. Phys. Res.* A **1016** 165777
[144] Norbury J W, Miller J, Adamczyk A M, Heilbronn L H, Townsend L W, Blattnig S R, Norman R B, Guetersloh S B and Zeitlin C J 2012 *Radiat. Meas.* **47** 315
[145] de Wet W C, Townsend L W, Ford W P, Werneth C M, Norman R B and Slaba T C 2020 *Nucl. Instrum. Methods. Phys. Res.* B **480** 115
[146] Ramsey C R, Townsend L W, Tripathi R K and Cucinotta F A 1998 *Phys. Rev.* C **57** 982
[147] Danielewicz P, Singh P and Lee J 2017 *Nucl. Phys.* A **958** 147
[148] Guss P P, Byrd R C, Howell C R, Pedroni R S, Tungate G, Walter R L and Delaroche J P 1989 *Phys. Rev.* C **39** 405
[149] Koning A J, Hilaire S and Goriely S 2008 *Nucl. Phys.* A **810** 13
[150] Koning A and Rochman D 2012 *Nucl. Data Sheets* **113** 2841
[151] Thompson I J 1988 *Comput. Phys. Rep.* **7** 167
[152] Molina A, Capote R, Quesada J M and Lozano M 2002 *Phys. Rev.* C **65** 034616
[153] Morillon B and Romain P 2004 *Phys. Rev.* C **70** 014601
[154] Capote R, Molina A and Quesada J M 2001 *J. Phys. G: Nucl. Part. Phys.* **27** B15
[155] Quesada J M, Capote R, Molina A and Lozano M 2003 *Comp. Phys. Commun.* **153** 97
[156] Quesada J M, Capote R, Molina A, Lozano M and Raynal J 2003 *Phys. Rev.* C **67** 067601
[157] Capote R, Soukhovitskii E S, Quesada J M and Chiba S 2005 *Phys. Rev.* C **72** 064610
[158] Soukhovitskii E S, Capote R, Quesada J M and Chiba S 2005 *Phys. Rev.* C **72** 024604
[159] Capote R, Chiba S, Soukhovitskiĭ E S, Quesada J M and Bauge E 2008 *J. of Nucl. Sc. Tech.* **45** 333
[160] Li R, Sun W, Soukhovitskiĭ E S, Quesada J M and Capote R 2013 *Phys. Rev.* C **87** 054611
[161] Quesada J M, Capote R, Soukhovitskii E S and Chiba S 2007 *Phys. Rev.* C **76** 057602
[162] Quesada J M, Soukhovitskii E S, Capote R and Chiba S 2013 *EPJ Web Conf.* **42** 02005
[163] Zhao X, Sun W, Capote R, Soukhovitskiĭ E S, Martyanov D S and Quesada J M 2020 *Phys. Rev.* C **101** 064618
[164] Lane A M 1962 *Phys. Rev. Lett.* **8** 171
[165] Lane A 1962 *Nucl. Phys.* **35** 676

[166] Mahzoon M H, Charity R J, Dickhoff W H, Dussan H and Waldecker S J 2014 *Phys. Rev. Lett.* **112** 162503
[167] Charity R J, Sobotka L G and Dickhoff W H 2006 *Phys. Rev. Lett.* **97** 162503
[168] Charity R J *et al* 2007 *Phys. Rev.* C **76** 044314
[169] Mahzoon M H, Atkinson M C, Charity R J and Dickhoff W H 2017 *Phys. Rev. Lett.* **119** 222503
[170] Atkinson M C, Blok H P, Lapikás L, Charity R J and Dickhoff W H 2018 *Phys. Rev.* C **98** 044627
[171] Pruitt C D, Charity R J, Sobotka L G, Atkinson M C and Dickhoff W H 2020 *Phys. Rev. Lett.* **125** 102501
[172] Atkinson M C, Mahzoon M H, Keim M A, Bordelon B A, Pruitt C D, Charity R J and Dickhoff W H 2020 *Phys. Rev.* C **101** 044303
[173] Pruitt C D 2022 Private communication
[174] Waldecker S J, Barbieri C and Dickhoff W H 2011 *Phys. Rev.* C **84** 034616
[175] Dussan H, Waldecker S J, Dickhoff W H, Müther H and Polls A 2011 *Phys. Rev.* C **84** 044319
[176] Pruitt C D *et al* 2020 *Phys. Rev.* C **102** 034601
[177] Potel G *et al* 2017 *Eur. Phys. J.* A **53** 178
[178] Hebborn C and Potel G 2023 *Phys. Rev.* C **107** 014607
[179] Kramer G J *et al* 1989 *Phys. Lett.* B **227** 199
[180] Giusti C and Pacati F D 1988 *Nucl. Phys.* A **485** 461
[181] Boffi S, Giusti C and Pacati F D 1980 *Nucl. Phys.* A **336** 416
[182] Atkinson M C and Dickhoff W H 2019 *Phys. Lett.* B **798** 135027
[183] King G B, Lovell A E, Neufcourt L and Nunes F M 2019 *Phys. Rev. Lett.* **122** 232502
[184] Phillips D R *et al* 2021 *J. Phys. G: Nucl. Part. Phys.* **48** 072001
[185] Pruitt C D, Escher J E and Rahman R 2023 *Phys. Rev.* C **107** 014602
[186] Rao C L, Reeves M III and Satchler G R 1973 *Nucl. Phys.* A **207** 182
[187] Lev A, Beres W P and Divadeenam M 1974 *Phys. Rev.* C **9** 2416
[188] Lev A and Beres W P 1974 *Phys. Rev.* C **10** 1223
[189] Coulter P W and Satchler G R 1977 *Nucl. Phys.* A **293** 269
[190] Vinh Mau N 1970 *Theory of Nuclear Structure* (Vienna: IAEA) p 931
[191] Bernard V and Van Giai N 1979 *Nucl. Phys.* A **327** 397
[192] Dover C B and Van Giai N 1972 *Nucl. Phys.* A **190** 373
[193] Vinh Mau N and Bouyssy A 1976 *Nucl. Phys.* A **257** 189
[194] Bouyssy A, Ngô H and Vinh Mau N 1981 *Nucl. Phys.* A **371** 173
[195] Osterfeld F, Wambach J and Madsen V A 1981 *Phys. Rev.* C **23** 179
[196] Osterfeld F and Madsen V A 1981 *Phys. Rev.* C **24** 2468
[197] Osterfeld F and Madsen V A 1985 *Phys. Rev.* C **32** 108
[198] Lassaut M and Vinh Mau N 1982 *Nucl. Phys.* A **391** 118
[199] Dermawan H, Osterfeld F and Madsen V A 1982 *Phys. Rev.* C **25** 180
[200] Leeb H and Osterfeld F 1985 *Phys. Rev.* C **32** 789
[201] Hao T V N, Loc B M and Phuc N H 2015 *Phys. Rev.* C **92** 014605
[202] Nhan Hao T V, Nhu Le N, Koh M H, Quang Hung N, Ngoc Duy N, Pham V N T and Hoang Tung N 2018 *Int. J. Mod. Phys.* E **27** 1850052
[203] Hoang Tung N, Quang Tam D, Pham V N T, Lam Truong C and Hao T V N 2020 *Phys. Rev.* C **102** 034608
[204] Blanchon G, Dupuis M, Arellano H F and Vinh Mau N 2015 *Phys. Rev.* C **91** 014612
[205] Blanchon G, Dupuis M and Arellano H F 2015 *Eur. Phys. J.* A **51** 165
[206] Blanchon G, Dupuis M, Bernard R N and Arellano H F 2017 *Eur. Phys. J.* A **53** 88
[207] Mizuyama K and Ogata K 2012 *Phys. Rev.* C **86** 041603
[208] Hao T V N, Loc B M and Phuc N H 2015 *Phys. Rev.* C **92** 014605
[209] Mizuyama K and Ogata K 2014 *Phys. Rev.* C **89** 034620
[210] Hilaire S and Girod M 2007 *Eur. Phys. J.* A **33** 237
[211] Mizuyama K, Le N N, Thuy T D and Hao T V N 2019 *Phys. Rev.* C **99** 054607
[212] Mizuyama K, Cong Quang H, Dieu Thuy T and Nhan Hao T V 2021 *Phys. Rev.* C **104** 034606
[213] Kuprikov V, Pilipenko V and Soznik A 2006 *Phys. At. Nucl.* **69** 6
[214] Kuprikov V, Pilipenko V, Soznik A, Tarasov V and Shlyakhov N 2009 *Phys. At. Nucl.* **72** 975
[215] Pilipenko V V, Kuprikov V I and Soznik A P 2010 *Phys. Rev.* C **81** 044614
[216] Pilipenko V V and Kuprikov V I 2012 *Phys. Rev.* C **86** 064613
[217] Xu Y, Guo H, Han Y and Shen Q 2014 *J. Phys. G: Nucl. Part. Phys.* **41** 015101

[218] Lopez-Moraña J and Viñas X 2021 *J. Phys. G: Nucl. Part. Phys.* **48** 035104
[219] Xu Y, Guo H, Han Y and Shen Q 2017 *Phys. Rev.* C **96** 024621
[220] Dover C B and Van Giai N 1971 *Nucl. Phys.* A **177** 559
[221] Anh N L and Loc B M 2021 *Phys. Rev.* C **103** 035812
[222] Bortignon P, Broglia R, Bes D and Liotta R 1977 *Phys. Rep.* **30** 305
[223] Idini A 2013 Renormalization effects in nuclei *PhD Thesis* University of Milan
[224] Idini A, Barranco F and Vigezzi E 2012 *Phys. Rev.* C **85** 014331
[225] Idini A, Barranco F, Vigezzi E and Broglia R 2011 *J. Phys. Conf. Ser.* **312** 092032
[226] Potel G, Idini A, Barranco F, Vigezzi E and Broglia R A 2013 *Phys. Rev.* C **87** 054321
[227] Idini A, Potel G, Barranco F, Vigezzi E and Broglia R A 2015 *Phys. Rev.* C **92** 031304
[228] Broglia R A, Bortignon P F, Barranco F, Vigezzi E, Idini A and Potel G 2016 *Phys. Scr.* **91** 063012
[229] Potel G, Idini A, Barranco F, Vigezzi E and Broglia R A 2017 *Phys. Rev.* C **96** 034606
[230] Friedrich H 1981 *Phys. Rep.* **74** 209–75
[231] Ljungberg J, Carlsson B G, Rotureau J, Idini A and Ragnarsson I 2022 *Phys. Rev.* C **106** 014314
[232] Wintgen D, Friedrich H and Langanke K 1983 *Nucl. Phys.* A **408** 239
[233] Lukyanov V, Kadrev D, Zemlyanaya E, Antonov A, Lukyanov K, Spasova K and Gaidarov M 2014 *Bull. Russ. Acad. Sci.: Phys.* **78** 1101
[234] Escher J and Jennings B K 2002 *Phys. Rev.* C **66** 034313
[235] Dickhoff W H and Barbieri C 2004 *Prog. Part. Nucl. Phys.* **52** 377
[236] Barbieri C and Jennings B K 2005 *Phys. Rev.* C **72** 014613
[237] Barbieri C and Carbone A 2017 *Self-Consistent Green's Function Approaches* (Berlin: Springer) p 571
[238] Rotureau J 2020 *Front. Phys.* **8** 285
[239] Burrows M B, Launey K D, Baker R B, Sargsyan G H, Dytrych T and Draayer J P 2021 *Ab initio* optical potentials for elastic scattering at low energies using the symmetry- adpated no-core shell model *APS Division Nucl. Phys. Meeting* **2021**
[240] Somà V, Barbieri C and Duguet T 2014 *Phys. Rev.* C **89** 024323
[241] Hagen G, Papenbrock T, Hjorth-Jensen M and Dean D J 2014 *Rep. Prog. Phys.* **77** 096302
[242] Somà V, Duguet T and Barbieri C 2011 *Phys. Rev.* C **84** 064317
[243] Somà V 2020 *Front. Phys.* **8** 340
[244] Somà V, Navrátil P, Raimondi F, Barbieri C and Duguet T 2020 *Phys. Rev.* C **101** 014318
[245] Arthuis P, Barbieri C, Vorabbi M and Finelli P 2020 *Phys. Rev. Lett.* **125** 182501
[246] Somà V, Barbieri C, Duguet T and Navrátil P 2021 *Eur. Phys. J.* A **57** 1
[247] Somà V, Cipollone A, Barbieri C, Navrátil P and Duguet T 2014 *Phys. Rev.* C **89** 061301
[248] Barbieri C, Duguet T and Somà V 2022 *Phys. Rev.* C **105** 044330
[249] Idini A, Barbieri C and Navrátil P 2019 *Phys. Rev. Lett.* **123** 092501
[250] Marchisio M A, Barnea N, Leidemann W and Orlandini G 2003 *Few Body Syst.* **33** 259
[251] Dagotto E 1994 *Rev. Mod. Phys.* **66** 763
[252] Nevo Dinur N, Barnea N, Ji C and Bacca S 2014 *Phys. Rev.* C **89** 064317
[253] Burrows M B *et al* 2022 in preparation
[254] Launey K D, Dytrych T and Draayer J P 2016 *Prog. Part. Nucl. Phys.* **89** 101
[255] Dytrych T, Launey K D, Draayer J P, Rowe D J, Wood J L, Rosensteel G, Bahri C, Langr D and Baker R B 2020 *Phys. Rev. Lett.* **124** 042501
[256] Launey K D, Mercenne A and Dytrych T 2021 *Annu. Rev. Nucl. Part. Sci.* **71** 253
[257] Dreyfuss A C, Launey K D, Escher J E, Sargsyan G H, Baker R B, Dytrych T and Draayer J P 2020 *Phys. Rev.* C **102** 044608
[258] Ruotsalainen P *et al* 2019 *Phys. Rev.* C **99** 051301
[259] Henderson J *et al* 2018 *Phys. Lett.* B **782** 468–73
[260] Williams J *et al* 2019 *Phys. Rev.* C **100** 014322
[261] Launey K D, Mercenne A, Sargsyan G H, Shows H, Baker R B, Miora M E, Dytrych T and Draayer J P 2018 Emergent clustering phenomena in the framework of the ab initio symmetry-adapted no-core shell model *Proc. of the 4th Int. Workshop on 'State of the Art in Nuclear Cluster Physics' (SOTANCP4)* vol 2038 (*AIP Conf. Proc.*) *(Galveston, Texas48, May 2018)*
[262] Hupin G, Quaglioni S and Navrátil P 2015 *Phys. Rev. Lett.* **114** 212502
[263] Dohet-Eraly J, Navrátil P, Quaglioni S, Horiuchi W, Hupin G and Raimondi F 2016 *Phys. Lett.* B **757** 430–6

[264] Calci A, Navrátil P, Roth R, Dohet-Eraly J, Quaglioni S and Hupin G 2016 *Phys. Rev. Lett.* **117** 242501
[265] Hupin G, Quaglioni S and Navrátil P 2019 *Nat. Commun.* **10** 351
[266] Kravvaris K, Quinlan K R, Quaglioni S, Wendt K A and Navrátil P 2020 *Phys. Rev.* C **102** 024616
[267] Kravvaris K, Quaglioni S, Hupin G and Navrátil P 2020 arXiv:2012.00228
[268] Kravvaris K, Navrátil P, Quaglioni S, Hebborn C and Hupin G 2022 arXiv:2202.11759
[269] Hebborn C, Hupin G, Kravvaris K, Quaglioni S, Navrátil P and Gysbers P 2022 *Phys. Rev. Lett.* **129** 042503
[270] Mercenne A, Launey K, Dytrych T, Escher J, Quaglioni S, Sargsyan G, Langr D and Draayer J 2022 *Comp. Phys. Comm.* **280** 108476
[271] Idini A and Barbieri C 2022 in preparation
[272] Hagen G, Papenbrock T and Dean D J 2009 *Phys. Rev. Lett.* **103** 062503
[273] Navrátil P 2004 *Phys. Rev.* C **70** 054324
[274] Johnson R C 2017 *Phys. Rev.* C **95** 064610
[275] Johnson R C 2019 *Phys. Rev.* C **99** 044608
[276] Rotureau J *et al* 2017 *Phys. Rev.* C **95** 024315
[277] Rotureau J *et al* 2018 *Phys. Rev.* C **98** 044625
[278] Arthuis P, Barbieri C, Pederiva F and Roggero A 2023 *Phys. Rev.* C arXiv:2203.16167
[279] Prokof'ev N V and Svistunov B V 2008 *Phys. Rev.* B **77** 125101
[280] Francis N C and Watson K M 1953 *Phys. Rev.* **92** 291
[281] Siciliano E R and Thaler R M 1977 *Phys. Rev.* C **16** 1322–32
[282] Ernst D J, Londergan J T, Miller G A and Thaler R M 1977 *Phys. Rev.* C **16** 537–55
[283] Tandy P C and Thaler R M 1980 *Phys. Rev.* C **22** 2321
[284] Crespo R, Johnson R C and Tostevin J A 1992 *Phys. Rev.* C **46** 279
[285] Vorabbi M, Gennari M, Finelli P, Giusti C, Navrátil P and Machleidt R 2022 *Phys. Rev.* C **105** 014621
[286] Chinn C R, Elster C and Thaler R M 1993 *Phys. Rev.* C **47** 2242
[287] Takeda G and Watson K M 1955 *Phys. Rev.* **97** 1336
[288] Goldberger M L and Watson K M 1964 *Collision Theory* (New York: Wiley)
[289] Picklesimer A and Thaler R M 1981 *Phys. Rev.* C **23** 42
[290] Chinn C R, Elster C and Thaler R M 1993 *Phys. Rev.* C **48** 2956
[291] Chinn C R, Elster C, Thaler R M and Weppner S P 1995 *Phys. Rev.* C **51** 1418
[292] Vorabbi M, Gennari M, Finelli P, Giusti C, Navrátil P and Machleidt R 2021 *Phys. Rev.* C **103** 024604
[293] Holt J W, Kaiser N and Weise W 2009 *Phys. Rev.* C **79** 054331
[294] Holt J W, Kaiser N and Weise W 2010 *Phys. Rev.* C **81** 024002
[295] Burrows M *et al* 2020 *Phys. Rev.* C **102** 034606
[296] Wolfenstein L and Ashkin J 1952 *Phys. Rev.* **85** 947
[297] Wolfenstein L 1954 *Phys. Rev.* **96** 1654
[298] Elster C and Weppner S P 1998 *Phys. Rev.* C **57** 189
[299] Arellano H F and Bauge E 2007 *Phys. Rev.* C **76** 014613
[300] Elster C, Cheon T, Redish E F and Tandy P C 1990 *Phys. Rev.* C **41** 814
[301] Crespo R, Johnson R C and Tostevin J A 1990 *Phys. Rev.* C **41** 2257
[302] Arellano H F, Brieva F A and Love W G 1990 *Phys. Rev.* C **41** 2188
Arellano H F, Brieva F A and Love W G 1990 *Phys. Rev.* C **42** 1782
[303] Aguayo F J and Arellano H F 2008 *Phys. Rev.* C **78** 014608
[304] Arellano H F and Bauge E 2011 *Phys. Rev.* C **84** 034606
[305] Durant V, Capel P, Huth L, Balantekin A and Schwenk A 2018 *Phys. Lett.* B **782** 668–74
[306] Durant V, Capel P and Schwenk A 2020 *Phys. Rev.* C **102** 014622
[307] Durant V and Capel P 2022 *Phys. Rev.* C **105** 014606
[308] Chamon L C, Carlson B V, Gasques L R, Pereira D, De Conti C, Alvarez M A G, Hussein M S, Cândido Ribeiro M A, Rossi E S and Silva C P 2002 *Phys. Rev.* C **66** 014610
[309] Pereira D, Lubian J, Oliveira J, de Sousa D and Chamon L 2009 *Phys. Lett.* B **670** 330–5
[310] Furumoto T, Horiuchi W, Takashina M, Yamamoto Y and Sakuragi Y 2012 *Phys. Rev.* C **85** 044607
[311] Minomo K, Kohno M and Ogata K 2017 *Phys. Rev.* C **96** 059906
[312] Khoa D T, Phuc N H, Loan D T and Loc B M 2016 *Phys. Rev.* C **94** 034612

[313] Holt J W and Whitehead T R 2022 arXiv:2201.13404
[314] Whitehead T R, Lim Y and Holt J W 2019 *Phys. Rev.* C **100** 014601
[315] Whitehead T R, Lim Y and Holt J W 2020 *Phys. Rev.* C **101** 064613
[316] Sammarruca F, Coraggio L, Holt J W, Itaco N, Machleidt R and Marcucci L E 2015 *Phys. Rev.* C **91** 054311
[317] Holt J W, Kaiser N, Miller G A and Weise W 2013 *Phys. Rev.* C **88** 024614
[318] Holt J W, Kaiser N and Miller G A 2016 *Phys. Rev.* C **93** 064603
[319] Bogner S K, Schwenk A, Furnstahl R J and Nogga A 2005 *Nucl. Phys.* A **763** 59
[320] Hebeler K, Bogner S K, Furnstahl R J, Nogga A and Schwenk A 2011 *Phys. Rev.* C **83** 031301
[321] Gezerlis A, Tews I, Epelbaum E, Gandolfi S, Hebeler K, Nogga A and Schwenk A 2013 *Phys. Rev. Lett.* **111** 032501
[322] Coraggio L, Holt J W, Itaco N, Machleidt R, Marcucci L E and Sammarruca F 2014 *Phys. Rev.* C **89** 044321
[323] Drischler C, Carbone A, Hebeler K and Schwenk A 2016 *Phys. Rev.* C **94** 054307
[324] Rios A 2020 *Front. Phys.* **8** 387
[325] Melendez J A, Wesolowski S and Furnstahl R J 2017 *Phys. Rev.* C **96** 024003
[326] Whitehead T R, Lim Y and Holt J W 2021 *Phys. Rev. Lett.* **127** 182502
[327] Amos K, Dortmans P J, von Geramb H V, Karataglidis S and Raynal J 2000 *Adv. Nucl. Phys.* **25** 275
[328] Arellano H F and Bauge E 2011 *Phys. Rev.* C **84** 034606
[329] Dupuis M, Karataglidis S, Bauge E, Delaroche J P and Gogny D 2008 *Phys. Lett.* B **665** 152
[330] Dupuis M 2017 *Eur. Phys. J.* A **53** 1
[331] Dupuis M, Haouat G, Delaroche J P, Bauge E and Lachkar J 2019 *Phys. Rev.* C **100** 044607
[332] Dupuis M, Bauge E, Hilaire S, Lechaftois F, Péru S, Pillet N and Robin C 2015 *Eur. Phys. J.* A **51** 1
[333] Cortés M L *et al* 2018 *Phys. Rev.* C **97** 044315
[334] Cheon T, Takayanagi K and Yazaki K 1985 *Nucl. Phys.* A **437** 301
[335] Dupuis M and Bauge E 2016 *EPJ Web Conf.* **122** 06001
[336] Maris P *et al* 2022 *Phys. Rev.*C **106** 064002
[337] Ekström A, Jansen G R, Wendt K A, Hagen G, Papenbrock T, Carlsson B D, Forssén C, Hjorth-Jensen M, Navrátil P and Nazarewicz W 2015 *Phys. Rev.* C **91** 051301
[338] Tews I *et al* 2022 *Few-Body Syst.* **63** 67
[339] Idini A *et al* 2019 *Phys. Rev. Lett.* **123** 092501
[340] Ross A, Titus L J and Nunes F M 2016 *Phys. Rev.* C **94** 014607
[341] Titus L J, Nunes F M and Potel G 2016 *Phys. Rev.* C **93** 014604
[342] Arellano H F and Blanchon G 2018 *Phys. Rev.* C **98** 054616
[343] Arellano H F and Blanchon G 2021 *Eur. Phys. J.* A **57** 27
[344] Faddeev L D 1961 *Soviet Phys. JETP* **12** 1014
[345] Johnson R C and Timofeyuk N K 2014 *Phys. Rev.* C **89** 024605
[346] Dinmore M J, Timofeyuk N K, Al-Khalili J S and Johnson R C 2019 *Phys. Rev.* C **99** 064612
[347] Dinmore M J, Timofeyuk N K and Al-Khalili J S 2021 *Phys. Rev.* C **104** 034614
[348] Hlophe L, Kravvaris K and Quaglioni S 2023 *Phys. Rev.*C **107** 014315
[349] Quaglioni S and Navrátil P 2009 *Phys. Rev.* C **79** 044606
[350] Navrátil P and Quaglioni S 2011 *Phys. Rev.* C **83** 044609
[351] Alt E O, Grassberger P and Sandhas W 1967 *Nucl. Phys.* B **2** 167
[352] Baroni S, Navrátil P and Quaglioni S 2013 *Phys. Rev. Lett.* **110** 022505
[353] Baroni S, Navrátil P and Quaglioni S 2013 *Phys. Rev.* C **87** 034326
[354] https://sites.google.com/view/opticalpotentials/
[355] Arellano H and Blanchon G 2019 *Phys. Lett.* B **789** 256–61
[356] Arellano H and Blanchon G 2021 *Comp. Phys. Commun.* **259** 107543
[357] Blanchon G, Dupuis M, Arellano H, Bernard R and Morillon B 2020 *Comp. Phys. Commun.* **254** 107340
[358] Soukhovitski E S, Chiba S, Iwamoto O, Shibata K, Fukahori T and Morogovskij G 2004 *Physics and numerical methods of optman: a coupled-channels method based on soft-rotator model for a description of collective nuclear structure and excitation* JAERII - Data/Code 2004-002 Japan Atomic Energy Research Institute

[359] Raynal J 1972 Optical-model and coupled-channel calculations in nuclear physics *International Atomic Energy Agency Report* IAEA-SMR-9/8 p 281 https://inis.iaea.org/collection/NCLCollectionStore/_Public/36/116/36116778.pdf
[360] Soukhovitski E S, Chiba S, Iwamoto O, Shibata K, Fukahori T and Morogovskij G 2005 *Programs Optman and Shemman Version 8 Report* JAERI Data/Code 2005-002 https://inis.iaea.org/collection/NCLCollectionStore/_Public/36/116/36116793.pdf
[361] Soukhovitskii E S, Chiba S, Capote R, Quesada J M, Kunieda S and Morogovskij G B 2008 *Supplement to Optman Code* JAERI-Data/Code 2008-025 https://jopss.jaea.go.jp/pdfdata/JAEA-Data-Code-2008-025.pdf
[362] Titus L J, Ross A and Nunes F 2016 *Comp. Phys. Commun.* **207** 499
[363] Rawitscher G H 1974 *Phys. Rev.* C **9** 2210
[364] Rawitscher G H 1975 *Phys. Rev.* C **11** 1152
[365] Rawitscher G H 1975 *Nucl. Phys.* A **241** 365
[366] Yahiro M and Kamimura M 1981 *Prog. Theor. Phys.* **65** 2046
[367] Sakuragi Y, Yahiro M and Kamimura M 1986 *Prog. Theor. Phys. Suppl.* **89** 136
[368] Yahiro M, Ogata K, Matsumoto T and Minomo K 2012 *Prog. Theor. Exp. Phys.* **2012** 01A206
[369] Cotanch S R and Vincent C M 1976 *Phys. Rev.* C **14** 1739
[370] Imanishi B, Ichimura M and Kawai M 1974 *Phys. Lett.* B **52** 267
[371] Johnson R and Tandy P 1974 *Nucl. Phys.* A **235** 56
[372] Ormand W E YAHFC https://github.com/LLNL/Yet-Another-Hauser-Feshbach-Code
[373] Herman M, Capote R, Carlson B, Obložinský P, Sin M, Trkov A, Wienke H and Zerkin V 2007 *Nucl. Data Sheets* **108** 2655
[374] Descouvemont P 2016 *Comp. Phys. Commun.* **200** 199
[375] https://nds.iaea.org/RIPL
[376] https://trwhitehead.com/WLH.html
[377] Frantz L M, Mills R L, Newton R G and Sessler A M 1958 *Phys. Rev. Lett.* **1** 340